D1.1 Future water supply availability and demand based on different RCP scenarios

W. Gernjak[1,2], A. Daaboub[3], N. Klamerth[1], L. Bosch[1], Á. Pedregal Montes[1], D. Mercado Bettin[4], E. Hernández Busto[3], Q. Plana Puig[3], A. Kleyböcker[5]

[1] ICRA – Catalan Institute for Water Research, Girona, Spain.

[2] ICREA – Catalan Institution for Research and Advanced Studies, Barcelona, Spain.

[3] Eurecat – Centre Tecnològic de Catalunya, Barcelona, Spain.

[4] CSIC-CEAB – Centre d'Estudis Avançats de Blanes, Blanes, Girona, Spain.

[5] KWB – Kompetenzzentrum Wasser Berlin, Berlin, Germany

Introductory Table

Project Ref. No.	HORIZON-CL6-2023-CLIMATE-01-2; GA No. 101136598
Project Title	Reliability and effectiveness of integrated alternative water resources management for regional climate change adaptation
Duration of the Project	2024-01-01 to 2027-12-31 (48 months)
WP/Task:	WP1 / Task 1.1
Document due Date:	2025-06-30
Actual Date of Delivery	2025-06-30
Leader of this Deliverable	ICRA
Dissemination Level	PUBLIC
Document Status	Submitted

This project has received funding from the European Union's Horizon Europe research and innovation programme under grant agreement No. 101136598. This document reflects only the views of RECREATE consortium, neither the European Commission nor any associated parties are responsible for any use that may be made of the information it contains.

Deliverable Information Sheet

Version	Date	Author	Document history/approvals
1	2025-06-06	Gernjak, Klamerth, Bosch, Pedregal (ICRA), Daaboub, Hernández Busto, Plana Puig (Eurecat), Bettin (CSIC), Kleyböcker (KWB)	First version created for review
2	2025-06-13	Reviewer 1 & 2: Klaasjan Raat (KWR) and Ioannis Zarikos (NCSRD), PMB and WP lead	Internal review
3	2025-06-18	Gernjak (ICRA) et al.	Revision completed
4	2025-06-17	Digu Aruchamy (EUT)	Quality check
5	2025-06-19	Gernjak (ICRA) et al.	Final Revision
6	2025-06-30	Digu Aruchamy (EUT)	Submission

Executive Summary

This report presents a comparative analysis of climate-related vulnerabilities in water systems across four European case studies: North Holland (Netherlands), Kalundborg (Denmark), Syros (Greece), and Costa Brava (Spain). Each region was evaluated through a four-dimensional framework—climate predictions, surface water availability, groundwater availability, and water demand—utilising downscaled climate projections and region-specific hydrological data. This harmonised framework facilitates both site-specific insights and meaningful cross-regional comparisons.

A key finding is that climate-induced hydrological changes are more evident in discharge and runoff trends than in precipitation. Rising temperatures are expected to intensify evapotranspiration and soil dryness, thereby reducing the conversion of rainfall into effective runoff. This exacerbates seasonal water stress and implies that runoff-based indicators should be prioritised over precipitation alone in future risk assessments. Furthermore, all regions display signs of increasing interannual variability, underscoring the necessity for systems designed not only for average trends but also for extremes.

North Holland does not experience a quantitative water deficit, but rather a qualitative one: salinisation risks arising from sea level rise and reduced Rhine discharge during dry periods. Lake IJssel, a vital freshwater resource, is susceptible to these dynamics, particularly when dry summers coincide with peak agricultural and domestic demand. With limited groundwater alternatives, adaptation must concentrate on international basin cooperation, freshwater retention, and demand regulation.

In Kalundborg, the water system is rooted in circularity and industrial symbiosis. Climate projections indicate limited change in overall water availability, but more frequent low-flow periods in summer could jeopardise ecological flows and seasonal demands. Groundwater remains relatively stable but is vulnerable to potential shifts in industrial and agricultural usage. Although current demand is managed efficiently, future challenges may arise if industrial growth alters usage patterns.

Syros exemplifies vulnerability in insular, semi-arid contexts. With no permanent streams and water systems already stretched, the island faces a disproportionate decline in runoff due to climate change, despite only modest alterations in rainfall. Groundwater resources are saline and limited, while escalating tourist demand worsens the situation. Furthermore, groundwater recharge is projected to decline markedly under RCP4.5 and even more severely under RCP8.5, suggesting increasing water stress over time. Although desalination plays a crucial role in resilience, its energy costs and infrastructure requirements demand a shift towards demand-side management and efficient water use.

In Costa Brava's Muga catchment, the Darnius-Boadella Reservoir is particularly sensitive to prolonged droughts, as evidenced by critically low levels during the 2021–2024 period. Projections indicate a 20–30% decline in runoff, particularly in spring and summer, accompanied by increasing interannual variability. Regarding groundwater, forecasts show a consistent decrease in availability across most climate scenarios, with the most severe losses projected under RCP8.5. Given the region's agricultural and tourism intensity, pressures on water allocation are anticipated to rise. Without enhanced forecasting, decentralised storage, and improved irrigation efficiency, both human and environmental systems may face escalating risks.

Despite their differences, all four case studies demonstrate that water resilience is influenced by the interplay of climate signals, system capacity, and socio-economic demand. Insights on storage capacity, governance flexibility, and demand-side adaptation will be vital as the RECREATE project develops regionally grounded yet transferable strategies for climate-smart water management across Europe in line with the recently released European Water Resilience Strategy.

Table of Contents

List of Abbreviations

CDS	*(Copernicus) Climate Data Store*
CMIP	*Coupled Model Intercomparison Project Phase*
CNN	*Convolutional Neural Network*
CORDEX	*Coordinated Regional Climate Downscaling Experiment*
CS	*Case Study*
CSV	*Comma separated values*
ERA5	*ECMWF Reanalysis v5*
EU	*European Union*
GCM	*Global Climate Model*
GLDAS	*Global Land Data Assimilation System*
GWS	*Groundwater Storage*
LSTM	*Long Short-Term Memory*
NASA	*National Aeronautics and Space Administration*
RCM	*Regional Climate Model*
RCP	*Representative Concentration Pathway*
SMHI	*Swedish Meteorological and Hydrological Institute*
SSP	*Shared Socioeconomic Pathway*
WHO	*World Health Organization*

List of Figures

List of Tables

1. Introduction and Objectives

1.1 Aim and scope of this document

Ensuring the long-term resilience and sustainability of water resources is one of the most pressing challenges of the 21st century. In response to increasing pressures from climate change, urbanisation, and changing consumption patterns, the RECREATE project (Reliability and Effectiveness of Integrated Alternative Water Resources Management for Regional Climate Change Adaptation, https://recreate4water.eu/project) has been launched to explore and develop innovative solutions for the utilisation of alternative water resources. The overarching goal of RECREATE is to secure a sustainable water supply under future climate and socioeconomic conditions. By focusing on circular approaches and integrating advanced technologies, the project contributes to building resilient water management strategies for Europe and beyond.

To operationalise these goals, RECREATE conducts in-depth analyses of four diverse case studies across Europe. These include North Holland in the Netherlands (CS1) Kalundborg in Denmark (CS2), known for its industrial symbiosis practices, characterised by complex water systems and high population density; Syros in Greece (CS3), a small island facing acute water scarcity; and Costa Brava in Spain (CS4), a coastal region with an established tradition of water reuse. These case studies have been carefully selected to represent a broad spectrum of climatic, hydrological, and socioeconomic conditions, offering a robust basis for comparative analysis and generalisation of findings.

This technical report, designated as Deliverable D1.1 of the RECREATE project, focuses on the development of baseline scenarios that are essential for assessing future trajectories in water supply and demand. The baseline scenarios encompass general climate parameters, including average and extreme temperatures, as well as precipitation patterns, alongside variables related to water availability, such as surface water and groundwater resources. In addition, the report considers the evolution of water demand, influenced by demographic shifts, economic activities, and technological developments. Establishing these baselines is a foundational step toward identifying future vulnerabilities and designing adaptive responses.

To construct these scenarios, a multidisciplinary methodological framework has been adopted. Climate projections are based on data from the Coupled Model Intercomparison Project Phase 5 (CMIP5), accessed through the Copernicus Climate Data Store (CDS). This data is processed and downscaled to produce regionally relevant insights into future climatic conditions under various emission trajectories. The assessment of groundwater dynamics incorporates state-of-the-art modelling techniques that integrate hydrological, geological, and climatic inputs to simulate both current and projected groundwater availability. Water demand estimations are derived through workshops, ensuring that regional knowledge, behavioural trends, and governance factors are reflected in the scenario development process.

All projections and scenario narratives are framed within the shared socioeconomic pathways (SSPs), a set of globally recognised frameworks that describe plausible future developments in demographics, economics, technology, and policy. Specifically, this report considers SSP1 (Sustainability), SSP2 (Middle of the Road), and SSP5 (Fossil-fuelled Development), each of which is paired with corresponding Representative Concentration Pathways (RCPs): RCP2.6, RCP4.5, and RCP8.5, respectively. This combination of SSP-RCP frameworks allows for the exploration of a wide range of futures, encompassing both optimistic and pessimistic developments in climate and socioeconomic conditions (O'Neill, 2017).

It is important to note that the objective of this report is not to provide precise quantitative predictions, but rather to highlight qualitative trends and potential trajectories that are critical for the strategic planning of future project activities. By focusing on indicative trends, rather than exact forecasts, RECREATE acknowledges the inherent uncertainties in long-term modelling and adopts a scenario-based planning approach that can accommodate a range of outcomes. These trends will serve as guiding inputs for subsequent phases of the project, including the development of adaptive water reuse strategies and the evaluation of their feasibility under varying future conditions.

1.2 Document structure

This report is structured to provide a robust and comparative assessment of climate-related water system vulnerabilities across four European regions: North Holland (Netherlands), Kalundborg (Denmark), Syros (Greece), and Costa Brava (Spain). The overarching aim is to understand how projected climate changes, notably shifts in hydrology and water demand, may impact the future reliability and resilience of local and regional water supplies.

The document begins with Section 1, which introduces the background, scope, and rationale of the study, including the selection of case studies and the relevance of addressing both supply and demand dimensions under climate stress.

Section 2 outlines the methodological framework used to conduct the assessment. Rather than structuring the analysis by case study at the outset, the methodology is organised along four core dimensions:

- Climate Projections
- Surface Water Availability
- Groundwater Availability
- Water Demand Scenarios

For each dimension, the report presents the general modelling approach, data sources (including ensemble climate models and downscaled hydrological simulations), and analytical assumptions. Within each sub-section, case study-specific methods or contextual adjustments are described, ensuring both consistency and flexibility across diverse regional settings.

Section 3 presents the results, following the same structure: findings are first categorised by the four analytical themes listed above, and within each theme, results are provided for all four case studies. This structure facilitates comparative insights across regions under each water system component, making it easier to identify patterns, outliers, and key vulnerabilities that cut across geographies.

Section 4 comprises the conclusions, synthesising the main findings. It begins with general observations on trends and methodological implications, followed by individual summaries for each case study that reflect on climate, surface water, groundwater, and demand outcomes. The section concludes with a cross-case synthesis, identifying both common challenges and region-specific adaptation pathways.

This structure ensures that the reader gains both thematic depth and regional specificity while supporting the overarching goal of identifying transferable lessons for climate-resilient water planning within the RECREATE project beyond.

2. Methodology

2.1 Climate and Hydrology Predictions

A foundational component of the RECREATE project's scenario development involves analysing climate data to understand baseline and projected trends in key hydrometeorological variables. To ensure the robustness and relevance of this analysis within the European context, we conducted a comprehensive evaluation of the Copernicus Climate Data Store (CDS), with a focus on identifying datasets that offer both spatial and temporal coverage suitable for the four case study regions (Hersbach et al., 2023).

The Copernicus Climate Data Store serves as a centralised repository for climate datasets derived from both global and regional climate models, as well as from reanalysis products and observational records. Our objective was to select model combinations that offer consistent temporal resolution, spatial granularity, and completeness for the variables of interest across different Representative Concentration Pathways and Shared Socioeconomic Pathways (van Vuuren et al., 2011; O'Neill et al., 2017).

The evaluation process began by screening the CDS catalogue for available ensembles of Coupled Model Intercomparison Project Phase 5 (CMIP5; (Taylor et al., 2012)) and Coordinated Regional Downscaling Experiment (CORDEX; (Kotlarski et al., 2014)) models. CMIP5 data was chosen despite newer CMIP6 climate data being available. However, hydraulic models based on CMIP6 climate data have not yet been issued at the time of the edition of this report. Therefore, for consistency all data was based on CMIP5.

Special attention was given to the availability of RCM-GCM (Regional Climate Model – Global Climate Model) pairings that provide bias-corrected data at appropriate spatial resolutions for European applications. Datasets were selected based on their inclusion of historical (baseline) and future (scenario) simulations for the following climate variables:

- **Air temperature** (2m above ground level): Daily values for monthly and seasonal mean, minimum, and maximum temperatures—critical for understanding thermal regimes and evapotranspiration patterns.
- **Mean evaporation flux**: A key variable for estimating potential evapotranspiration and informing water balance models.
- **Precipitation**: Total daily precipitation values are essential for simulating runoff, soil moisture, and recharge.
- **Discharge**: Modelled daily streamflow data used to assess surface water availability under changing climate conditions. In the absence of a river this equals run-off.

Climate datasets were obtained at a daily resolution over a total of 125 years, encompassing a historical period (1971–2005) and future projections (2006–2095). This temporal consistency facilitates high-resolution time series analysis and seasonal aggregations across both baseline and scenario periods.

Following this evaluation, a subset of seven RCM-GCM combinations was selected to ensure comprehensive spatial and temporal coverage across the case study regions, as well as to allow for ensemble-based uncertainty assessment. The selected model combinations are as follows:

Table 1 Combination of Global and Regional Climate Model

Global Climate Model (GCM)	Regional Climate Model (RCM)	Institution(s)
HadGEM2-ES	RACMO22E	UK Met Office / KNMI (Netherlands)
HadGEM2-ES	RCA4	UK Met Office / SMHI (Sweden)
MPI-ESM-LR	REMO2009	MPI-M (Germany)
MPI-ESM-LR	RCA4	MPI-M / SMHI (Germany / Sweden)
EC-EARTH	CCLM4-8-17	ICHEC / CLM-Community (Ireland / EU)
EC-EARTH	RACMO22E	ICHEC / KNMI (Ireland / Netherlands)
EC-EARTH	RCA4	ICHEC / SMHI (Ireland / Sweden)

For the variable river discharge, the downscaled outputs from these seven climate model combinations were further processed through two hydrological models available via the CDS: E-HYPEgrid, developed by the Swedish Meteorological and Hydrological Institute (SMHI; (Arheimer et al., 2012)), and VIC-WUR, implemented by Wageningen University and Research (Hamman et al., 2018). This led to a total of 14 discharge model combinations, supporting robust ensemble modelling of streamflow dynamics across diverse hydroclimatic conditions.

All selected datasets were initially downloaded as compressed ZIP archives containing NetCDF (ncf) files. These were systematically extracted and processed using Python, leveraging libraries such as xarray, netCDF4, pandas, and numpy (Hoyer & Hamman, 2017). Scripts were developed to automate the extraction of time series data for each of the four RECREATE case study regions. This process involved:

- Subsetting spatial grids to isolate the relevant geographic locations.
- Extracting daily values for the four variables (temperature, evaporation, precipitation, and discharge).
- Structuring the extracted time series into a harmonised format.
- Exporting the final data into CSV files, with metadata included to identify case study, model combination, variable, climate scenario and time slice.

The coordinates used as reference extraction points for each case study are listed in Table 2.

Table 2 GPS reference points for the 4 Case Studies

Case Study	Location Description	Latitude	Longitude
CS1 North Holland	Central case area	52.67°N	4.70°E
CS2 Kalundborg	Central case area	55.68°N	11.09°E
CS3 Syros	Central case area	37.43°N	24.91°E
CS4 Costa Brava (inland)	Boadella Reservoir zone	42.36°N	2.79°E
CS4 Costa Brava (coast)	Coastal activities zone	42.27°N	3.18°E

The Costa Brava case study was divided into two distinct locations to reflect the significant differences in both climatic conditions and water use dynamics between the inland catchment, which supplies the Boadella Reservoir (the primary source of the drinking water supply), and the coastal zone, where urbanisation, tourism, and agriculture drive concentrated water demand.

The final output of the climate data extraction and formatting process was a comprehensive comma separated values (CSV) table containing approximately 20 million rows, with each row representing one data point (i.e. one daily observation for a specific variable, location, model combination, and scenario). The table structure allows for rapid filtering and aggregation by case study, time period, or variable, facilitating downstream analysis and integration with other project components such as groundwater simulation and water demand assessments.

All further data processing, post-CSV generation, was conducted in the latest version of RStudio (Team, 2023), where the extracted time series were cleaned, aggregated, and analysed to support trend identification and visualisation. This included seasonal decomposition, ensemble averaging, anomaly detection, and preparation of figures for reporting. Coding and scripting tasks were supported using OpenAI's ChatGPT (GPT-4), which facilitated code debugging, explanation, and documentation.

2.2 General Groundwater modelling approach

We developed a pixel-level temporal continuity downscaling approach, assuming each pixel as an independent unit (Xue et al., 2024). For each pixel, time series sequences were extracted and split into training, validation, and testing subsets. To capture groundwater storage (GWS) fluctuations and assess the impact of climate change on groundwater availability, we employed three relevant and widely available climatic predictors: actual evapotranspiration and temperature as proxies for aquifer discharge, and precipitation as a mechanism of recharge. These predictors, available at an original spatial resolution of 0.1°, were used to model GWS at each pixel using a one-dimensional Convolutional Neural Network coupled with a Long Short-Term Memory architecture (1D CNN-LSTM) model. As outlined in the flowchart (Figure 1), the methodology included downloading climate data from Copernicus (ERA5-Land) and NASA (GLDAS-V2.2). GWS data were resampled using bilinear interpolation to 0.1° resolution to align with the climatic predictors, and specific grid cells corresponding to study locations were selected. Location-specific 1D CNN-LSTM models were then developed from the aligned datasets. Model optimisation was conducted through hyperparameter tuning using an iterative approach. The validated models were subsequently used to project GWS using bias-corrected climate model outputs.

2.2.1 Modelling and climate impact assessment

- ***Model Architecture***

To prevent data leakage into the model, data from 2019 to 30 June 2024 was reserved to test the model's accuracy and uncertainty. 90 % of the data prior to 2019 was used to train the proposed model, while the remaining ten per cent was reserved for validation and hyperparameter optimisation.

We developed a Hybrid 1D CNN-LSTM model to predict GWS storage fluctuations. The model consists of an input layer followed by a 1D convolutional layer with a fixed kernel size (size of 3) and an optimised number of filters. This is succeeded by a Max pooling layer and a Monte-Carlo dropout layer with an optimised rate to prevent the model from overfitting and quantify prediction uncertainty during inference. Next, an LSTM layer with an optimised number of units is applied, followed by another Monte-Carlo dropout layer. Then we added a fully connected dense layer with an optimised number of neurons and finally an output layer. To introduce non-linearity into the model, a ReLU activation function is employed.

- ***Hyperparameter optimization and model training***

We used the Adam optimizer with a maximum of 100 epochs and a tuned learning rate between 10^{-4} and 10^{-2}. To prevent overfitting, early stopping was applied with a patience of 15 epochs. Hyperparameters tuning was performed using the Optuna framework (Akiba et al., 2019) and MSE as an objective function, optimising the hyperparameters presented in Table 3

- **Model Evaluation *and* Explainability**

To assess the accuracy of the developed model, several metrics were computed. These metrics include the Root Mean Square Error (RMSE), Mean Absolute Error (MAE), coefficient of determination (R^2), Kling Gupta efficiency (KGE) (Kling et al., 2012) and the Percent Bias (pbias).

Model interpretability for GWS predictions was achieved using SHapley Additive exPlanations (SHAP) (Lundberg et al., 2017). SHAP is a tool that decomposes the black-box models' output into additive feature contributions. It employs game theory principles to calculate SHAP values, assigning importance scores to each input parameter based on their marginal contributions (Lundberg et al., 2020).

To assess whether the model can reliably simulate such future conditions, we tested its performance on modified historical data that reflect extreme climate scenarios. According to IPCC AR4, the projected change in the mean temperature is likely (with a probability greater than 66%) to range between 2 and 4.5 °C (Solomon, 2007). Therefore, we increased the temperature by 4.5 °C and decreased the precipitation by 40%. By doing so, we aimed to evaluate the model's robustness under conditions that approximate those expected in a warmer future.

- **Climate change impact assessment**

Two specific grid cells models were developed to infer monthly changes in GWS. For each specific grid, the corresponding trained model was used to compute GWS projections based on temperature, precipitation and actual evapotranspiration. Seven combinations of different GCMs and Regional Climate Models from EURO-CORDEX under three emission pathway scenarios (RCP2.6, RCP4.5, and RCP8.5) were simulated. The spatial resolution of the climate model data is 0.1, which fits perfectly with ERA5-Land historical data used for model development and training.

Before feeding this climate data into the model, the raw datasets were first regridded to ERA5-Land mesh and subsequently bias-corrected using a distribution mapping algorithm (Teutschbein & Seibert, 2012). Specifically, a quantile mapping approach with a Gamma distribution was employed to correct precipitation, empirical quantile mapping was applied for evaporation, while a Gaussian distribution (normal) was used to adjust temperature data (D'Oria et al., 2017). For this purpose, the IBICUS package was used (Spuler et al., 2024), using calibration based on the overlapping historical period (ERA5 vs. EURO-CORDEX, 1970-2005), and then applied to the future CORDEX data.

The nonparametric Mann-Kendall test (Mann, 1945; Kendall, 1975) was applied to evaluate the monotonic trends of the projected GWS time series.

To compare future projections with the historical reference period, we first computed the annual mean of GWS for the reference period (1970-2005). Then, for each RCP scenario and time period, the annual mean across the seven climate models was calculated. The relative percent change was then derived by comparing these values to the ERA5 historical mean. For seasonal analysis, the mean GWS for each season during the historical baseline was calculated separately. Then, for each scenario-period combination, seasonal means were computed in the same manner, and the corresponding seasonal percent changes were determined. Based on the projected GWS changes, a detailed assessment of annual and seasonal trends, as well as relative deviations from the historical baseline, was conducted.

Table 3 Ranges of tuned Hyperparameters for Optung framework

Hyperparameter	
Sequence length	1-12 months
Number of convolutional filters	16-256
Dropout rate	0.2-0.5
LSTM layer size	16-128 units
Dense layer size	16-256 units
Learning rate	10^{-4} to 10^{-2}
Batch size	16-64
Kernel size	3
Activation function	ReLu

MaxPool size: padding	Same
Optimizer	Adam
Loss	Huber
Epochs	100

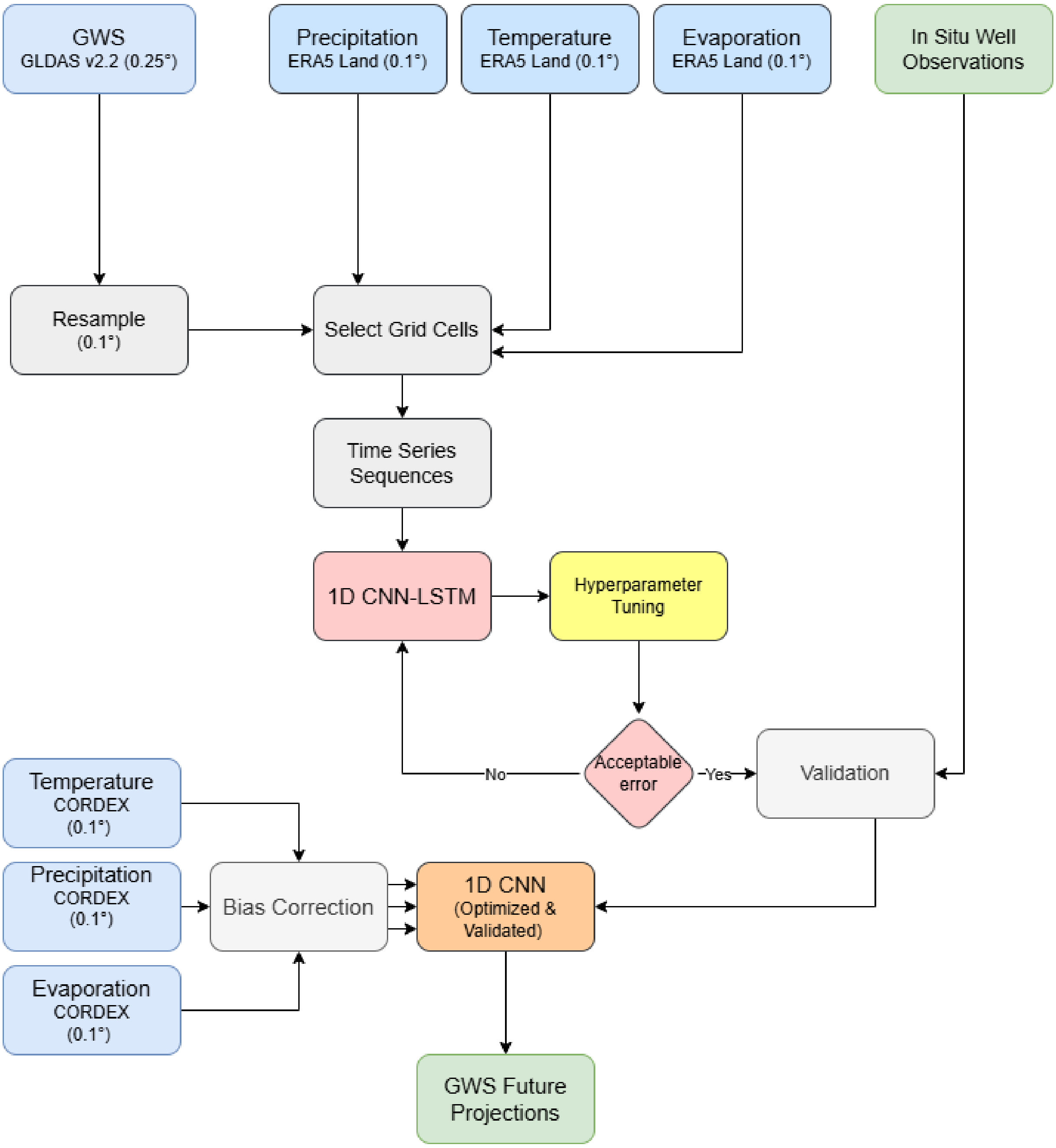

Figure 1 Flowchart of the proposed methodology

2.2.2 CS4 Costa Brava

The Muga aquifer system is situated in the northeast of Spain, encompassing an area of approximately 850 km^2 (see Figure 2). It is primarily comprised of porous materials, with Quaternary detrital deposits resting atop Neogene detrital sediments from the Empordà basin (Pulido-Velazquez et al., 2022). Table 4 illustrates the coordinates of the selected grid cells of interest that intersect with the Muga aquifer system.

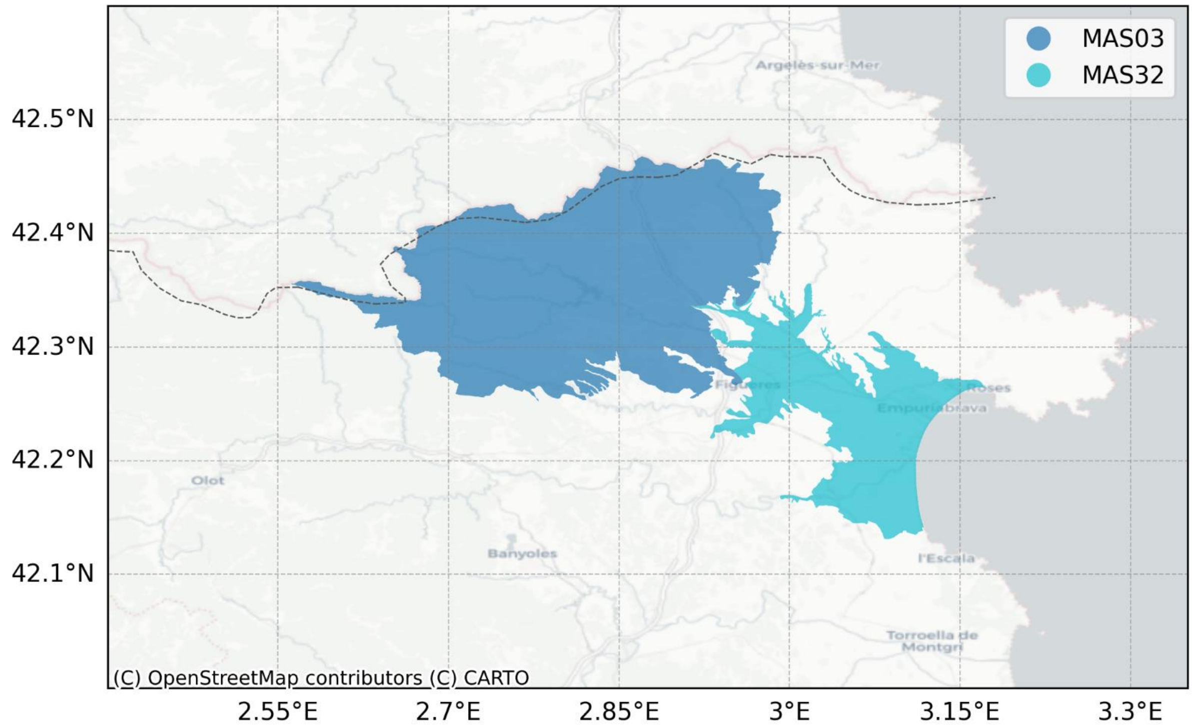

Figure 2 The Muga Aquifer System

Table 4 Coordinates of selected grid cells

ID	Latitude	Longitude	Aquifer
FFM1	42.1889	3.1086	Fluviodeltaic del Fluvià -Muga
CAM1	42.3401	2.8818	Conca Alta de la Muga

To meet the goal of this task, we first retrieved the GWS change data from the GLDAS-2.2 dataset covering the period from February 2003 to June 2024. Specifically, we downloaded the NASA_GLDAS_V022_CLSM_G025_DA1D product from NASA, which assimilates GRACE data provided by the Centre for Space Research (CSR) into the Catchment Land Surface Model (CLSM) within the NASA Land Information System (LIS). This dataset ingests satellite and in situ observations through advanced land surface modelling and data assimilation techniques (Li et al., 2019). GLDAS-2.2 is provided at a spatial resolution of 0.25°. The CSR mascon solution used for assimilation is based solely on GRACE observations and is independent of external total water storage (TWS) estimates or auxiliary models (Save et al., 2016).

Next, the downloaded data was post-processed and reprojected to the same Coordinate Reference System (CRS) to extract time series corresponding to the GLDAS-2.2 grid cells intersecting our area of interest Figure 3. Thereafter, we resampled the GWS_tavg to a monthly temporal scale, then we regridded it to a spatial resolution of 0.1° using the bilinear interpolation method (to match with ERA5-Land and EURO-CORDEX resolutions).

- ***Climate* data**

Historical meteorological data, including precipitation, temperature, and actual evapotranspiration, were sourced from ERA5-Land dataset from Copernicus Climate Change Service (C3S) (Copernicus Climate Change Service, 2022). This dataset is a global reanalysis product that integrates observational data with numerical weather model outputs (Muñoz Sabater, 2019). It provides a temporal resolution of monthly averages and a spatial resolution of 0.1° (Figure 4). We pre-processed it by aggregating monthly average precipitation and evapotranspiration values to obtain monthly totals. Temperature data were converted from Kelvin to degrees Celsius for consistency with commonly used climate metrics.

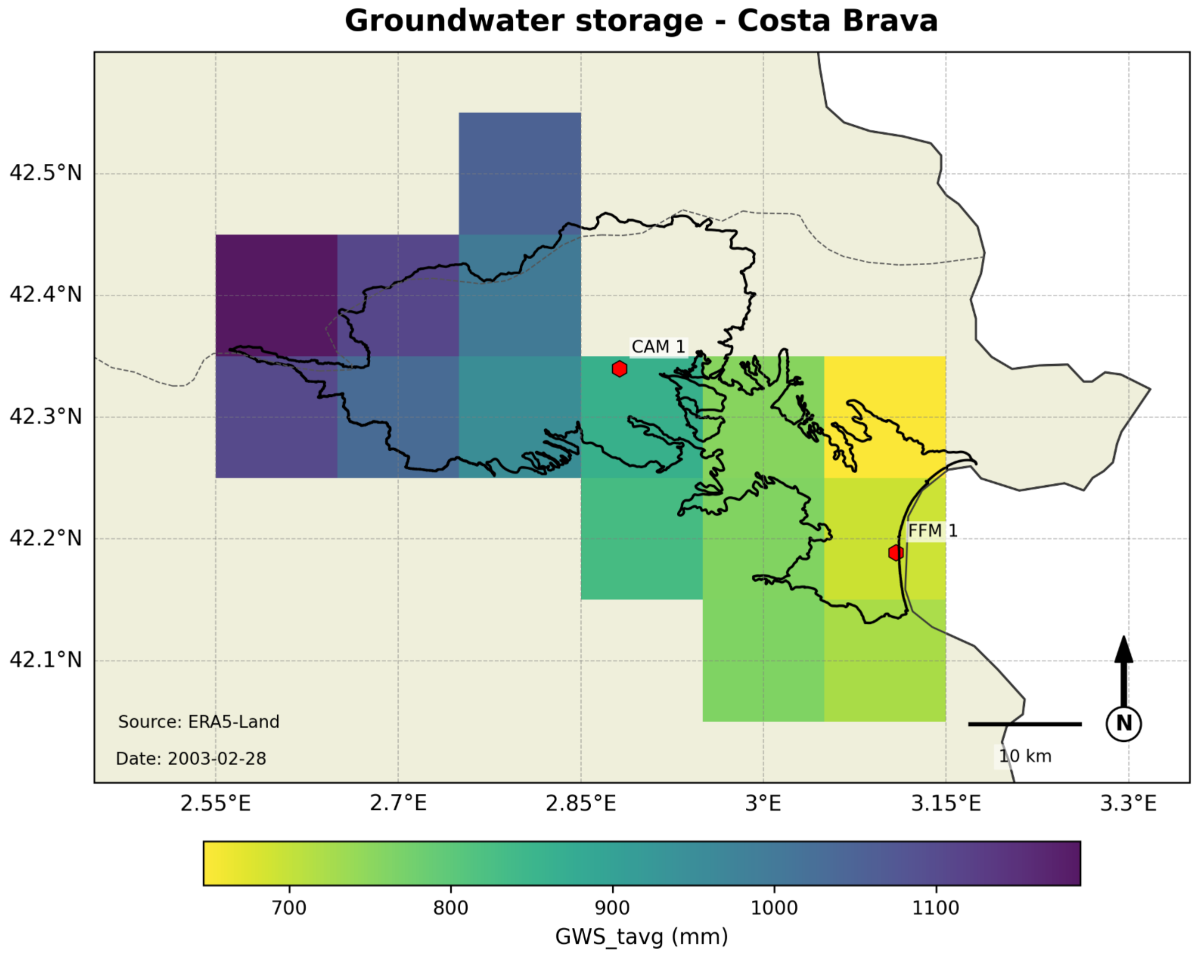

Figure 3 Groundwater storage average (Target variable)

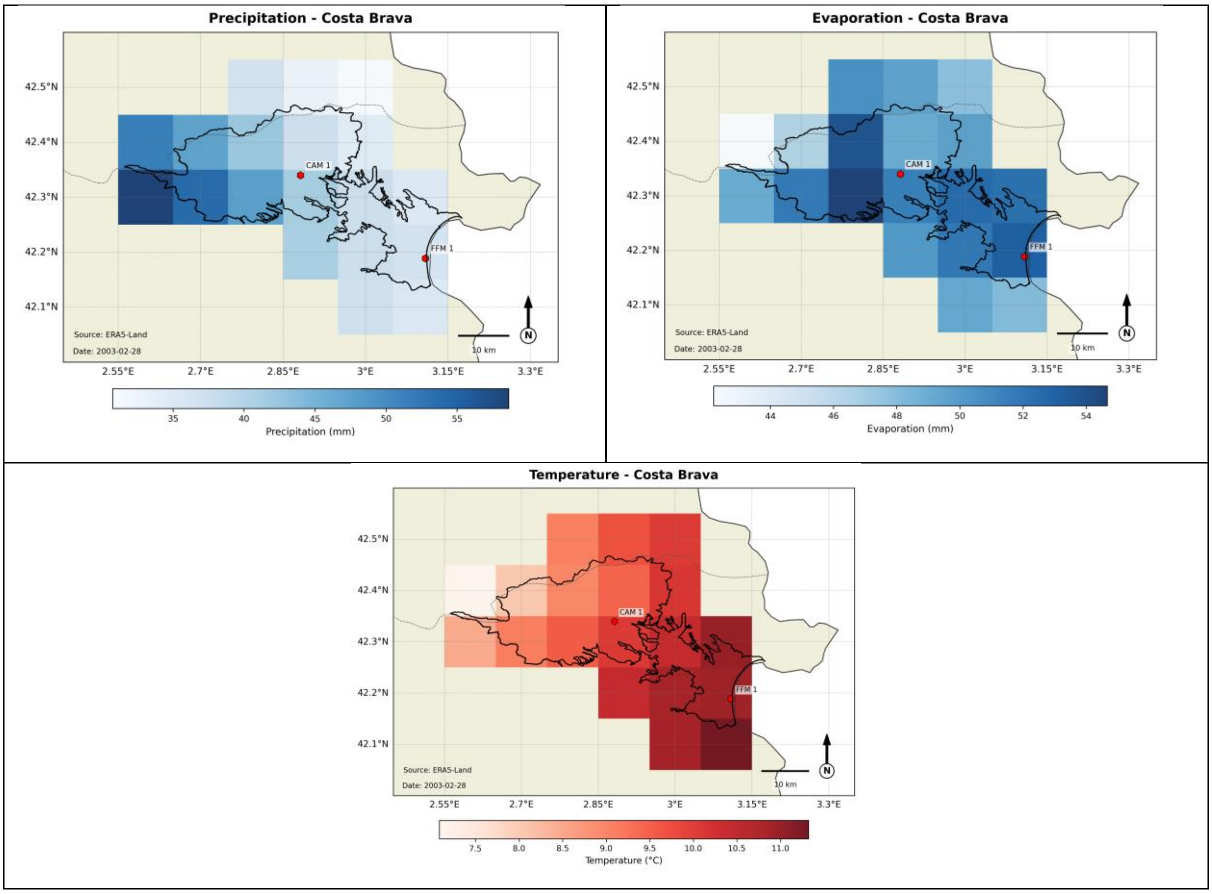

Figure 4 Monthly data of precipitation, Temperature and actual Evapotranspiration

2.2.3 CS2 Kalundborg

The same methodology developed for the Costa Brava case study, with some adaptations, was applied to the Kalundborg case. Specifically, we utilised the same data sources to extract climate variables to train the model, namely ERA5-Land data from the Copernicus Climate Data Store (Muñoz Sabater, 2019). The primary modification lies in the target variable: in this case, groundwater level, which is conceptually aligned with the framework proposed by (Wunsch et al., 2022). Groundwater level data were obtained from the Groundwater Monitoring Network (GGMN) of IGRAC (IGRAC, 2025). The GGMN is a web-based platform that aggregates and disseminates groundwater monitoring data from national institutions worldwide.

Table 5 and Figure 5 present the geographic coordinates of the selected monitoring wells. These locations were selected based on the origin of Kalundborg's water supply, with nearby locations used when direct data were unavailable. For wells KLND02 and KLND03, we enhance model learning by introducing months as an auxiliary variable. The remaining procedures for model evaluation and climate change impact assessment follow the same approach as in the Costa Brava case study.

Figure 5 Map of Kalundborg CS showing the location of the selected wells for model training

Table 5 Coordinates of selected grid cells

ID	Lat	Lon	zone
KLND 01	55.43	11.3	~Gørlev
KLND02(371536)	55.68	11.56	Holbæk
KLND03 (326189)	55.686	11.427	Deigvad

2.2.4 CS3 Syros

Since the GRACE does not cover the Syros case study due to the small size of the Island, and also due to the absence of historical registered piezometric data, the groundwater recharge is estimated based on Thornthwaite-Mather (T-M) procedure (Steenhuis & Van Der Molen, 1986)

- **Thornthwaite-Mather *procedure***

The T-M procedure assumes that the soil has a specific soil-moisture storage capacity, with moisture added or subtracted monthly, depending on whether precipitation is greater or less than evapotranspiration, as long as it remains within the maximum capacity of soil moisture (soil moisture at field capacity) (Steenhuis & Van Der Molen, 1986). The rationale behind this is to estimate the percolation out of the root zone by calculating the water balances for the root zone. Specifically, deep percolation occurs when the amount of stored water exceeds the soil moisture at field capacity. Soil storage is also influenced by numerous factors, including soil texture, evaporation, and precipitation.

To implement T-M procedure, the following assumptions were made:

- The entire aquifer is considered a homogeneous recharge area.
- Land use and human intervention (pumping and irrigation return) are omitted.
- Capillarity rise was not considered.

As illustrated in the flowchart Figure 6, we first initialized the potential water loss and the soil moisture (we assumed that the soil moisture is initially at field capacity ($SM_0 = SM_{FC}$). Then the potential evapotranspiration (ET_o) was calculated using the Thornthwaite methodology (see part of data description). Based on the sign of difference between the precipitation (P) and the potential evapotranspiration, the following logic was followed:

- For months where $ET_o \geq P$, the amount of water stored in the root zone is calculated as:

$$SM_t = SM_{FC} \left(e^{-WL_t / SM_{FC}} \right) \tag{1}$$

Where the WL_t is the accumulated potential water loss due to soil dry out and can be obtained as follows:

$$WL_t = WL_{t-1} + (ET_{o(t)} - P_{(t)}) \tag{2}$$

And the actual evapotranspiration (ET_a) can be calculated as follows:

$$ET_a = P_{(t)} + SM_{t-1} \, (1 - e^{\frac{P(t) - ET_{o(t)}}{SM_{FC}}}) \tag{3}$$

And in this case the deep percolation/ recharge will not occur.

- For months where $ET_o \leq P$, we have two possibilities:
  - If the amount of water stored is less than the soil moisture field capacity, the storage will be incremented by the difference between the potential evapotranspiration and precipitation:

$$SM_t = SM_{t-1} + P_{(t)} - ET_{o(t)} \tag{4}$$

And the accumulated potential water loss can be obtained as:

$$WL_t = -SM_{FC} \ln\left[\left(SM_{t-1} + P_{(t)} - ET_{o(t)} \right) / SM_{FC} \right] \tag{5}$$

  - If on the other hand, the soil storage exceeds the storage at filed capacity, deep percolation will occur (Recharge). In this case the WL_t is set to 0.

$$DP = R = \begin{cases} P_{(t)} - ET_{o(t)} - SM_{FC} + SM_{t-1} & for\ P_{(t)} \geq ET_{o(t)}\ and\ SM_t = SM_{FC} \\ & else\ 0 \end{cases} \tag{6}$$

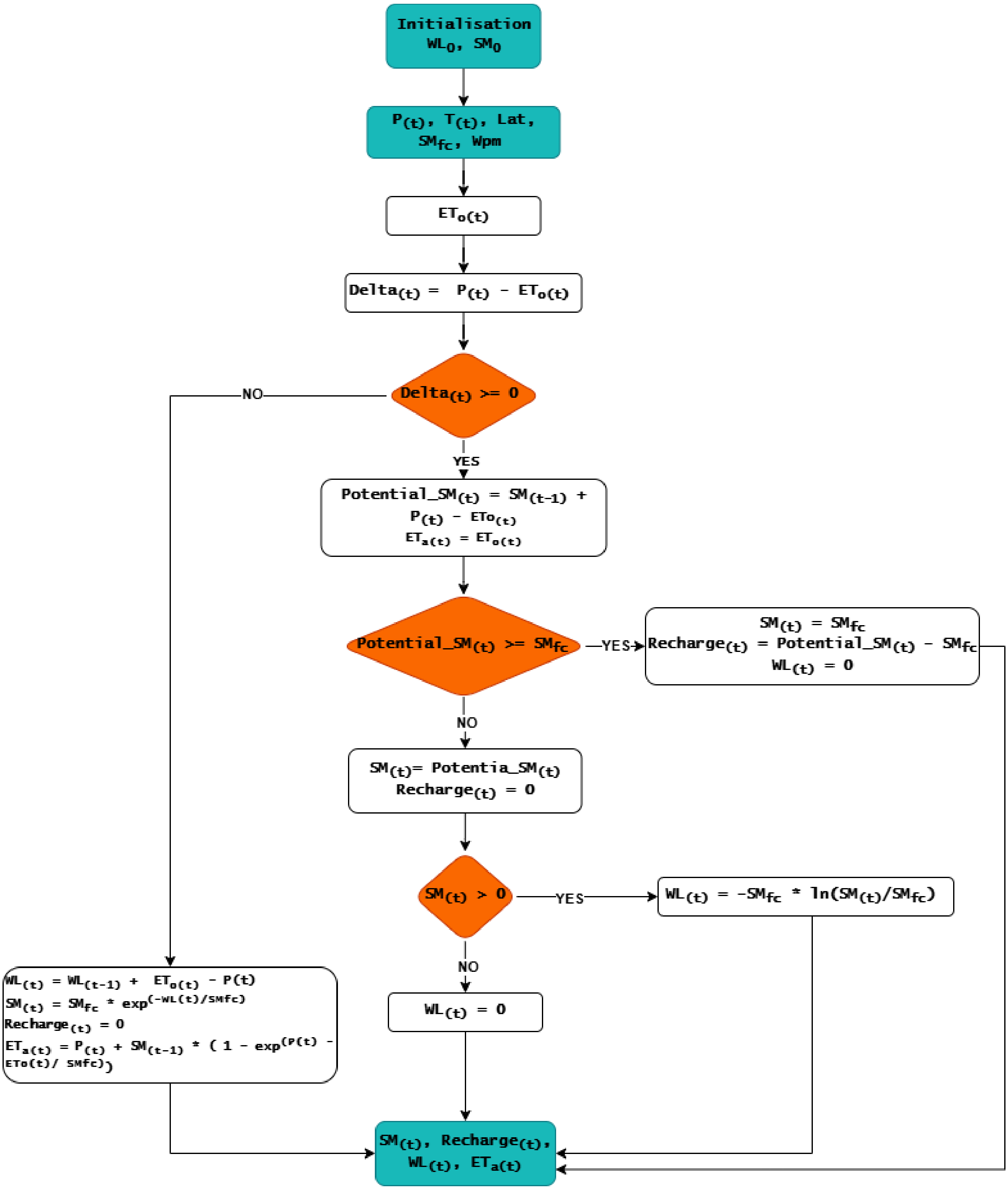

Figure 6 Flowchart of Thornthwaite-Mather procedure

- **Data description**
  - **Soil Hydraulic properties**

The M-T procedure integrates multiple soil hydraulic properties and meteorological variables to estimate the water balance. For this purpose, the soil-moisture storage capacity (SM_{FC}) was first calculated using Eq. (9). This variable depends on rooting depth of vegetation and the hydraulic parameters of the soil, including field capacity and permanent wilting point, which were derived per depth using established equations (eq. (7) and eq. (8)) (Table 6) (Allen et al., 1998). Regarding the rooting depth, Syros's flora is characterized by abundance of the Mediterranean species such as bushes and phrygana. The maximum rooting depth of these shrubs typically ranges from 0.6 to 1.2 meters. Accordingly, an effective rooting depth of approximately 60 cm was assumed for the purposes of this study.

Soil texture data, essential for these calculations, were acquired from OpenLAndMap geospatial dataset (Hengl et al., 2017; Hengl & MacMillan, 2018) (Figure 7). This data set provides global estimates of clay, sand, and organic carbon content (expressed as mass fractions in kg/kg) across six standardized soil depths (0, 10, 30, 60, 100, and 200 cm) at a spatial resolution of 250 meters. These estimates were generated through machine learning models trained on a global compilation of soil profile measurements and field samples.

Table 6 Equation summary for soil hydraulic characteristics

Parameter	Equation	eq	Reference
Water content at field capacity	$\theta_{33} = \theta_{33t} + (1.283 * \theta_{33t}^2 - 0.374 * \theta_{33t} - 0.015)$ $\theta_{33t} = -0.251 * S(\%) + 0.195 * C(\%) + 0.011 * OM(\%) + 0.006(S(\%) * OM(\%)) - 0.027(C(\%) * OM(\%)) + 0.452\,(S(\%) * C(\%)) + 0.299$	(7)	(Saxton & Rawls, 2006)
Water content at wilting point	$\theta_{1500} = \theta_{1500t} + (0.14 * \theta_{1500t} - 0.02)$ $\theta_{1500t} = -0.024\,S(\%) + 0.487\,C(\%) + 0.006\,OM(\%) + 0.005(S(\%) * OM(\%)) - 0.013(C(\%) * OM(\%)) + 0.068\,(S(\%) * C(\%)) + 0.031$	(8)	(Saxton & Rawls, 2006)
Soil-moisture storage capacity	$SM_{FC} = 1000(\theta_{FC} - \theta_{WP})Z_r$	(9)	(Allen et al., 1998)

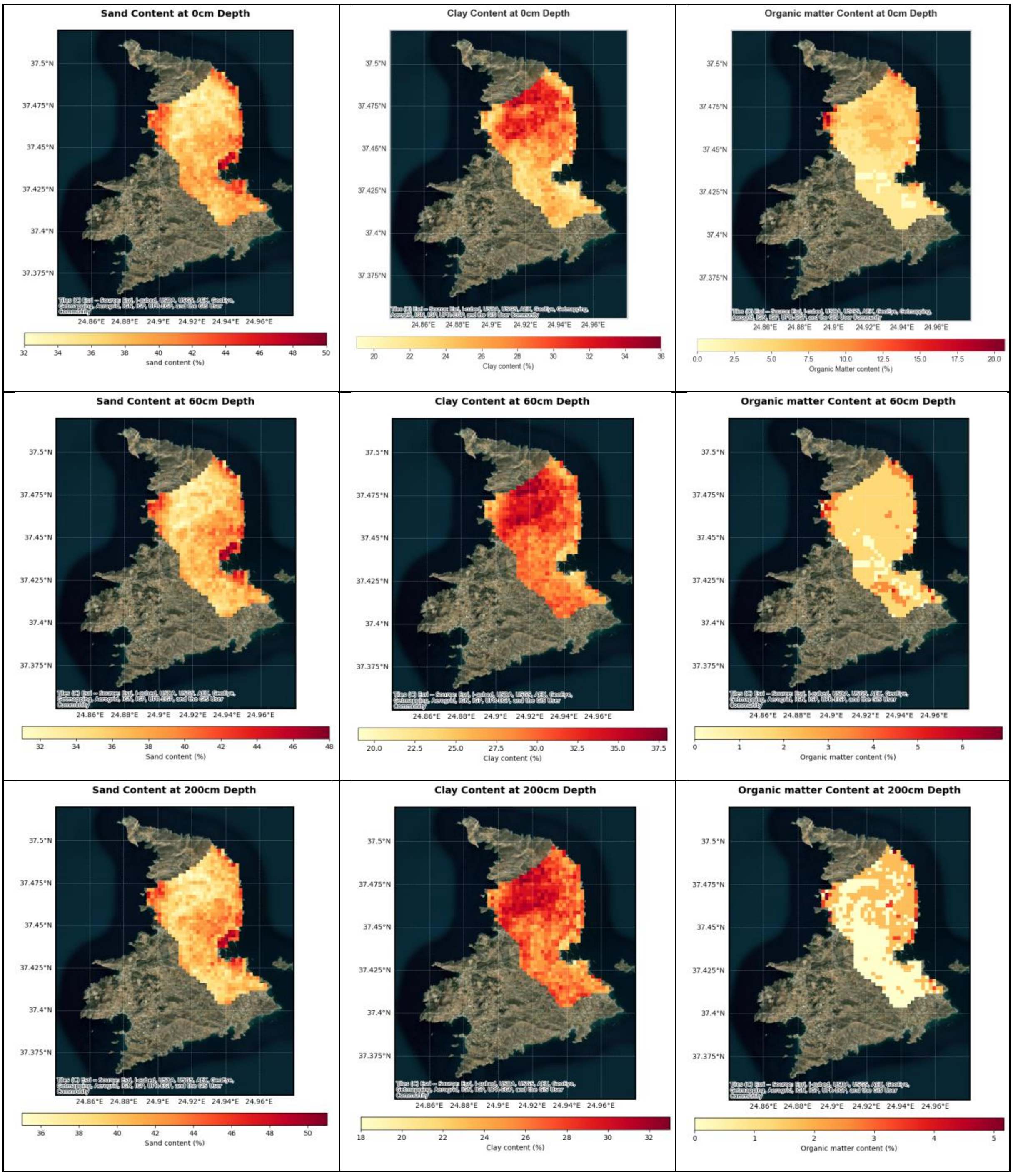

Figure 7 Syros Soil profile characteristics per depth (aquifer of Syros)

- **Precipitation and temperature**

For climate inputs, monthly precipitation and temperature data were sourced from the ERA5-Land reanalysis dataset (Muñoz Sabater, 2019) as described before in Costa Brava case study.

- **Potential Evapotranspiration**

The potential evapotranspiration was estimated using the Thornthwaite method (Thornthwaite, 1948). This method takes as input the mean temperature and the sunshine duration.

First, we calculated the Annual Heat Index, as the sum of the monthly heat indices:

$$I = \sum_{i=1}^{12} \left(\frac{T_i}{5}\right)^{1.514} \tag{10}$$

Then, an unadjusted Potential Evapotranspiration ($ET_{o_{undjusted}}$) is estimated by applying the formula (12). It considers 12 theoretical sunshine hours per day and there are 30 days per month.

$$ET_{o_{(undjusted)}} = 16 \left(10 \frac{T_i}{I}\right)^{\alpha} \tag{11}$$

Where:

$$\alpha = 0.49239 + (I * 1.792 * 10^{-2}) - (I^2 * 7.71 * 10^{-5}) + (I^3 * 6.75 * 10^{-7}) \tag{12}$$

The estimated $ET_{o_{(undjusted)}}$ is after adjusted according to the real theoretical sunshine duration by altitude, and the number of days for each month.

$$ET_o = 16 \left(10 \frac{T_i}{I}\right)^{\alpha} \frac{N}{12} \frac{d}{30} \tag{13}$$

Where N is the theoretical sunshine duration for each month, and d is the number of days in each month.

$$N = \frac{24}{\pi} \omega_s \tag{14}$$

ω_s is the sunset hour angle (in radians):

$$\omega_s = arcos(-\tan\varphi \tan\delta) \tag{15}$$

$$\delta = 23.45 \sin\left(360 \frac{284+n}{365}\right) \tag{16}$$

where φ is the latitude and δ is the declination, n is the ordinal number of the day in solar calendar (Jin et al., 2005).

2.3 Development of Demand Scenarios

The assessment of future water demand in the four case studies followed a multi-step, integrated methodology that combines climate projections, stakeholder engagement, and socio-economic analysis. Key factors considered include population forecasts (where available), competing sectoral demands, projected growth in industry and tourism, water availability, and water quality constraints.

To draw a robust baseline, a comprehensive dataset was compiled for each Case Study to establish current conditions and inform scenario development. This included:

- Current water usage by sector (residential, industrial, agricultural, and tourism)
- Population size and growth trends
- Main economic drivers (e.g., industry, agriculture, tourism)
- Existing water infrastructure

- Circular economy initiatives, including water reuse programs (existing or planned)

Scenarios were developed using the Shared Socioeconomic Pathways (SSPs), which describe plausible global futures based on varying trends in demographics, economic development, technology, and environmental policy. The chosen pathways were:

- SSP1 – Sustainability-focused growth
- SSP2 – Middle-of-the-road development
- SSP5 – Fossil-fuelled development with high economic and resource growth

These pathways were contextualised to reflect local dynamics in each case study region.

Water demand was projected for each major sector using tailored assumptions and parameters:

- Residential/Municipal Demand: Based on projected population growth or decline, water efficiency improvements (e.g., low-flow appliances, greywater reuse), and behavioural shifts such as increased urban density and changes in per capita use.
- Industrial Demand: Informed by the expected expansion of key sectors, technological advancements in water use and treatment, integration of circular economy principles, and process-specific water requirements.
- Agricultural Demand: Modelled considering climate-driven changes in evapotranspiration, shifts in crop types, irrigation intensity, and the uptake of precision agriculture and water-saving practices.
- Tourism Demand: Accounted for seasonal variability, infrastructure development (e.g., accommodation, recreational facilities), and climate-related changes in visitor numbers.

This methodological framework ensures that each scenario is both locally grounded and comparably aligned, providing a robust foundation for long-term planning and policy development across various European regions.

3. Results

3.1 Climate Projections

3.1.1 Temperature

Temperature is a key driver of the hydrological cycle and the broader climate system. Changes in air temperature influence numerous processes such as evaporation, snowmelt, plant phenology, energy demand, water demand, and the frequency and intensity of extreme weather events including droughts, heatwaves, and storms. In the context of the RECREATE project, understanding projected temperature change is critical for shaping future adaptation strategies across the four European case studies. Each case study is analysed through ensemble mean projections from seven GCM–RCM combinations, with shaded areas representing the standard deviation of the ensemble, indicating the range of model uncertainty. The time series extends from 1971 to 2100, covering a historical baseline and three RCP scenarios: RCP 2.6 (low emissions), RCP 4.5 (intermediate emissions), and RCP 8.5 (high emissions). The seasonal and annual plots provide a holistic view of long-term trends. As a further note, it shall be repeated that the reported temperatures are mean temperatures (i.e., not daily peak temperatures).

Table 7 Projected Temperature Increase Relative to 1981–2000

Case Study	Scenario	2026–2045	2046–2065	2066–2085
North Holland	RCP 2.6	+1.0°C	+1.4°C	+1.6°C
North Holland	RCP 4.5	+1.3°C	+2.1°C	+2.8°C
North Holland	RCP 8.5	+1.7°C	+3.3°C	+4.8°C
Kalundborg	RCP 2.6	+0.8°C	+1.2°C	+1.3°C
Kalundborg	RCP 4.5	+1.1°C	+1.9°C	+2.5°C
Kalundborg	RCP 8.5	+1.5°C	+3.0°C	+4.5°C
Syros	RCP 2.6	+1.2°C	+1.8°C	+2.2°C
Syros	RCP 4.5	+1.8°C	+3.1°C	+4.0°C
Syros	RCP 8.5	+2.5°C	+4.3°C	+5.7°C
Costa Brava	RCP 2.6	+1.1°C	+1.6°C	+2.0°C
Costa Brava	RCP 4.5	+1.6°C	+2.6°C	+3.5°C
Costa Brava	RCP 8.5	+2.3°C	+4.0°C	+5.3°C

North Holland shows annual means rising toward 14°C under RCP 8.5 (*Figure 8*). Seasonal changes are the strongest in summer. The projections suggest that summer temperatures could rise from approximately 17°C to over 21°C under high-emission scenarios, substantially raising the risk of heatwaves in this densely populated and highly urbanized delta region. Winters could become milder by as much as 3.5°C, reducing heating energy demand while also raising the likelihood of rainfall instead of snow, potentially altering seasonal hydrology. Spring and autumn also see steady warming, which might extend growth seasons and groundwater recharge timing. Overall, seasonal warming is most accentuated in summer, reflecting broader European patterns, but with compound risks in flat, low-lying areas sensitive to sea-level and storm surge influences.

Kalundborg exhibits a warming trend across all RCPs, rising from approximately 8.5°C historically to over 12.5°C under RCP 8.5 (*Figure 9*). Seasonal warming is most pronounced in summer (~4°C by 2100 under RCP 8.5). The seasonal disaggregation indicates that the summer season in Kalundborg is anticipated to warm by more than 3.5°C under RCP 8.5, in comparison to the historical baseline. Winters warm at a slower rate (~2.5°C), but still significantly affect heating demand and ecosystem cycles. Spring and autumn experience a steady increase of ~2–3°C, which may influence crop growth phases and alter growing seasons. The annual cycle remains relatively stable, yet temperature extremes in summer could become more frequent and severe, impacting freshwater availability and industrial cooling needs in this region known for its energy-intensive industrial symbiosis model.

Syros, with the warmest baseline, could reach 23°C annually by 2100 under RCP 8.5 (*Figure 10*). Summer increases may approach 30°C, posing serious challenges for water supply and heat resilience. Seasonal warming is highly uneven, with summers rising by up to 5–6°C, amplifying existing water stress and tourism-related pressures. Spring and autumn are also subject to 3–4°C increases, which may shift phenological cycles and exacerbate wildfire risks. Winters, traditionally mild, are projected to increase modestly by 2.5–3°C, further reducing precipitation in solid form and lowering freshwater recharge. This Mediterranean case study exhibits the most extreme seasonal warming and is emblematic of climate vulnerability in semi-arid regions. The projections suggest adaptation measures must address both extreme summer conditions and longer transitional dry periods in spring and autumn.

Costa Brava experiences intermediate warming, with annual means increasing from approximately 12.5°C to over 17.5°C under RCP 8.5 (*Figure 11*). Significant seasonal warming occurs in summer, particularly inland. The inland zone feeding the Darnius-Boadella Reservoir shows summer warming of about 5°C under RCP 8.5, while the coastal zone warms by approximately 4°C, narrowing the temperature gradient that traditionally supports microclimatic diversity. Winter warming ranges from 2.5 to 3°C, likely diminishing snowmelt contributions. Autumn and spring follow similar warming trajectories, yet their implications differ: spring warming may extend the growing season, while autumn warmth could postpone dormancy and impact vine and fruit maturation. This dual-natured case study (coastal vs inland) exemplifies how seasonal warming will affect both supply (reservoir recharge) and demand (tourism, agriculture), necessitating geographically differentiated adaptation strategies.

The ensemble-based projections reveal a clear, seasonally differentiated warming trend across all RECREATE case studies. Summer emerges as the most sensitive season, particularly under RCP 8.5. The findings underscore the necessity to design climate-resilient water management strategies that incorporate seasonal dynamics, model uncertainty, and socio-economic pathways. Achieving the Paris Agreement goals remains a critical threshold to avert the most disruptive impacts, especially in the Mediterranean regions. The implications extend beyond temperature itself, as warming induces changes in evaporation, drought frequency, and hydrological regimes.

Figure 8: Annual and seasonal temperature for North Holland

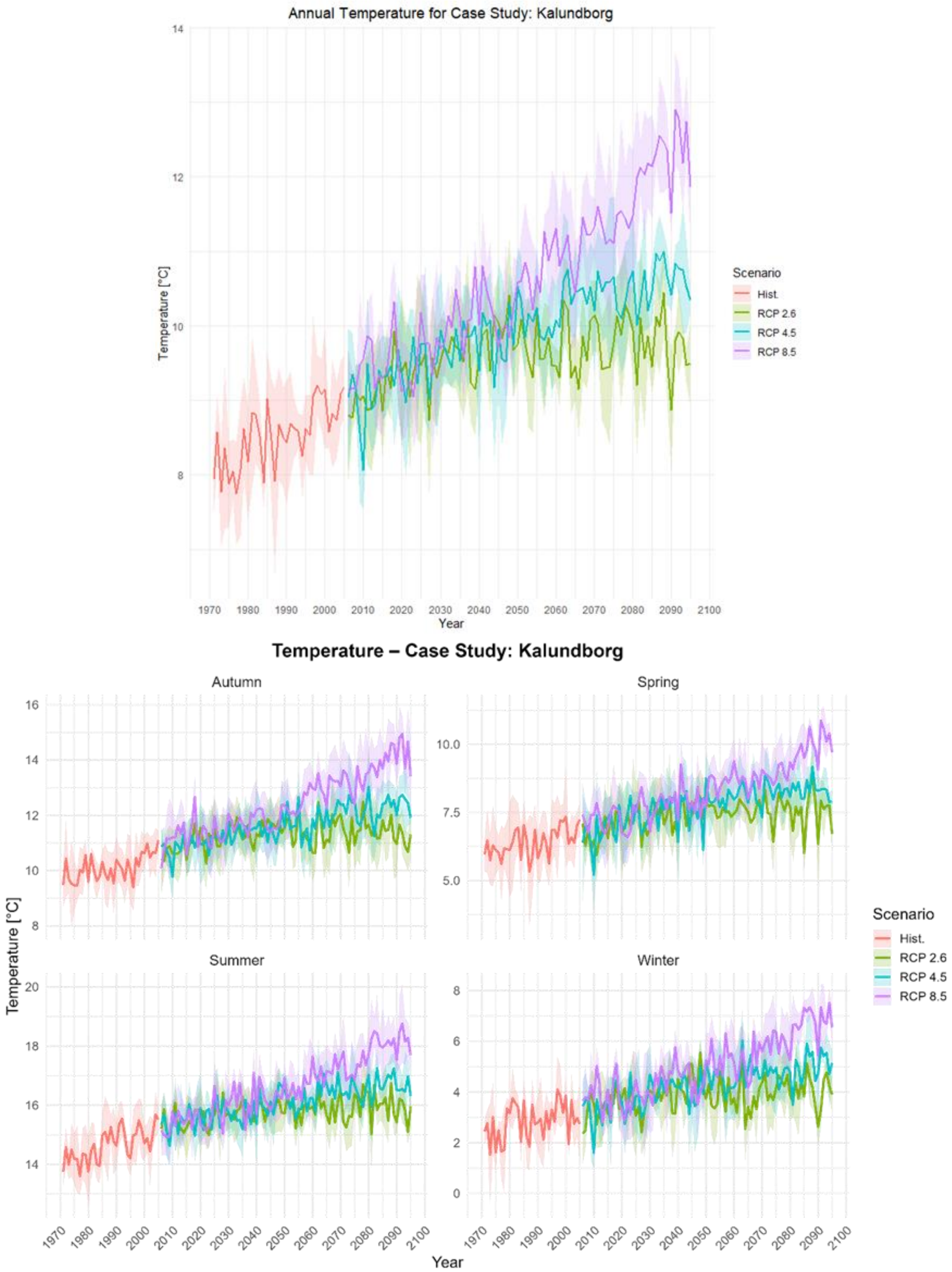

Figure 9: Annual and seasonal temperature for Kalundborg

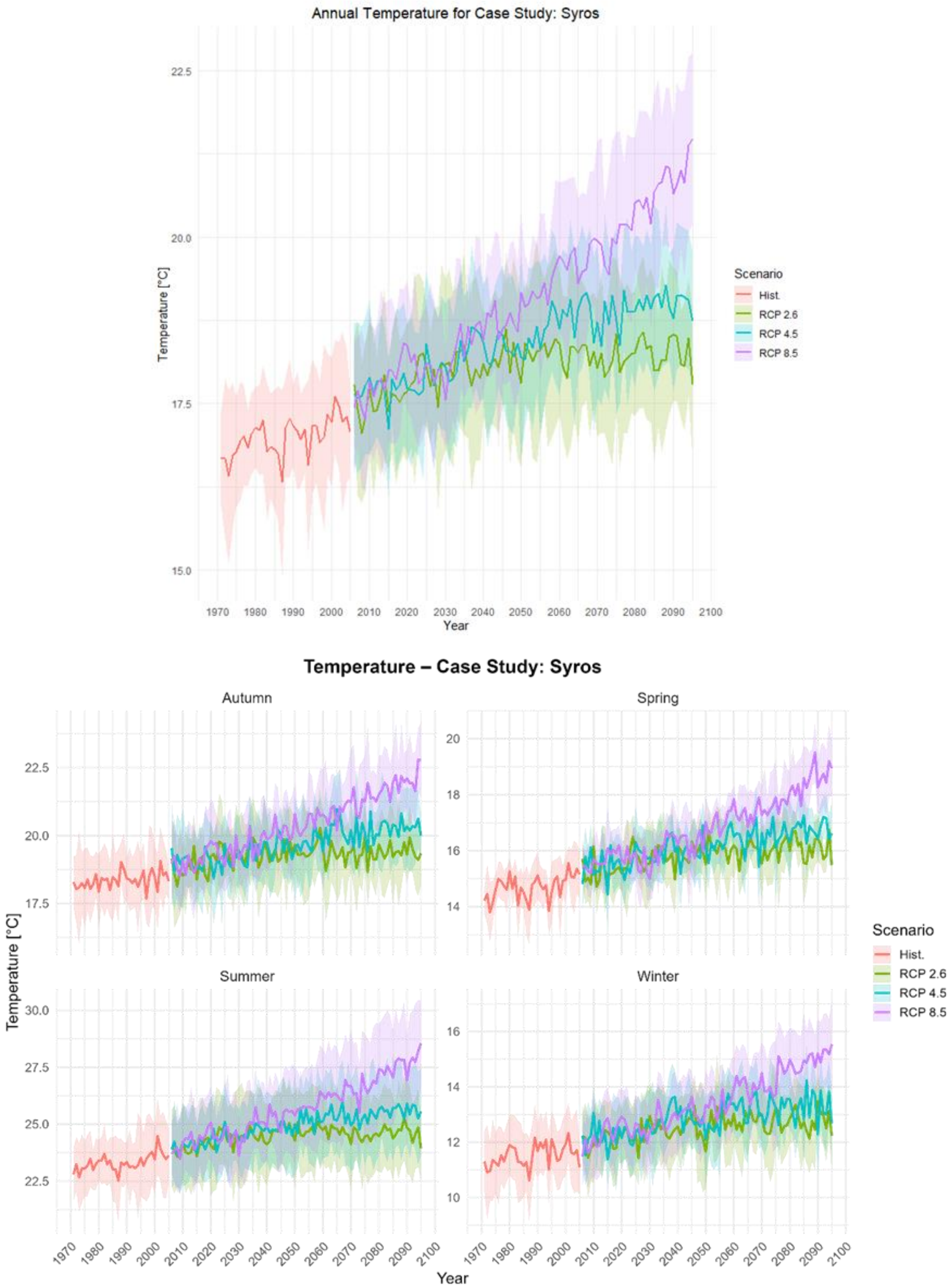

Figure 10: Annual and seasonal temperature for Syros

Figure 11. Annual and seasonal temperature for Costa Brava

Temperature Extremes and Heat Spells

The climate data used in this report originates from the Copernicus Climate Data Store and is based on *daily average temperatures*, rather than daily maximums. While this distinction is significant, average daily temperatures serve as a reliable indicator of heat-related stress. For instance, a mean daily temperature of 30°C often corresponds to peak daytime temperatures of 35°C or higher—thresholds defined by the World Health Organization (WHO) and national meteorological services to identify hazardous heat events. This correlation has been substantiated in climatological analyses throughout Europe (Casanueva et al., 2019).

Furthermore, such conditions are typically associated with so-called tropical nights—nights that do not drop below 25°C—posing an additional public health hazard by disrupting sleep and exacerbating cardiovascular and respiratory risks (Gasparrini et al., 2015).

Projected climate scenarios suggest a significant rise in the number of days with mean temperatures surpassing 30°C in both Syros and Costa Brava. These exceedances are most noticeable in summer and under the high-emissions RCP 8.5 scenario.

In Syros (CS3), summer days above 30°C increase from fewer than 2 historically to nearly 12 by 2085 under RCP 8.5. Inland Costa Brava follows a similar pattern, increasing from near-zero to approximately 11 days. Coastal Costa Brava exhibits a more moderated but significant rise, reaching around 9 days by century's end.

The probability of experiencing at least one summer heat spell—defined here as periods with multiple consecutive days exceeding a mean temperature of 30°C—is also set to increase dramatically. In Syros and Costa Brava (both inland and coastal), this probability reaches 30–50% by mid-century and rises to over 60% by 2085 under RCP 8.5. These projections represent a conservative estimate of days when peak temperatures could exceed 35°C, aligning with WHO thresholds for heat-health alert systems (World Health Organisation, 2009).

These changes also suggest an increasing frequency of tropical nights, particularly in urbanised or low-ventilation areas. From a health policy perspective, this supports the enhancement of early warning systems, social vulnerability mapping, and integration with urban cooling strategies as encouraged by the EU Climate Adaptation Strategy and national heat-health action plans (European Environmental Agency, 2024).

Table 8 Summary of Temperature Extremes (Mean Temp >30°C) in Mediterranean Case Studies

Case Study	**Δ Days >30°C (Hist. → 2085)**	**Prob. ≥1 Heat Spell (2085, RCP 8.5)**	**Notable Features**
Syros	<2 → ~12	>60%	Strongest increase; tropical nights likely
Costa Brava Inland	~0 → ~11	~55%	Pronounced inland warming
Costa Brava Coast	~0 → ~9	~45%	Moderated by maritime influence

Table 9 Summary of Emerging Temperature Extremes (>25°C) in Northern Case Studies

Case Study	**Δ Days >25°C (Hist. → 2085)**	**Prob. ≥1 Heat Spell (2085, RCP 8.5)**	**Notable Features**
North Holland	~0.5 → ~2.6	~25%	Emerging spells; urban vulnerability rising
Kalundborg	~0 → ~1.1	~10%	First signs of future heat exposure

Although extreme heat remains relatively rare in the Kalundborg and North Holland case studies, a clear upward trend emerges for days exceeding a mean temperature of 25 °c—a lower, yet still health-relevant, threshold in cooler climates.

In North Holland, such days increase from under 1 to more than 2.5 days by the end of the century under RCP 8.5. Kalundborg experiences a rise from virtually zero to over 1 day in the same timeframe.

While these values do not fulfil standard heat spell definitions (typically >3 consecutive days), they do indicate the emergence of heat spells in some models. Given that our data represents ensemble means across seven models, this means that in some realisations, heat spells do occur even if the average duration across models remains low. Hence, to simplify interpretation, we emphasise probability rather than average duration.

Indeed, under RCP 8.5, the likelihood of experiencing at least one heat spell each summer (defined here as one or more consecutive days with a mean temperature exceeding 25 °C) increases to 20–25% in North Holland and up to 10% in Kalundborg. Although these values may seem low, they signify a structural shift in the baseline climate, one that brings new public health implications for populations previously unaccustomed to heat risk.

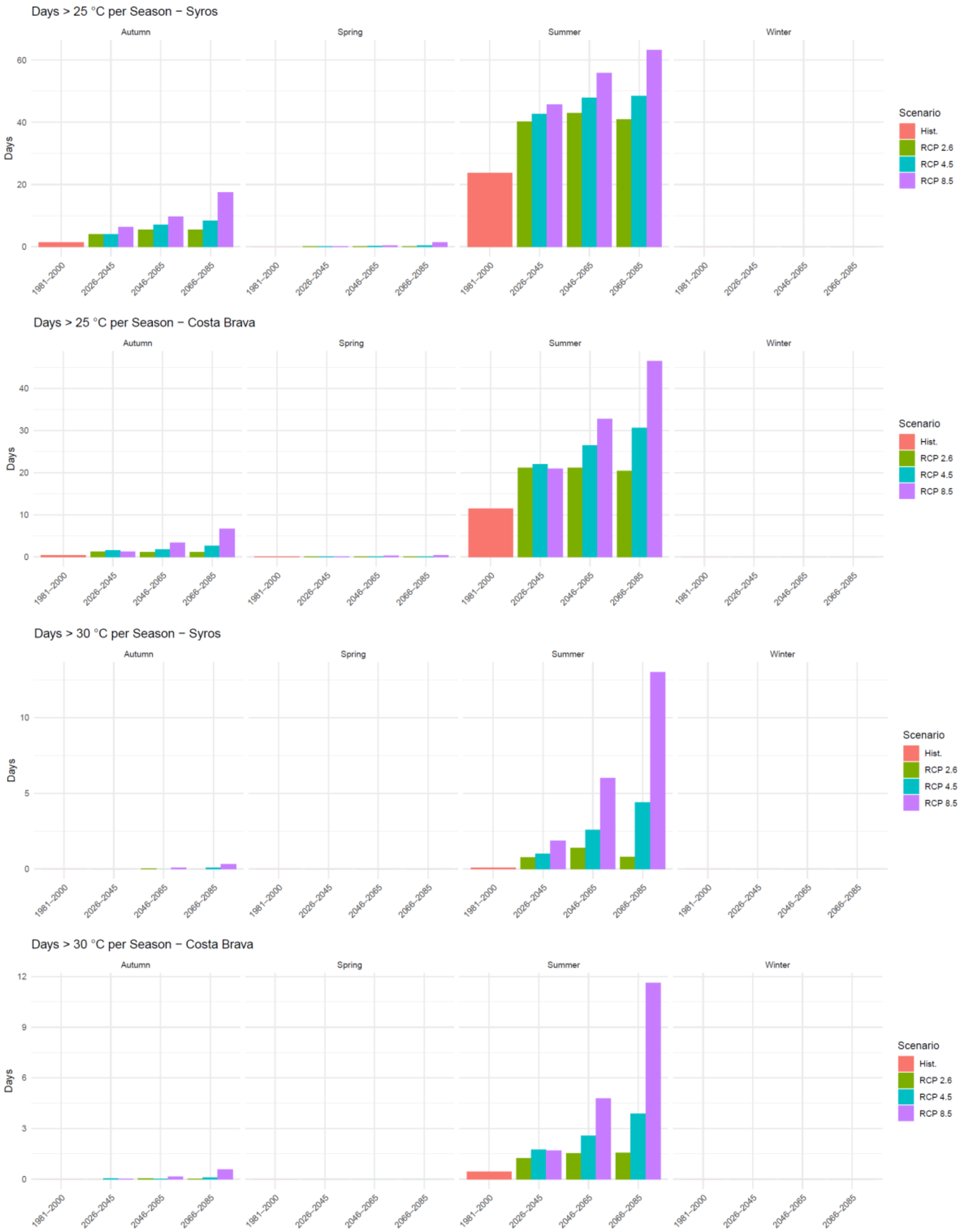

Figure 12. Expected hot days per season for the Mediterranean case studies.

3.1.2 Precipitation

Seasonal definitions in this analysis follow meteorological conventions: Winter (December–February), Spring (March–May), Summer (June–August), and Autumn (September–November).

The following table summarizes the percent change in mean seasonal precipitation for each case study compared to the historical reference period (1981–2000), based on ensemble averages across the selected GCM-RCM models. Only spring and summer are highlighted due to their critical relevance for agriculture, ecosystem activity, and water supply planning. The results reflect the mid-term projection period (2026–2045) under three RCP scenarios.

Table 10 Changes to precipitation in the reference period used (1981-2000) for spring and summer

Case Study	Season	Scenario	Period	% Change from Reference
North Holland	Spring	RCP 2.6	2026–2045	6.7
North Holland	Spring	RCP 4.5	2026–2045	8.4
North Holland	Spring	RCP 8.5	2026–2045	9.6
North Holland	Summer	RCP 2.6	2026–2045	3.5
North Holland	Summer	RCP 4.5	2026–2045	4.1
North Holland	Summer	RCP 8.5	2026–2045	5.0
Kalundborg	Spring	RCP 2.6	2026–2045	4.2
Kalundborg	Spring	RCP 4.5	2026–2045	5.8
Kalundborg	Spring	RCP 8.5	2026–2045	7.1
Kalundborg	Summer	RCP 2.6	2026–2045	1.5
Kalundborg	Summer	RCP 4.5	2026–2045	0.9
Kalundborg	Summer	RCP 8.5	2026–2045	-2.3
Syros	Spring	RCP 2.6	2026–2045	-3.2
Syros	Spring	RCP 4.5	2026–2045	-5.1
Syros	Spring	RCP 8.5	2026–2045	-6.8
Syros	Summer	RCP 2.6	2026–2045	-10.5
Syros	Summer	RCP 4.5	2026–2045	-12.3
Syros	Summer	RCP 8.5	2026–2045	-14.9
Costa Brava	Spring	RCP 2.6	2026–2045	1.8
Costa Brava	Spring	RCP 4.5	2026–2045	0.5
Costa Brava	Spring	RCP 8.5	2026–2045	-2.4
Costa Brava	Summer	RCP 2.6	2026–2045	-5.1
Costa Brava	Summer	RCP 4.5	2026–2045	-6.8
Costa Brava	Summer	RCP 8.5	2026–2045	-8.2

North Holland exhibits relatively strong increases in spring precipitation, ranging from +6.7% (RCP 2.6) to +9.6% (RCP 8.5). This growth is significant in a region where spring precipitation supports both groundwater recharge (especially relevant for the coastal dunes used for drinking water supply) and early-season crop development, particularly for floriculture and horticulture. If such trends materialise, the region could benefit from reduced irrigation pressure in spring.

Summer precipitation changes are also positive, ranging from +3.5% to +5.0% across the RCP spectrum. These changes are significant given North Holland's vulnerability to water quality degradation in summer due to risks of eutrophication and saline intrusion. A wetter summer may alleviate these pressures to some extent, although this depends on the intensity and distribution of rainfall events. Overall, North Holland's projections suggest a moderately advantageous shift in precipitation during key growth periods, albeit with uncertainties about the frequency of extreme events including the occurrence of summer droughts, which may put challenges to agriculture. It should also be noted that while precipitation trends may be positive, this positive trend may be at least partially cancelled by increased evapotranspiration.

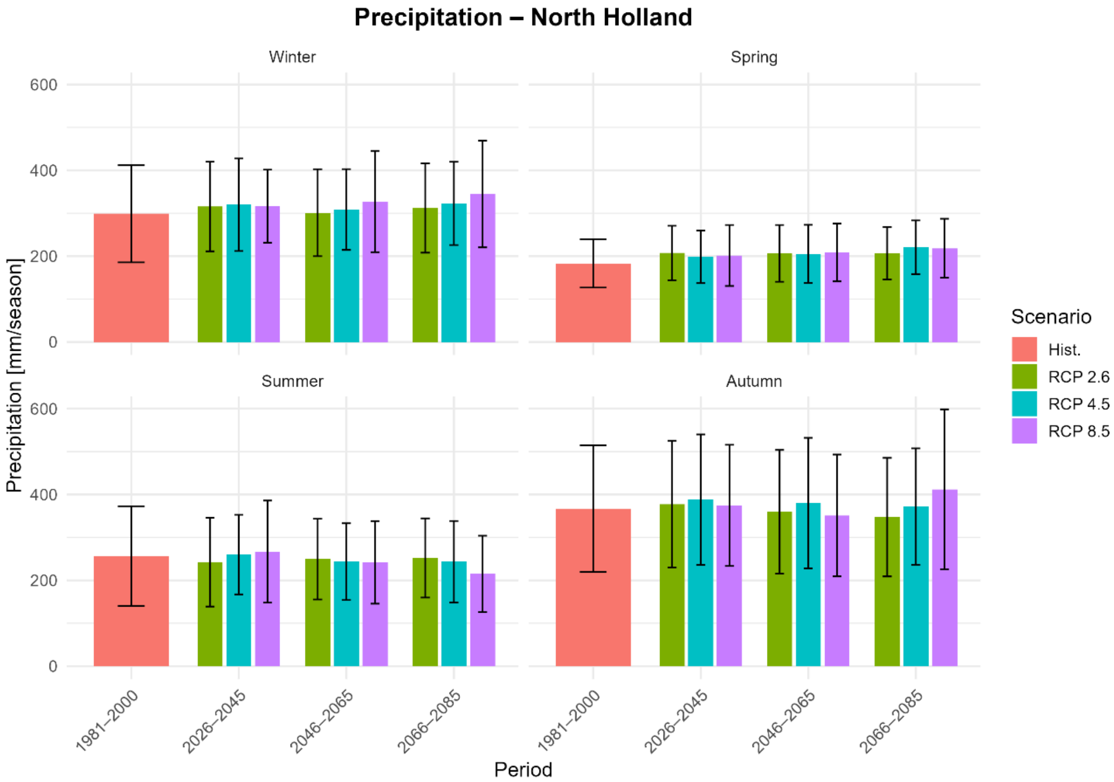

Figure 13. Seasonal precipitation trends for North Holland

In Kalundborg, projected changes in precipitation during spring and summer remain moderate across all RCP scenarios. For spring, the projected increases range from +4.2% under RCP 2.6 to +7.1% under RCP 8.5 for the mid-term future (2026–2045). This consistent upward trend suggests potential for improved soil moisture recharge and reduced water stress for spring crops. However, the modest magnitude of change indicates that existing agricultural practices may largely remain viable, although variability between years may increase.

Summer projections are more uncertain, exhibiting a weak signal for change. Slight increases under RCP 2.6 (+1.5%) and RCP 4.5 (+0.9%) contrast with a minor decrease under RCP 8.5 (-2.3%). This variability highlights that while summer rainfall may not drastically diminish, inter-annual differences could stress irrigation-dependent sectors. In the context of Kalundborg's industrial water use and thermoelectric cooling, even small reductions in summer precipitation could impact water balance planning.

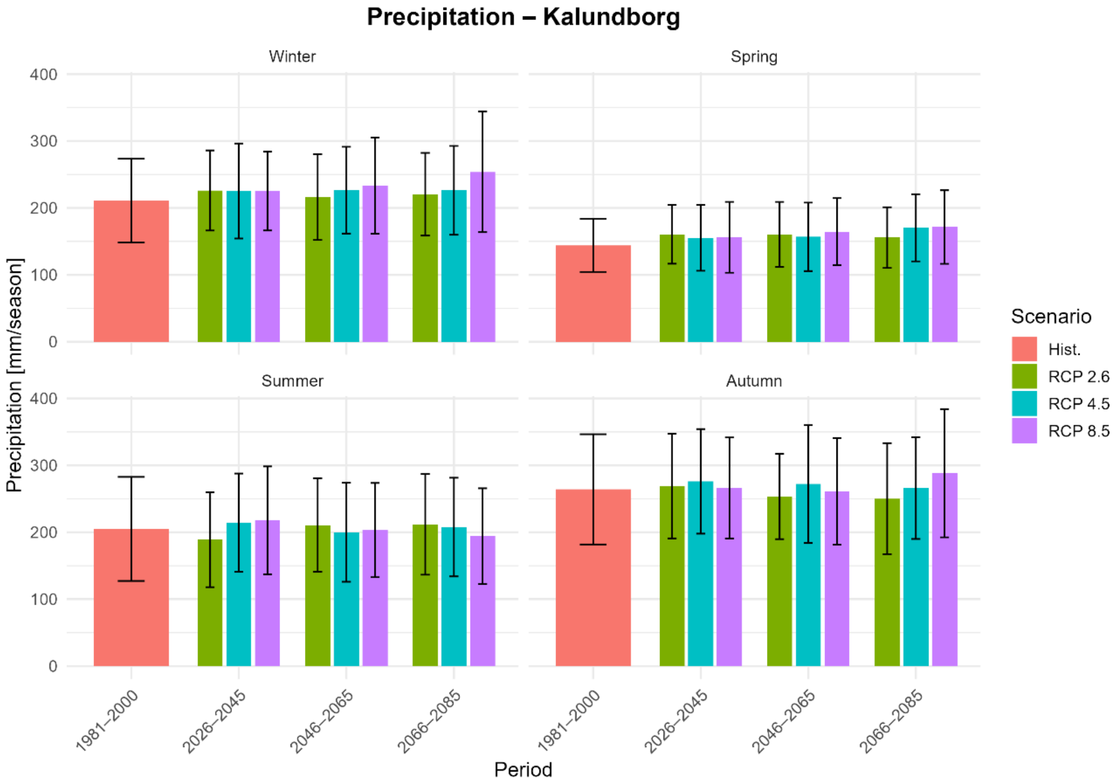

Figure 14. Seasonal precipitation trends for Kalundborg

Syros, situated in the semi-arid Cyclades, faces a significantly different trajectory. Projections indicate a continued decrease in precipitation during both spring and summer. Spring precipitation is expected to decline by −3.2% (RCP 2.6) to −6.8% (RCP 8.5), which could exacerbate already arid conditions and strain agricultural and ecological systems.

The decline is even more pronounced in summer, ranging from −10.5% to −14.9%. These results reinforce concerns that Syros will experience increasing seasonal dryness, which may challenge even drought-tolerant crops and stress groundwater resources used for both agriculture and tourism. Reduced summer precipitation, combined with rising temperatures, would likely increase evapotranspiration and exacerbate desertification risks. Strategic shifts towards water-efficient cropping systems and rainwater harvesting could be crucial in this context.

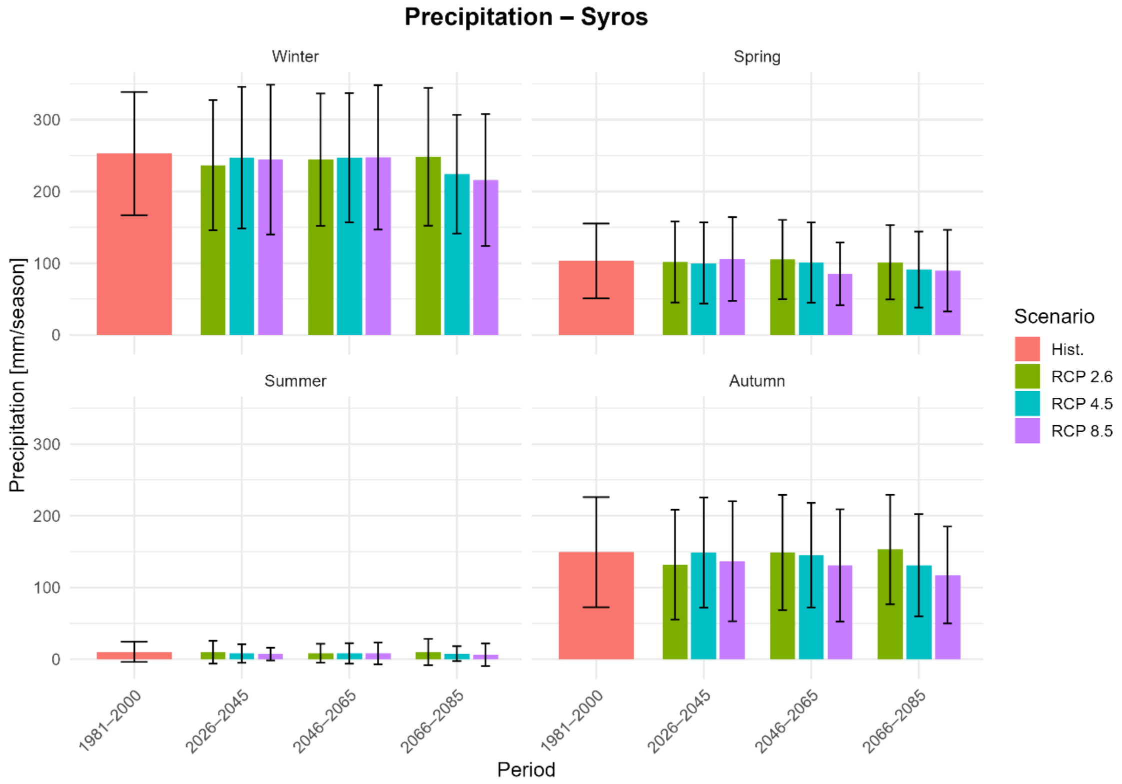

Figure 15. Seasonal precipitation trends for Syros

Costa Brava presents a mixed picture. In spring, changes are modest and near zero. A small increase is projected under RCP 2.6 (+1.8%), stagnation under RCP 4.5 (+0.5%), and a minor decrease under RCP 8.5 (−2.4%). While these values are not drastic, they suggest that spring rainfall will not change significantly, implying that any future agricultural planning will need to account for existing variability rather than rely on substantial seasonal wetting.

In contrast, summer precipitation is projected to decline more clearly. Reductions of −5.1%, −6.8%, and −8.2% are anticipated for RCP 2.6, RCP 4.5, and RCP 8.5, respectively. This reinforces the broader Mediterranean trend of increasing summer aridity, which has implications for crops such as grapes, olives, and stone fruits. These reductions could heighten irrigation demand at a time when water availability from reservoirs may be limited due to lower inflows and increased evaporation.

The Costa Brava case study also includes a comparison between inland and coastal sub-regions. While the general trends in precipitation are similar, the inland areas (feeding the Boadella Reservoir) typically exhibit slightly lower baseline summer precipitation but comparable percentage declines. The coastal areas, while benefiting from slightly higher mean precipitation, show equally sharp declines, suggesting that both regions will face significant water management challenges. The loss of the coastal-inland gradient, driven by uniform drying trends, implies a reduced microclimatic buffering capacity.

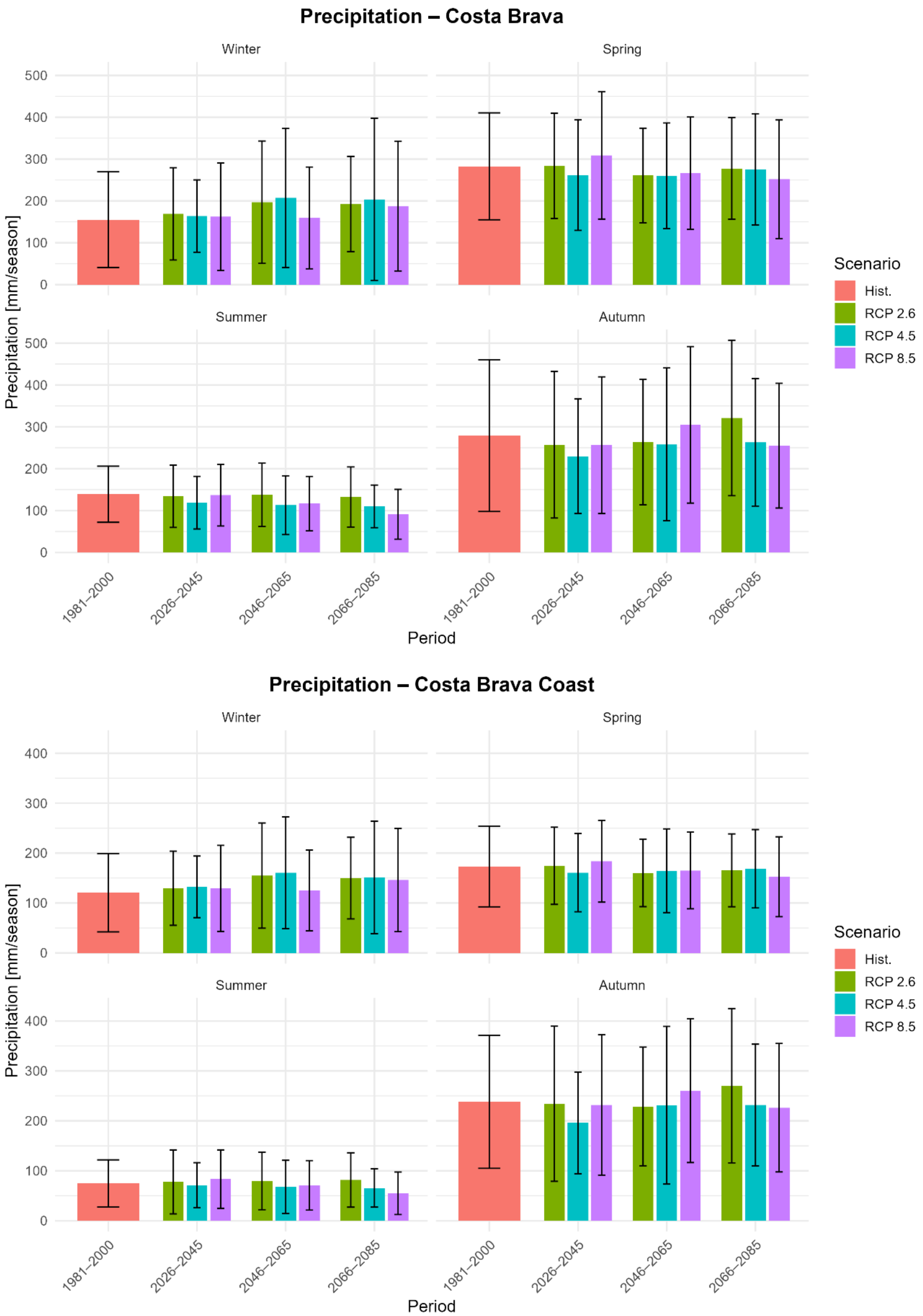

Figure 16. Seasonal precipitation trends for Costa Brava (inland) and Costa Brava Coast

Precipitation Extremes

This analysis is based on daily precipitation data from the Copernicus Climate Data Store, derived from seven combinations of global and regional climate models (GCM-RCM ensembles). Here, we focus on daily rainfall events exceeding 25 mm, a threshold commonly used by national meteorological agencies to flag intense but not exceptional precipitation. Although this value is lower than the categories of “torrential” rainfall (e.g. >50 mm or >100 mm), it serves as a robust indicator of disruptive events such as urban flooding, local erosion, or pressure on drainage systems—especially when aggregated seasonally.

The use of 25 mm/day as a threshold also aligns better with the capabilities of the models employed. Higher thresholds (e.g. >100 mm/day) remain extremely rare in the simulations, which is consistent with the known limitation of RCMs to represent convective, short-duration rainfall bursts due to their coarse spatial resolution (typically 10–50 km) and smoothed temporal aggregation. Studies such as (Prein et al., 2015) and (Fowler et al., 2021) emphasised that genuinely extreme sub-daily events necessitate convection-permitting models, which were not employed here.

Across the case studies, Costa Brava and Syros demonstrate the most consistent increase in both the number and seasonal probability of events exceeding 25 mm/day. In Costa Brava, the average number of rainfall days per month exceeding 25 mm rises significantly in autumn, reaching 1.3 days/month by 2085 under RCP 8.5, compared to 0.6 days historically. The probability of experiencing at least one such event per season increases from approximately 40–50% to over 75% under the same scenario.

Syros, while drier overall, also exhibits a distinct upward trend. In autumn, the likelihood of experiencing at least one event exceeding 25 mm per day rises from historically under 40% to nearly 70% by the century's end under RCP 8.5. Spring likewise demonstrates subtle improvements, indicating that future precipitation in the Aegean may become more intense, even if total rainfall declines.

For North Holland and Kalundborg, the >25 mm/day threshold captures emerging patterns of extreme precipitation that are not apparent at higher thresholds. In North Holland, for example, autumn probabilities for >25 mm events rise from approximately 50% historically to over 90% under RCP 8.5 by the end of the century. In Kalundborg, summer and autumn probabilities increase to 30–40% during the same period, marking a clear departure from the historical baseline.

These developments align with IPCC assessments that northern and central Europe will experience an increase in the frequency and severity of heavy rainfall, even in areas traditionally characterised by moderate, steady precipitation (IPCC, 2021).

The increase in frequency and probability of intense rainfall events exceeding 25 mm/day—particularly in autumn for Mediterranean areas and increasingly in summer-autumn for northern regions—has direct implications for infrastructure resilience. Urban drainage systems, soil erosion controls, and flood early-warning systems ought to be revised to accommodate more intense bursts within shorter time frames. These findings support calls from the EU’s Adaptation Strategy and the European Environment Agency to strengthen local-scale risk mitigation efforts (European Commission, 2021) (European Environment Agency, 2020).

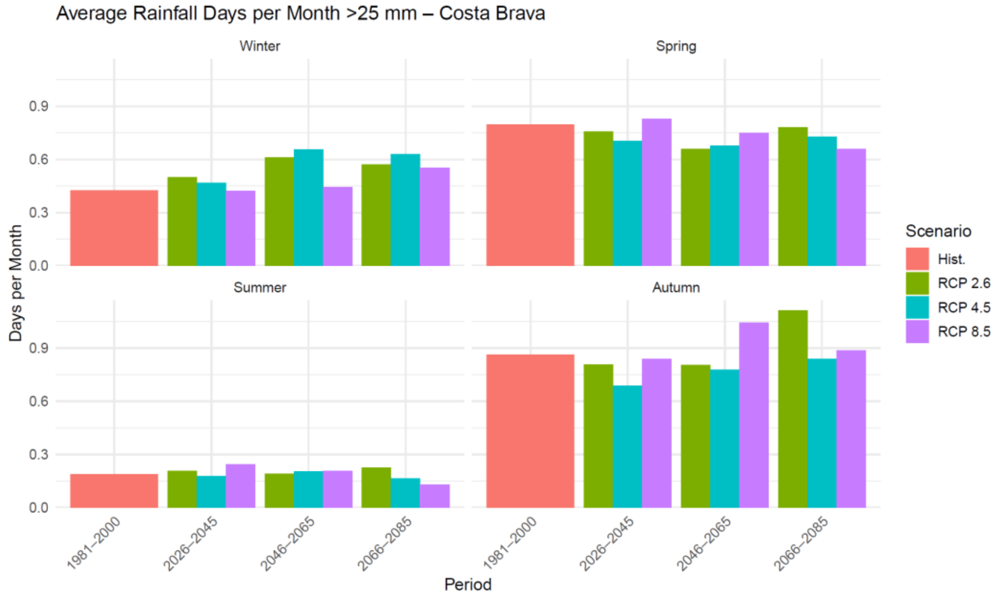

Figure 17. Average rainfall days per month >25 mm/day at the Costa Brava.

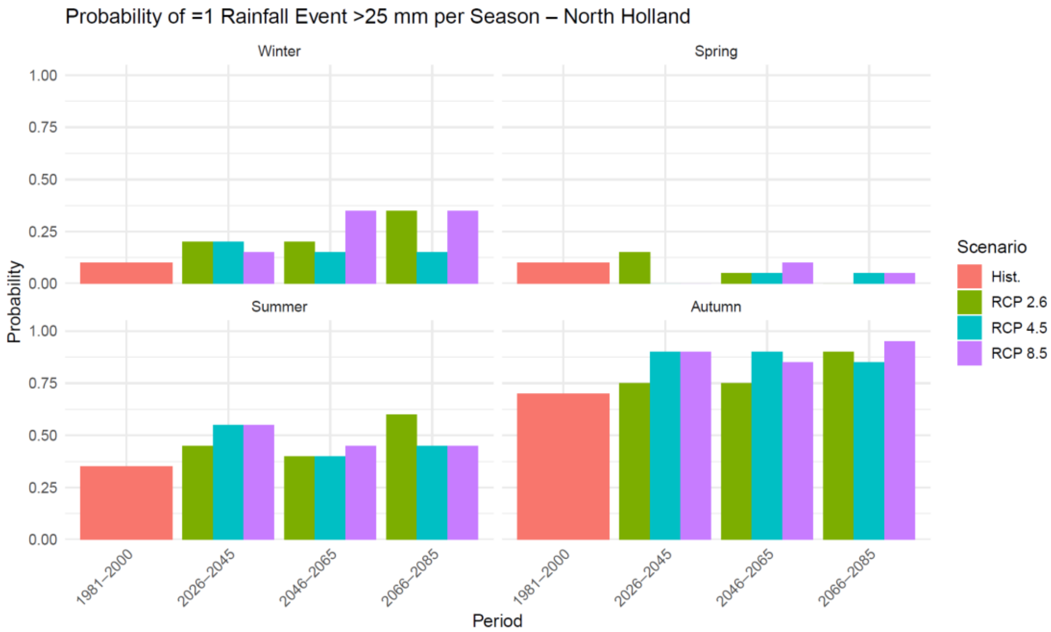

Figure 18. Probability of at least one rainfall event per month >25 mm/day in North Holland.

3.2 Surface Water availability

3.2.1 CS1 North Holland

In North Holland, the availability of freshwater critically depends on Lake IJssel (IJsselmeer), which acts as a buffer against salinity and a vital source of regional water supply. The reliability of the lake is increasingly threatened by two interacting pressures: sea level rise and reduced inflow from the River Rhine during dry spells. When the Rhine's discharge is low, less freshwater is available to maintain the hydraulic barrier that prevents seawater intrusion via the IJsselmeer's sluices and adjacent estuaries. At the same time, rising sea levels increase the upstream pressure of saline water, compounding the risk of salinization—especially in dry summers when water demand is highest.

This dual stress could undermine the freshwater function of Lake IJssel, impacting agriculture, water management of canals, polder areas and peatlands, and drinking water supply. Effective long-term adaptation strategies for drinking water must incorporate both Rhine discharge variability and sea level scenarios, as well as demands for IJsselmeer water for water management.

The data extracted from the Copernicus Climate Data Store within the context of RECREATE is unsuitable for modelling the complexities surrounding a large catchment like the River Rhine. Therefore, this report refers instead to existing detailed modelling and projections that have been published previously (Bonte & Zwolsman, 2010; Van der Brugge, 2024). The Dutch Delta Scenarios foresee a considerate decline of the 7-days summer minimum in Rhine discharge in 2050 of -8% to -18%. Also, the amount of water needed from the IJsselmeer for water management of canals, polders and peatlands is expected to double from the current 600 million m^3/yr (Van der Brugge, 2024).

3.2.2 CS2 Kalundborg

Kalundborg's surface water availability is intrinsically tied to the hydrological dynamics of Lake Tissø, the largest lake in western Zealand, which plays a central role in supporting local ecosystems, agriculture, and industry. As climate change continues to reshape hydrometeorological patterns, understanding future trends in precipitation and runoff becomes essential for sustainable water resource planning.

Using ensemble projections from the Copernicus Climate Data Store, we have analyzed seasonal trends in both precipitation and discharge across three future time slices—2026–2045, 2046–2065, and 2066–2085—under RCP8.5 scenarios. The ensemble combines outputs from seven Global/Regional Climate Model (GCM/RCM) pairs coupled with two hydrological models, thereby capturing a robust range of potential futures.

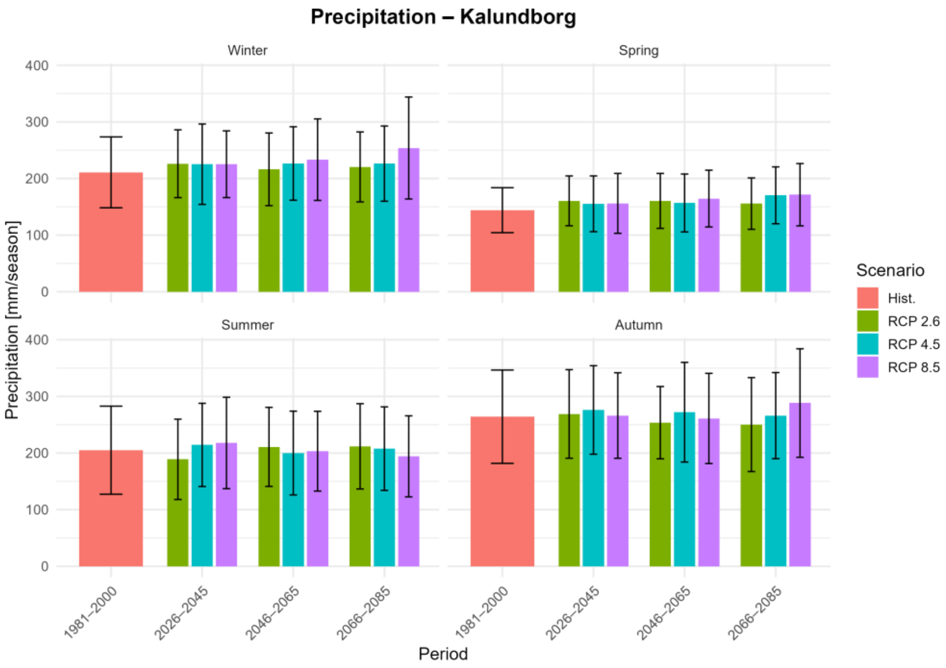

Figure 19. Seasonal precipitation patterns for Kalundborg.

Figure 19 illustrates projected seasonal precipitation across the ensemble. The historical baseline (1981–2000) serves as a reference. All seasons show moderate increases in precipitation compared to the historical baseline, particularly during winter and autumn. For instance, winter precipitation rises from approximately 210 mm to over 250 mm by the late 21st century for the RCP 8.5 scenario. This aligns with broader projections for northern Europe, where wetter winters are anticipated due to intensified westerly weather systems and a northward shift of storm tracks (Jacob et al., 2014).

Spring and summer exhibit more muted changes, with precipitation levels remaining mostly stable or slightly increasing. However, inter-model variability remains high during summer, as evidenced by wide error bars. This variability reflects uncertainties in convective rainfall modelling and regional feedbacks (Christensen & Christensen, 2007).

Figure 20 presents ensemble mean discharge values, providing a proxy for runoff potential across the Lake Tissø catchment. Discharge trends generally align with precipitation patterns, with winter and autumn displaying slight increases relative to the baseline. These seasons may contribute more to groundwater recharge and surface runoff, potentially enhancing lake inflows.

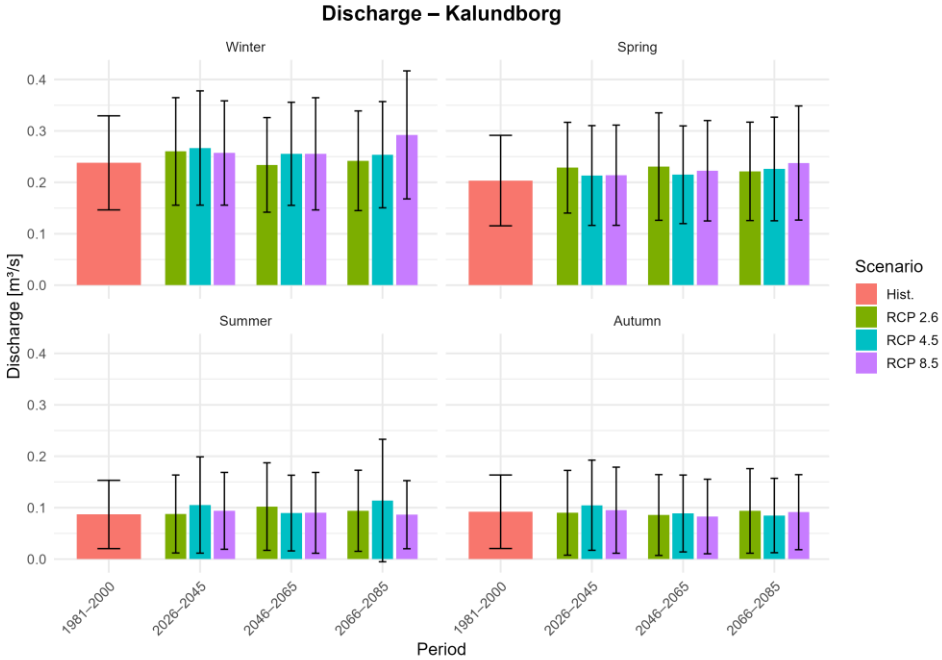

Figure 20. Seasonal discharge patterns for Kalundborg. Note, the discharge value reported here, is derived from the coordinate reported in the methodology section. It is not a river flow, but rather a value that is directly proportional to the run-off being generated by the catchment area.

However, summer and spring exhibit relatively stable discharge values, indicating that increased evapotranspiration may counterbalance higher rainfall. This has significant implications for water resource stress. While winter and autumn may provide more water, the ecological and industrial demand peaks during summer, when discharge remains stagnant and evaporation may further diminish net water availability. This aligns with findings by Hanasaki et al. (2013), who highlight the decoupling of water availability and demand under climate change (Hanasaki et al., 2013).

The net impact on Lake Tissø will depend on the interplay between seasonal inputs (precipitation and discharge) and losses (evaporation and withdrawals). While projected inflows during colder months may buffer the lake, persistent low flows in summer highlight the necessity for adaptive management—e.g., through seasonal storage optimisation or alternative water sourcing. Considering the industrial significance of Kalundborg, including the symbiotic resource-sharing system among local industries, it is essential to maintain lake water levels through informed hydrological modelling.

3.2.3 CS3 Syros

Climate projections from a 7-model ensemble indicate that precipitation will decline moderately under the RCP8.5 scenario, with winter and autumn totals decreasing by about 10–15% toward the end of the century. Yet, seasonal discharge — a proxy for runoff generation — shows much steeper reductions, particularly in winter, which may decline by up to 30% compared to the 1981–2000 baseline.

This divergence reflects a fundamental shift in hydrological behavior: increased temperatures will raise evaporation and soil moisture deficits, meaning that even when rainfall occurs, less water is converted into runoff.

These findings align with broader research on the Cyclades, which highlights the declining effectiveness of rain-fed systems under climate stress. A recent study on rainwater harvesting performance in the Cyclades confirms that increased evapotranspiration undermines long-term water security, even when rainfall remains relatively stable (Zarikos et al., 2023). Similarly, national assessments indicate that runoff efficiency is expected to decline across southern Greece, intensifying the challenges for small islands (Mimikou & Baltas, 2013).

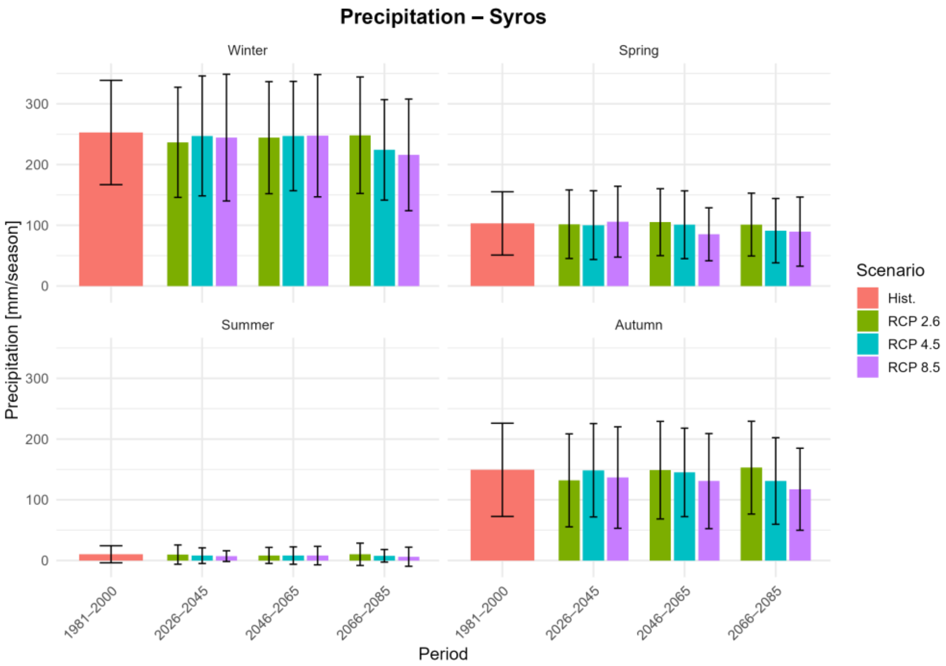

Figure 21. Seasonal precipitation patterns for Syros.

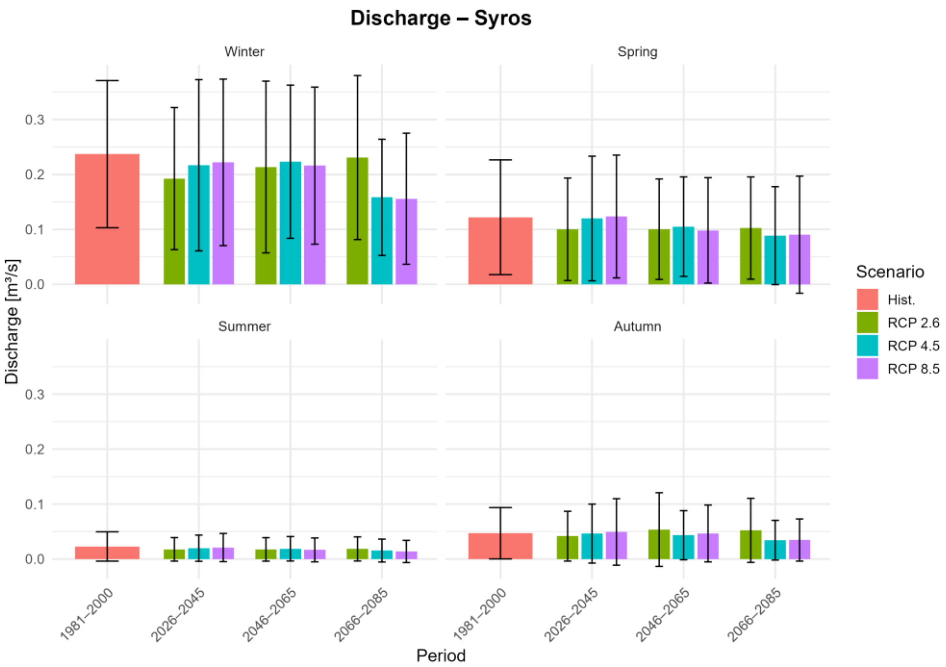

Figure 22. Seasonal discharge patterns (proxy for expected inflow to dams) for Syros.

3.2.4 CS4 Costa Brava

The Darnius-Boadella Reservoir, situated in the headwaters of the Muga River in northeastern Catalonia, is a critical water source for agriculture, urban supply, and ecosystems in this Case Study. With a storage capacity of approximately 61 hm³ and a catchment area of 182 km², its ability to buffer against hydrological variability is limited.

One aspect to highlight is that due to the extensive microclimate conditions caused by the topography of the Muga catchment, making precise discharge predictions is challenging. It is likely that additional models, such as locally calibrated SWAT+ models or similar hydrological tools, will be required to perform accurate quantitative assessments. This was also noted in recent work conducted by ICRA, where the hydrological model proved particularly difficult to calibrate for the Muga catchment (Laia Estrada, 2024). This may also explain the finding of why historical values derived from the Copernicus Climate Data Store actually indicated lower discharge values than future scenarios. Therefore, it seems appropriate to focus trend analysis more on the RCP2.6 scenario compared to the RCP8.5 scenario.

Climate projections from a 7-model ensemble indicate that while precipitation may decline only moderately (by about 10–15% under RCP8.5), runoff is expected to decrease more significantly, particularly in spring, summer, and autumn. For instance, spring discharge is projected to decline by approximately 25–30% by the 2066–2085 period when compared to the 2026-2045 period. This disproportionate reduction is attributed to increased temperatures leading to higher evapotranspiration rates and drier soil conditions, which reduce the efficiency of rainfall in generating runoff. These findings align with broader research on Mediterranean catchments, where studies have shown that even modest declines in precipitation can lead to substantial reductions in runoff due to increased evaporative demand.

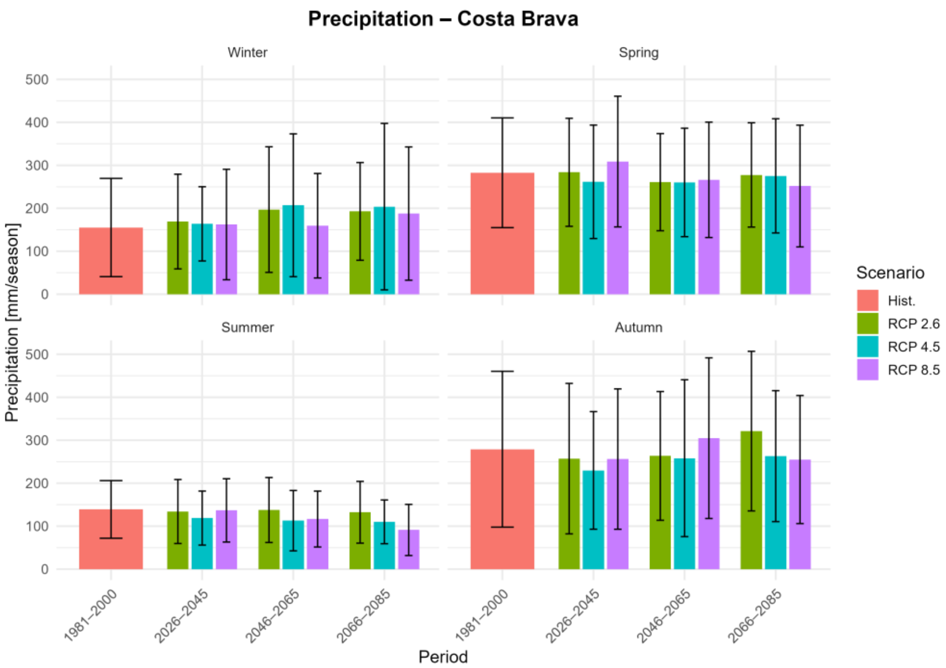

Figure 23. Seasonal precipitation patterns (proxy for expected inflow to dams) for Costa Brava west of the Darnius-Boadella reservoir.

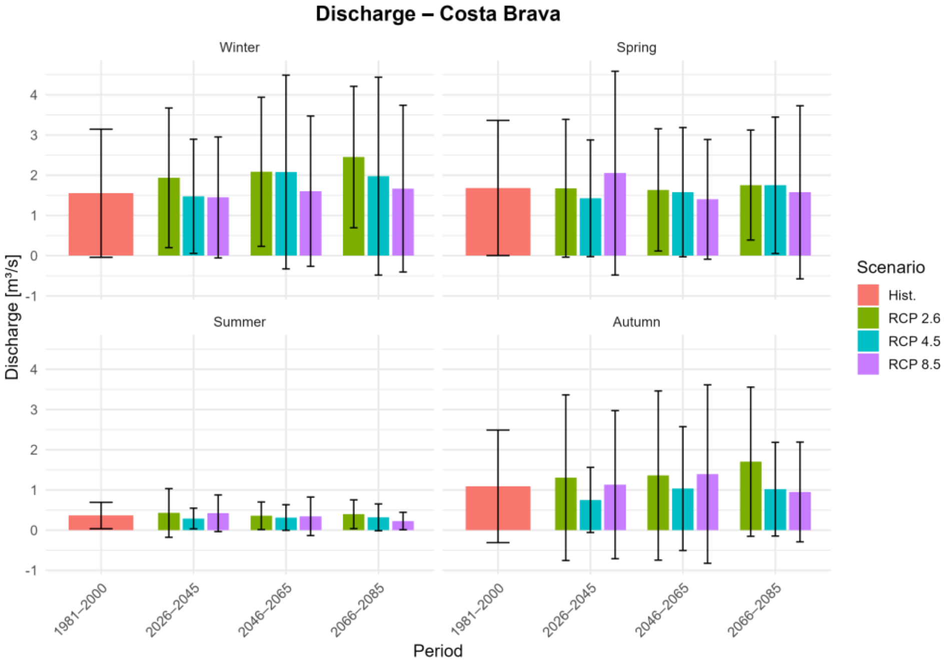

Figure 24. Seasonal discharge patterns (proxy for expected inflow to dams) for Costa Brava west of the Darnius-Boadella reservoir.

The projections also indicate an increase in interannual variability in discharge, particularly during spring and autumn, as evidenced by the widening error bars in model outputs. This variability heightens the risk of multi-year droughts, challenging the reliability of the reservoir. Recent events underscore this vulnerability. Between 2021 and early 2024, the Boadella Reservoir's volume fell to as low as 11.5% of its capacity, according to the Catalan Water Agency. Significant rainfall in late 2024 and early 2025 restored levels to above 80% by mid-2025. Such events illustrate the system's limited buffering capacity, especially when dry years occur consecutively.

Given the projected 30% decline in seasonal discharge and increasing variability, the resilience of the Boadella Reservoir is evidently at risk. Adaptive measures—such as enhancing water use efficiency, diversifying water sources, and implementing demand-side management—will be crucial to ensuring sustainable water availability in the face of climate change.

3.3 Groundwater availability

3.3.1 CS1 North Holland

Considering that the Case Study is currently not foreseeing to use groundwater and that the main water quantity and water quality concerns relate to the salinization of the Lake IJssel, groundwater modelling has not been performed for this Case Study.

3.3.2 CS2 Kalundborg

- **Modelling results**

The model demonstrates consistent and reasonably strong performance across the selected locations Table 11. For KLND01, the training set achieved an R² of 0.73, RMSE of 0.10, and KGE of 0.67, while the test set followed closely with an R² of 0.68, RMSE of 0.13, and KGE of 0.60 indicating good generalization and a low prediction bias of 1.89%. In the second KLND02 location, both train and test sets yielded identical R² values of 0.67, with low errors (RMSE of 0.17 and 0.16) and near-zero bias (pbias of 0.18% and -0.15%), pointing to model robustness. At KLND03, we obtained a comparable R² values of 0.62 on both sets, with low errors during training and the testing, and a higher KGE on the test set, suggesting reliable performance. As illustrated in Figure 25, the model's predictions closely match the observed groundwater level (GWL) dynamics over time which reinforces the model's effectiveness in simulating groundwater fluctuation behaviour during the test period.

Furthermore, the SHAP value analysis highlights the relative importance of input features on model output (Figure 26). Precipitation (P) stands as the most influential predictor, with high Precipitation values generally associated with a positive impact on GWL predictions. Evapotranspiration (ET_a) also shows a substantial contribution, where low ET_a tends to increase GWL.

Table 11 Model evaluation on test set

ID	Data set	R^2	RMSE	MAE	KGE	pbias
KLND01	Test	0.68	0.13	0.10	0.60	1.89
	Train	0.73	0.10	0.08	0.67	0.05
KLND02	Test	0.62	0.17	0.14	0.79	-0.12
	Train	0.62	0.19	0.15	0.63	1.01
KLND03	Test	0.67	0.16	0.12	0.70	-0.15
	Train	0.67	0.17	0.13	0.65	0.18

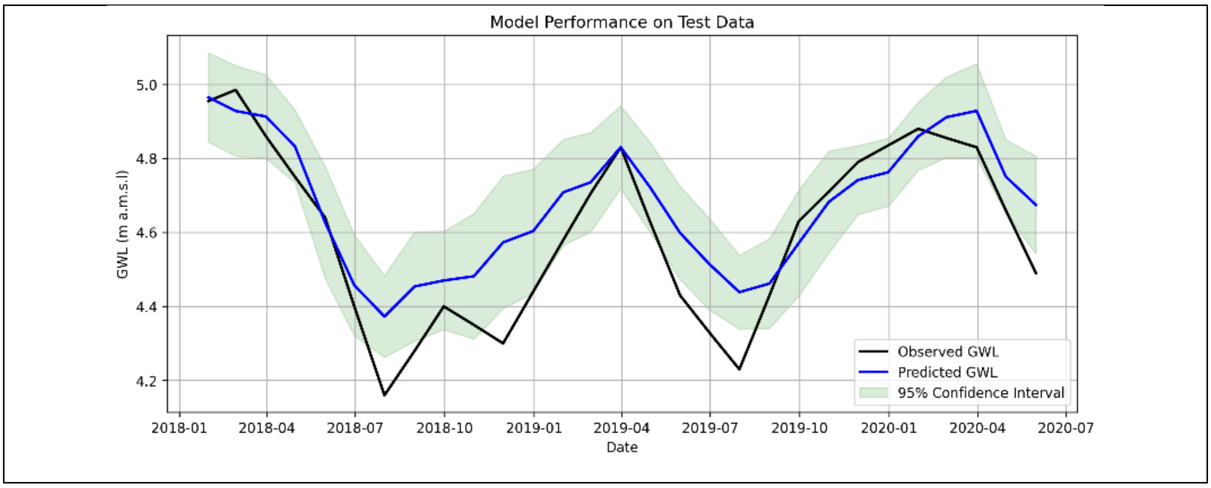

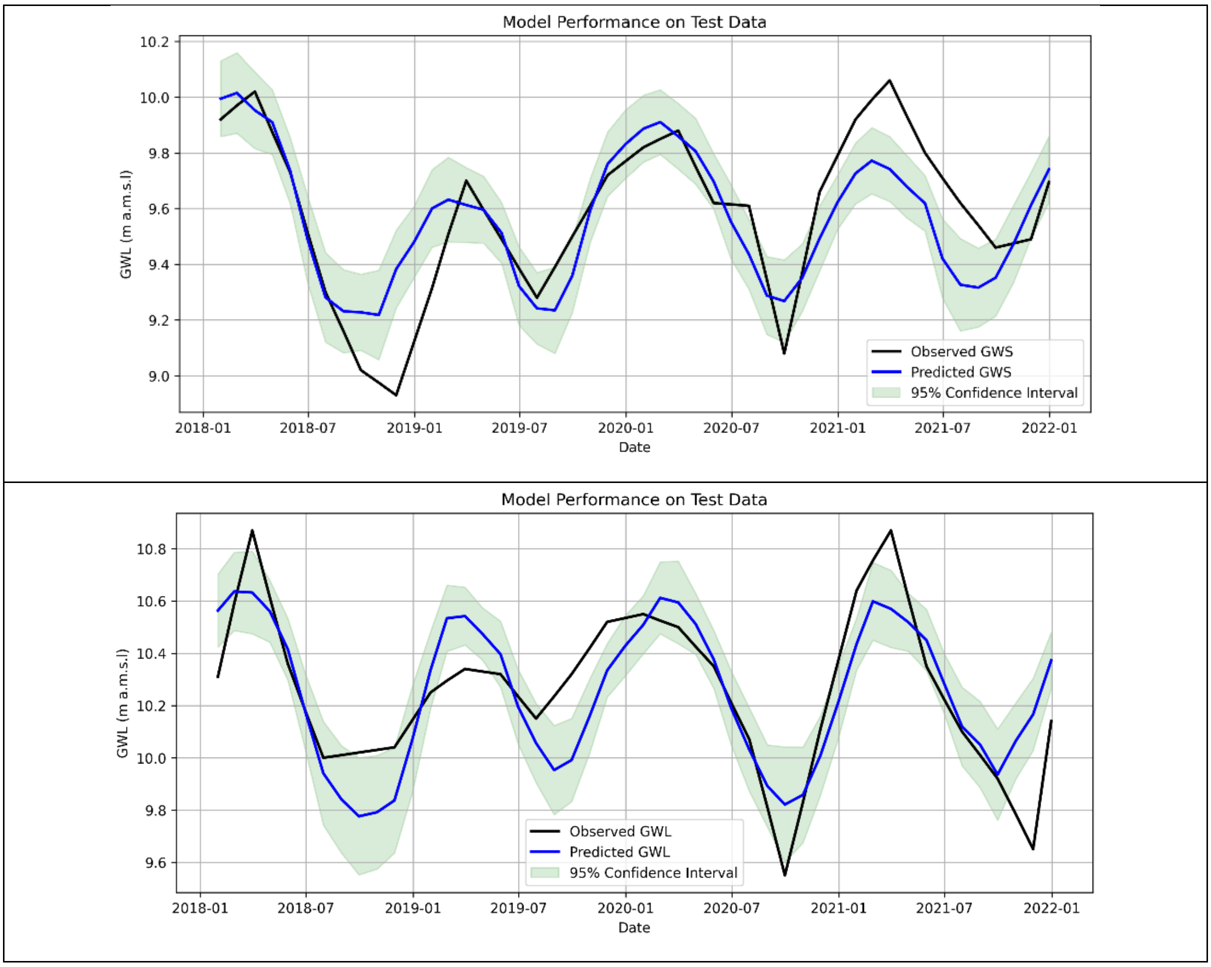

Figure 25 Model performance on test set

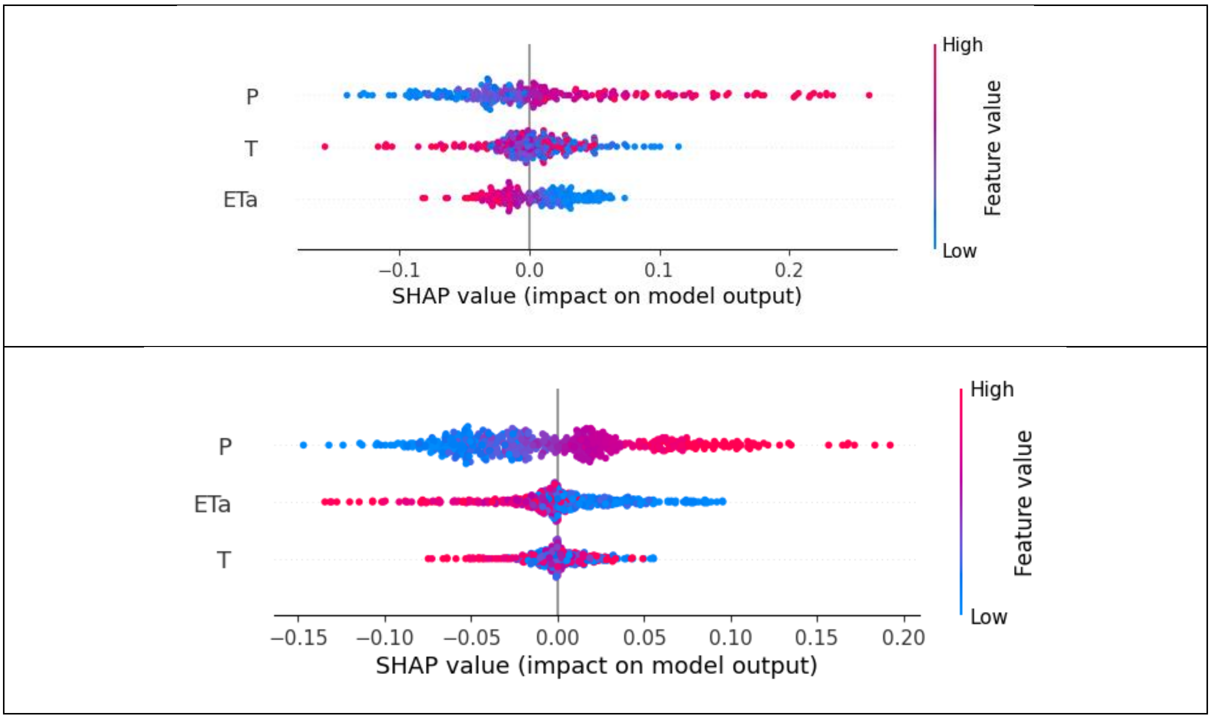

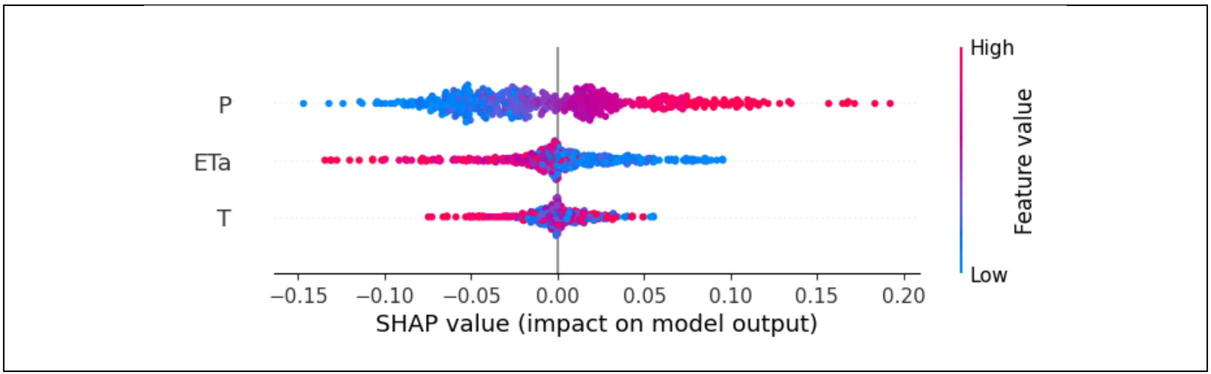

Figure 26 Beeswarm plot of SHAP analysis

- **Groundwater projections: KLND01**

As presented in Figure 27, it is evident that the groundwater level has an irregular pattern with many fluctuations between 2010 and 2100. Despite these variations, a significative declining trend average groundwater level compared to earlier years can be identified specially by the end of the century under the RCP4.5 (p-value < 0.05). The results also revealed a significant seasonal variation, with different seasons showing varying degrees of vulnerability to future climate conditions. Table 12 and Figure 28 show how seasonal groundwater dynamics may shift under different warming scenarios. The projected groundwater levels under all scenarios show a clear seasonal pattern relative to the 1970-2005 baseline, winter groundwater levels decline by about 0.09-0.12 m (1.8-2.4 %), while summer levels recover by 0.04-0.06 m (0.95-1.38 %). Under low-emission RCP2.6 and mid-range RCP4.5, summer gains stabilize near 1.2 % by mid-century, but under high-emission RCP8.5 they accelerate to 1.38 % by 2071-2100.

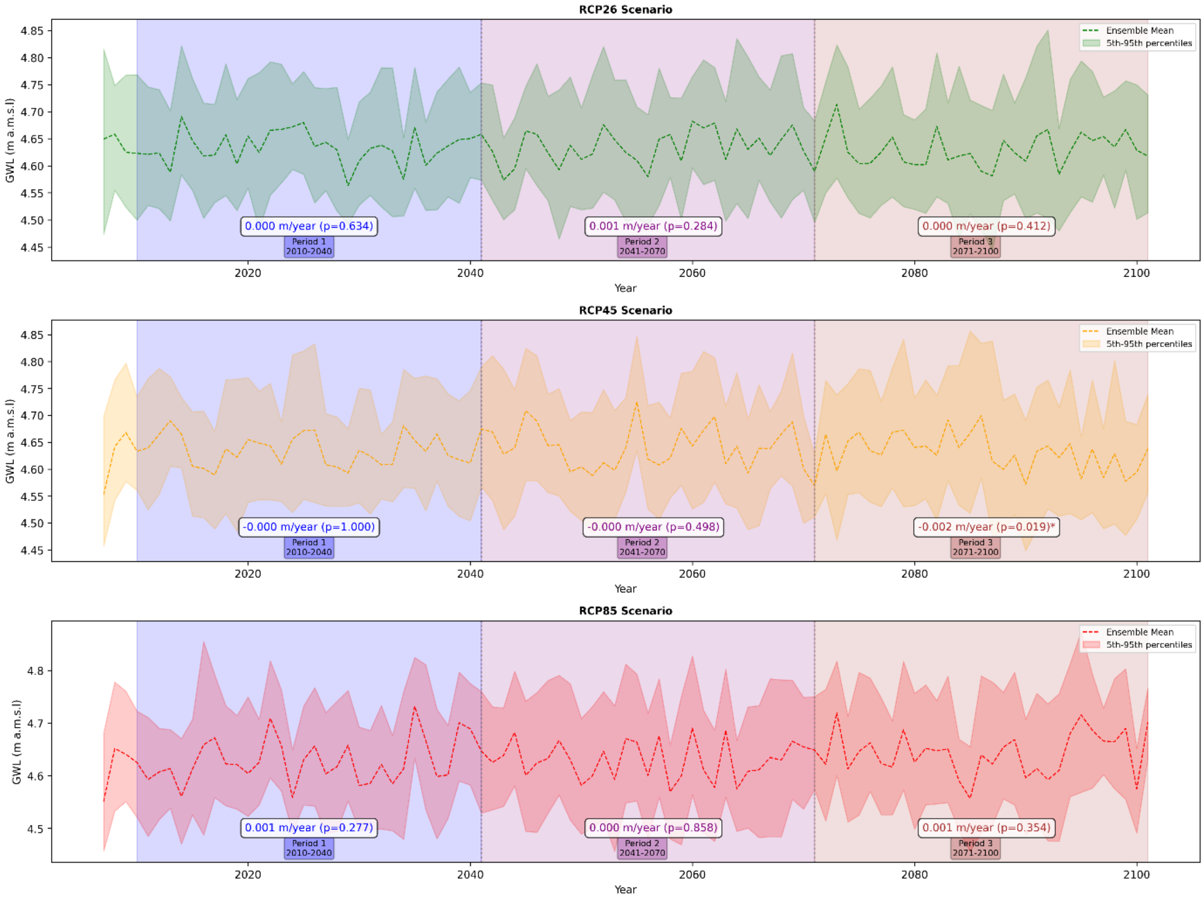

Figure 27 Projected Mean GWL (2010–2100) from Seven RCMs under RCP2.6, RCP4.5, and RCP8.5 for KLND01

Table 12 Seasonal change in GWL under different RCP scenarios and periods

Scenario	Period	Winter $\Delta GWL(m)$	Summer $\Delta GWL(m)$
RCP2.6	2010-2040	-0.099 (-2.07%)	+0.048 (+1.07%)
	2041-2070	-0.111 (-2.32%)	+0.055 (+1.21%)
	2070-2100	-0.110 (-2.29)	+0.043 (+0.95%)
RCP4.5	2010-2040	-0.106 (-2.20%)	+0.050 (+1.10%)
	2041-2070	-0.097 (-2.02%)	+0.056 (+1.24%)
	2070-2100	-0.103 (-2.15%)	+0.051 (+1.14%)
RCP8.5	2010-2040	-0.115 (-2.40%)	+0.049 (+1.09%)
	2041-2070	-0.108 (-2.24%)	+0.051 (+1.13%)
	2070-2100	-0.089 (-1.85%)	+0.062 (+1.38%)

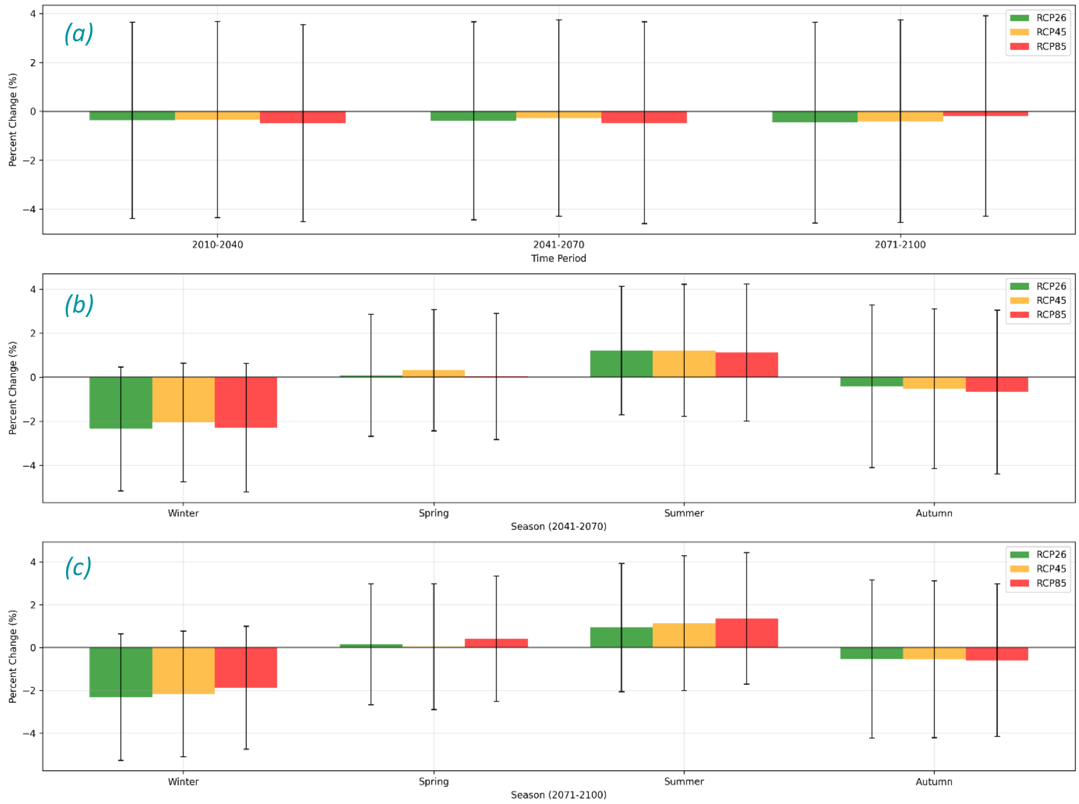

Figure 28 (a) GWL Change under RCP Scenarios by Period; (b-c) Seasonal GWL Percent Change (KLND01)

- **Groundwater level projection: KLND02**

The projected groundwater availability in this location exhibits contrasting responses across emission scenarios, with groundwater levels maintaining stability around 10.3-10.4 m above mean sea level under most conditions but showing concerning trends under high-emission pathways (RCP8.5) (Figure 29). While the RCP2.6 and RCP4.5 scenarios demonstrate minimal long-term changes with statistically non-significant trends (Mann Kendall p-value>0.05), the RCP8.5 scenario presents a statistically significant declining trend of -0.002 m/year during the critical mid-century period (2041-2070, p-value=0.030), indicating potential groundwater depletion under severe climate change conditions. Like previously observed in KLND01, we can identify a pronounced seasonal redistribution pattern across all scenarios, with summer months consistently showing positive changes (+2%) and winter months exhibiting negative changes (-1 to -2%), suggesting a fundamental shift in the hydrological (Figure 30). These results diverge from the findings of (Seidenfaden et al. (2022), who reported increased winter recharge; this discrepancy can be attributed primarily to differences in the selected baseline and the high uncertainty inherent in the simulated climate models.

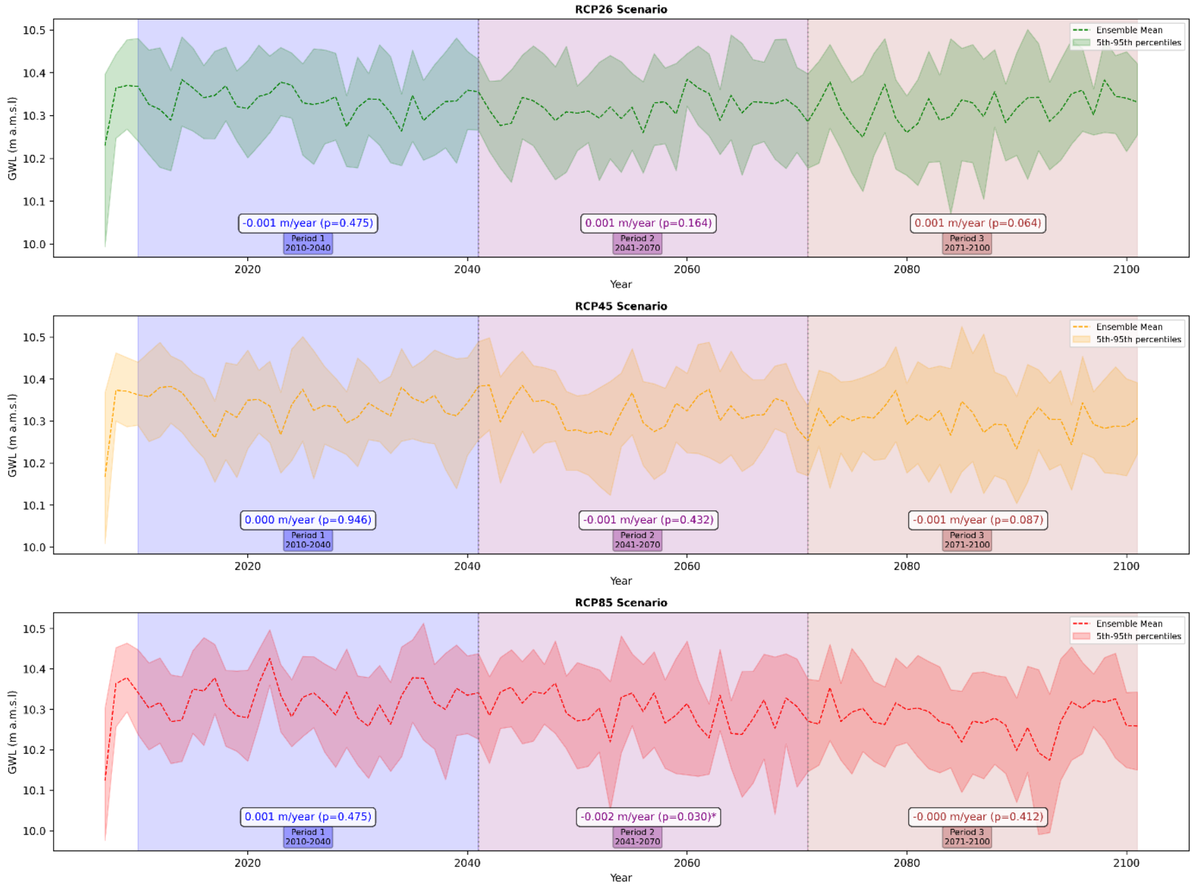

Figure 29 Projected Ensemble Mean GWL (2010-2100) under RCP2.6, RCP4.5, and RCP8.5(KLND02)

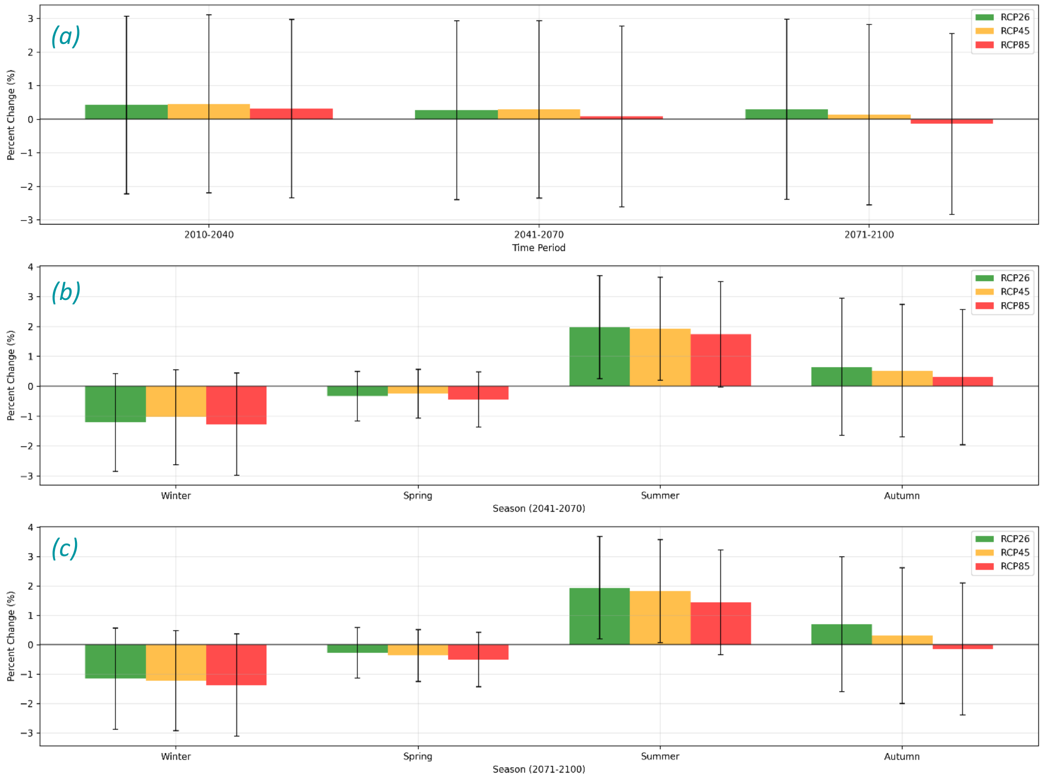

Figure 30 (a) GWL Change under RCP Scenarios by Period; (b-c) Seasonal GWL Percent Change (KLND02)

- **Groundwater level projection: KLND03**

As depicted in Figure 31, the ensemble projections show minimal long-term trends in groundwater levels, with annual rates changes in general inferior to 0.002m/year across all scenarios. Notably, as illustrated in Figure 32, distinct seasonal patterns emerge, particularly evident in 2041-2070 and 2071-2100 periods, where winter months show negative percent changes (approximately -2%) while summer months exhibit positive changes (+2%), suggesting a seasonal redistribution of groundwater recharge. The increasing variability observed under the RCP8.5 scenario, characterized by wider confidence intervals and more pronounced seasonal fluctuations, suggests that while mean groundwater availability remains stable, extreme climate conditions may introduce greater uncertainty.

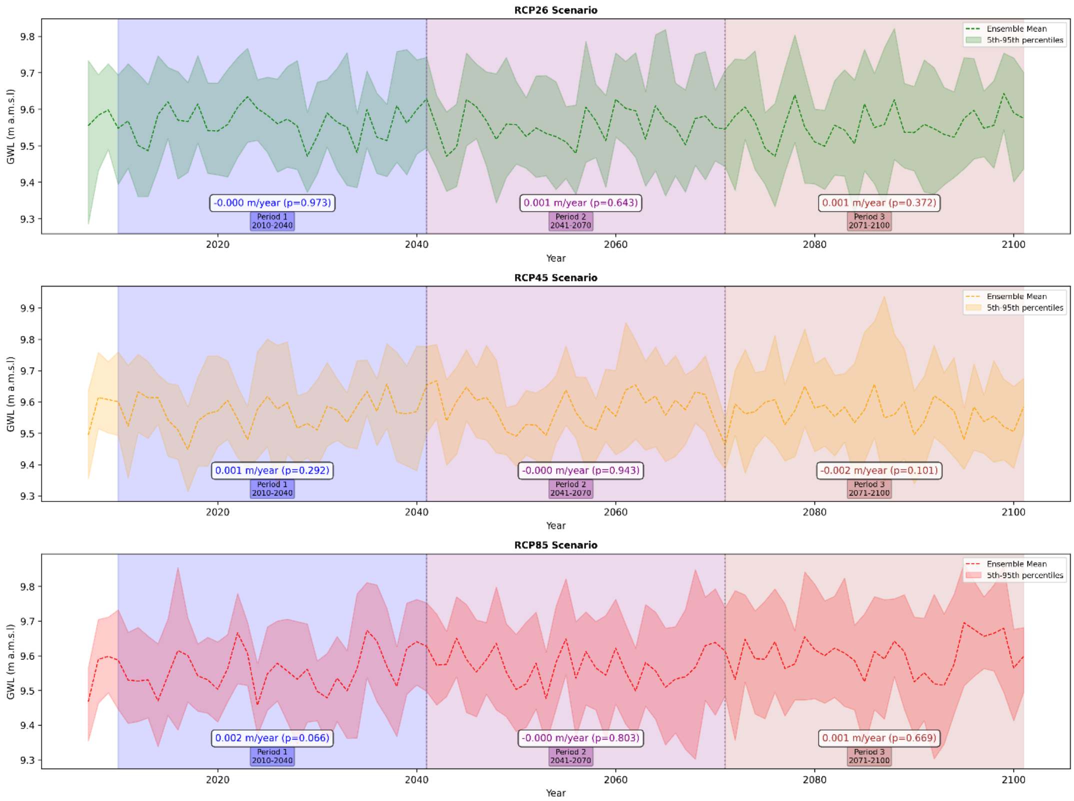

Figure 31 Projected Mean GWL (2010-2100) for KLND03

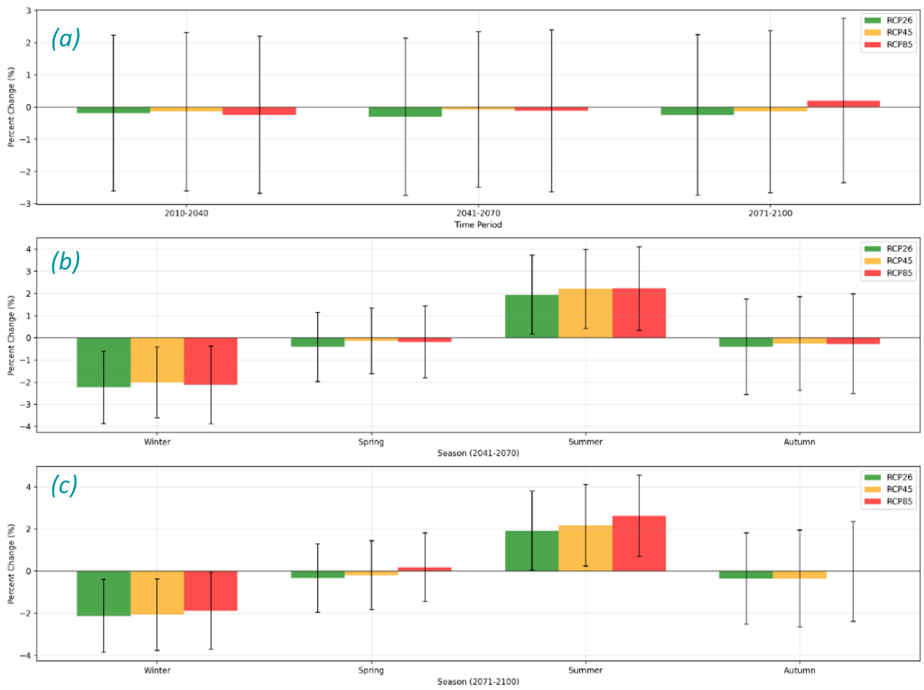

Figure 32 a) GWL Percent Change under RCP Scenarios by Period; (b-c) Seasonal GWL Percent Change (KLND03)

3.3.3 CS3 Syros

- **Modelling results**

Across the soil profile Figure 33, the mean Field Capacity (FC) is about 30.1 %, the mean Permanent Wilting Point (PWP) is 16.9 %, and the plant-available water (SM) is 72.57 mm

According to Table 13 and Figure 34, the simulation results using ERA5-Land historical climate data for the period 1970-2005 indicate a mean annual groundwater recharge of approximately 9.02 mm/year, which represents around 3% of the total annual precipitation (400.8 mm/year).

Table 13 T-M outputs for Syros Case Study

period	Total Precipitation	ETo	ETa	Recharge
1970-2005	400.8	1239.9	389.6	9.02

Note: All parameters are expressed in mm/year

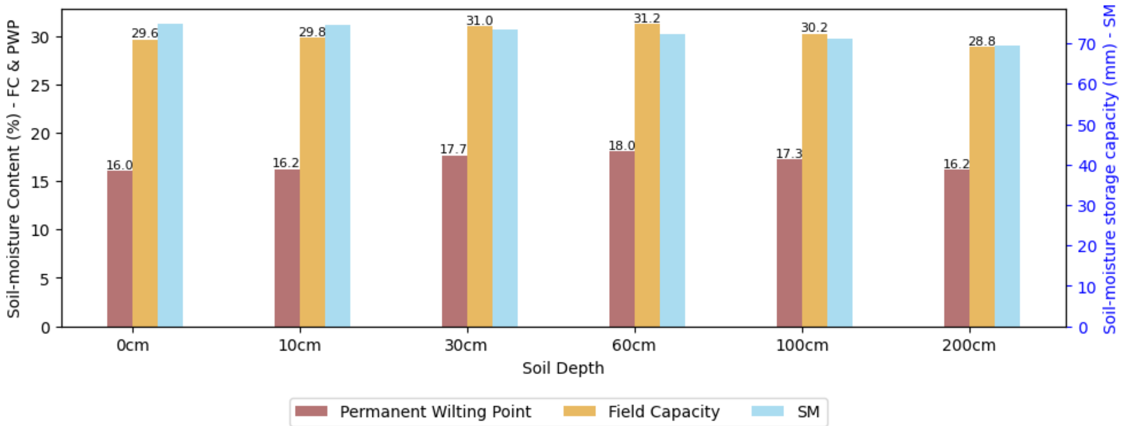

Figure 33 Syros soil hydraulic properties per depth

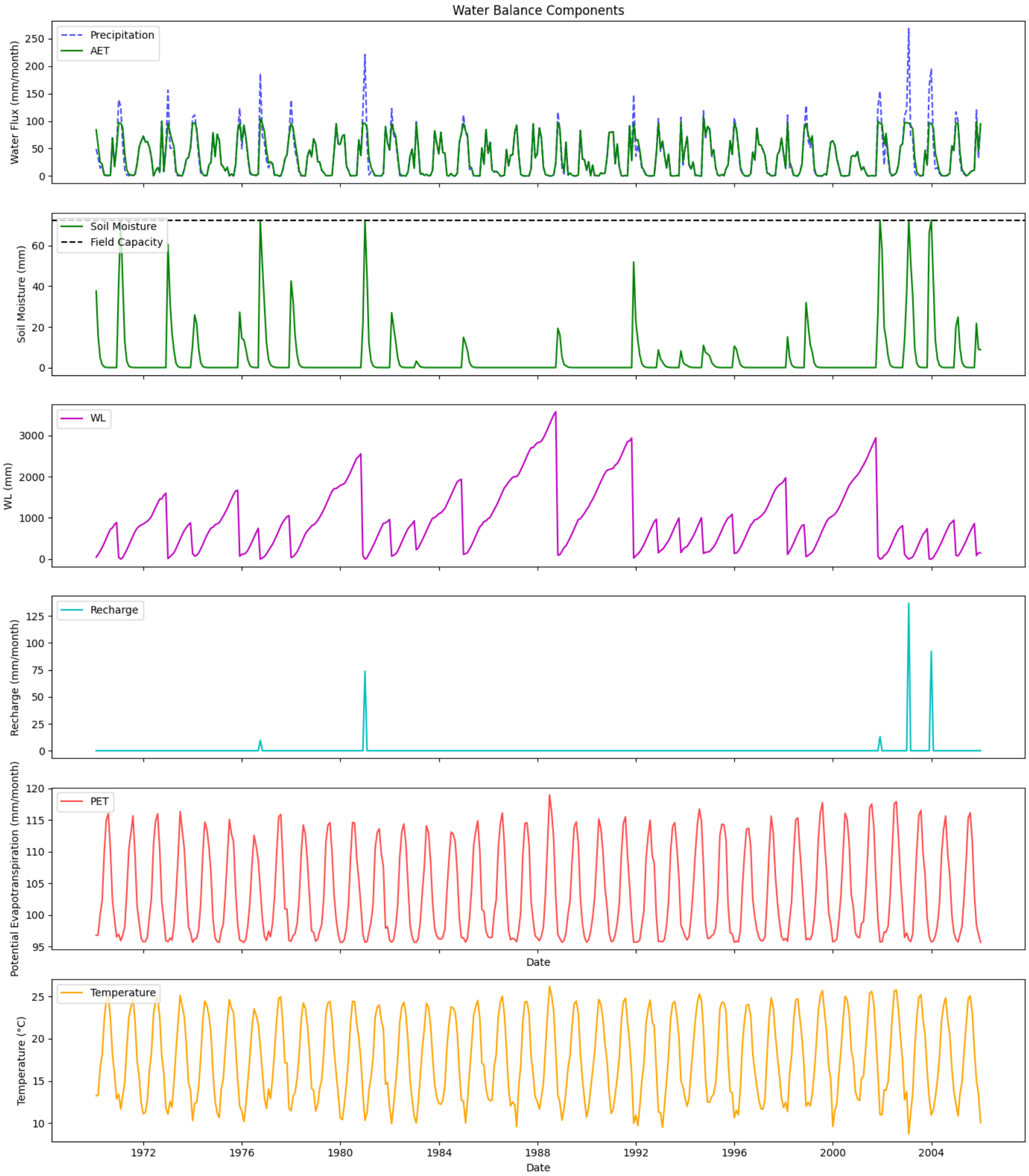

Figure 34 T-M simulation output of ERA5-Land for 1970-2024

- **Groundwater recharge projections**

According to Table 14, Figure 35, and Figure 36, different trends vary depending on the scenario and the period, relative to the 1970-2005 ERA5 baseline. Under RCP8.5, recharge declines by approximately -10% to -47% across all three future periods, with RCP4.5 also tending to decrease by the century's end, whereas RCP2.6 indicates a potential positive change. All projections demonstrate high uncertainty with standard deviations of ±4 - 12 mm, particularly, RCP2.6 displays high variability initially but shifts toward positive change by the end of the century. In general, higher-emission pathways correlate with more pronounced and persistent reductions in groundwater recharge. These results confirm that water stress in Syros will intensify due to constrained recharge, which will put in concern the water availability.

Over time, recharge projections under RCP4.5 and RCP8.5 indicate a clear decrease in shift, especially pronounced under RCP8.5, suggesting a progressive decline in recharge rates. Meanwhile, RCP2.6 remains relatively stable with moderate variability. The growing spread of values over time across all scenarios underscores increasing uncertainty and risk in water availability projections.

Table 14 Percent Change in Groundwater Recharge Compared to ERA5-Land Historical Baseline (1970-2005

Period	RCP	Ensemble Mean	Std	ERA5	Percent change
2010-2040	RCP2.6	5,96	± 4,71	9,04	-34,1
2010-2040	RCP4.5	10,92	± 8,56	9,04	20,75
2010-2040	RCP8.5	8,1	± 5,14	9,04	-10,38
2041-2070	RCP2.6	9,07	± 8,24	9,04	0,25
2041-2070	RCP4.5	12,43	± 12,41	9,04	37,39
2041-2070	RCP8.5	7,43	± 6,43	9,04	-17,8
2071-2100	RCP2.6	12,28	± 9,16	9,04	35,75
2071-2100	RCP4.5	4,64	± 4,33	9,04	-48,74
2071-2100	RCP8.5	4,81	± 3,78	9,04	-46,84

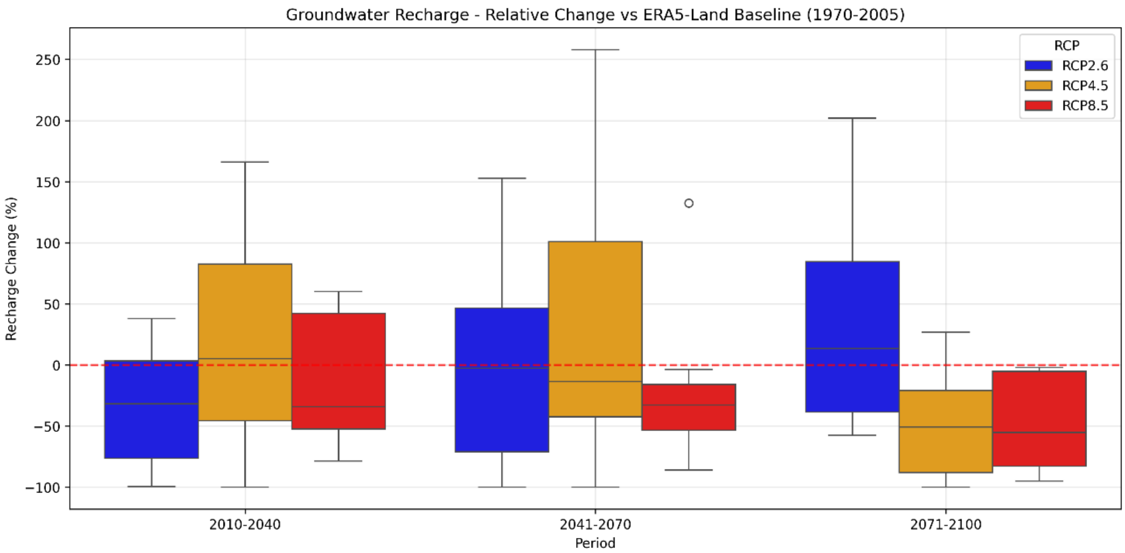

Figure 35 Distribution of groundwater recharge relative to ERA5-Land Baseline (1970-2005)

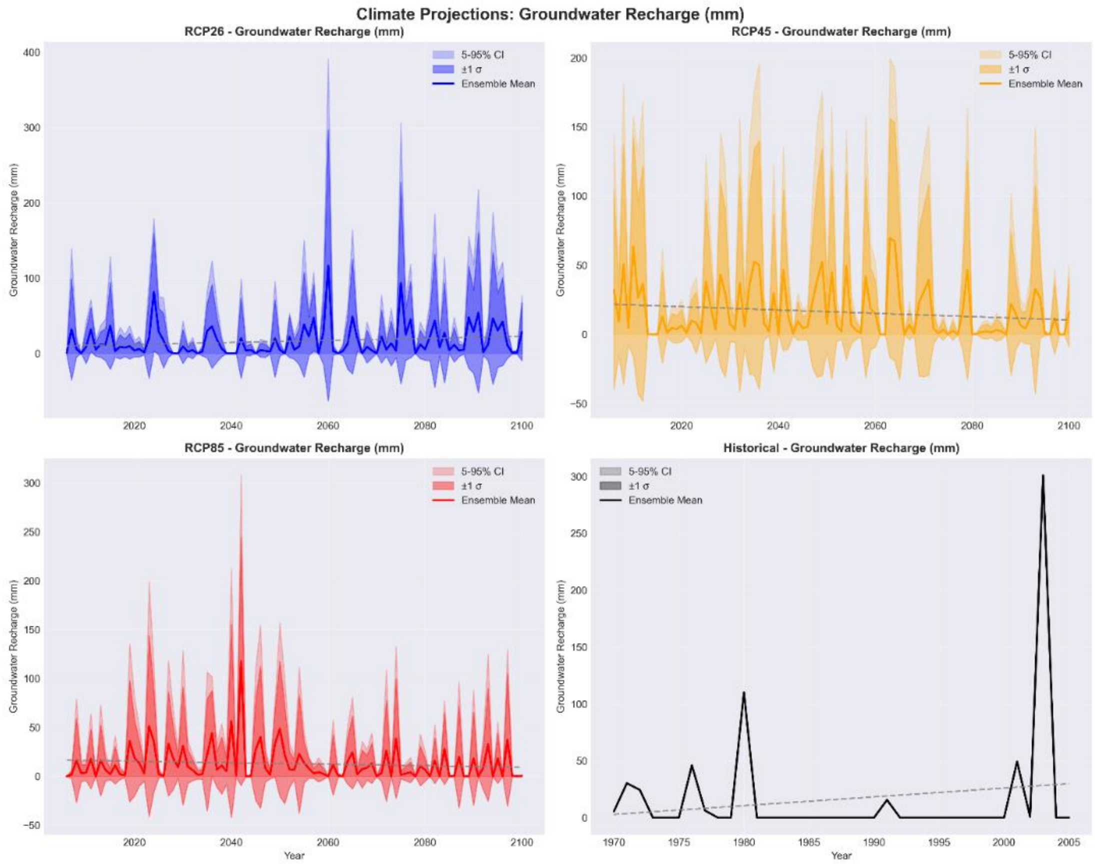

Figure 36 Projections results for Syros. Mean of seven Regional Climate Models predictions with uncertainty range (5th-95th percentiles)

3.3.4 CS4 Costa Brava

- **Modelling results**

For both locations, the models demonstrate high predictive accuracy, as illustrated in Figure 37. The simulated groundwater storage (GWS) closely fits the observed data, with KGE values of 0.93 for FFM1 and 0.75 for CAM1. A summary of performance metrics is presented in Table 15. The models exhibit low RMSE and MAE values, along with high coefficients of determination ($R^2 > 0.80$), confirming strong predictive skill. Additionally, the low pbias values further indicate minimal systematic bias, supporting the reliability of the model outputs.

Figure 38 presents a Beeswarm plot that ranks the input features (Y-axis) by the sum of the SHAP values of magnitudes. The x-axis represents the SHAP values, color-coded from blue (low values) to red (high values) to indicate the magnitude of impact. Each data point corresponds to a SHAP value for a specific predictor. According to the obtained results, GWS is most significantly influenced by precipitation, followed by the temperature, then the actual evapotranspiration. High precipitation values significantly increase GWS, while high temperature values decrease GWS. The SHAP values are consistent with known aquifer behaviour to changes in meteorological variables. Additionally, according to Figure 39**,** we can confirm the ability of the implemented models to simulate extreme conditions likely to be expected in the future.

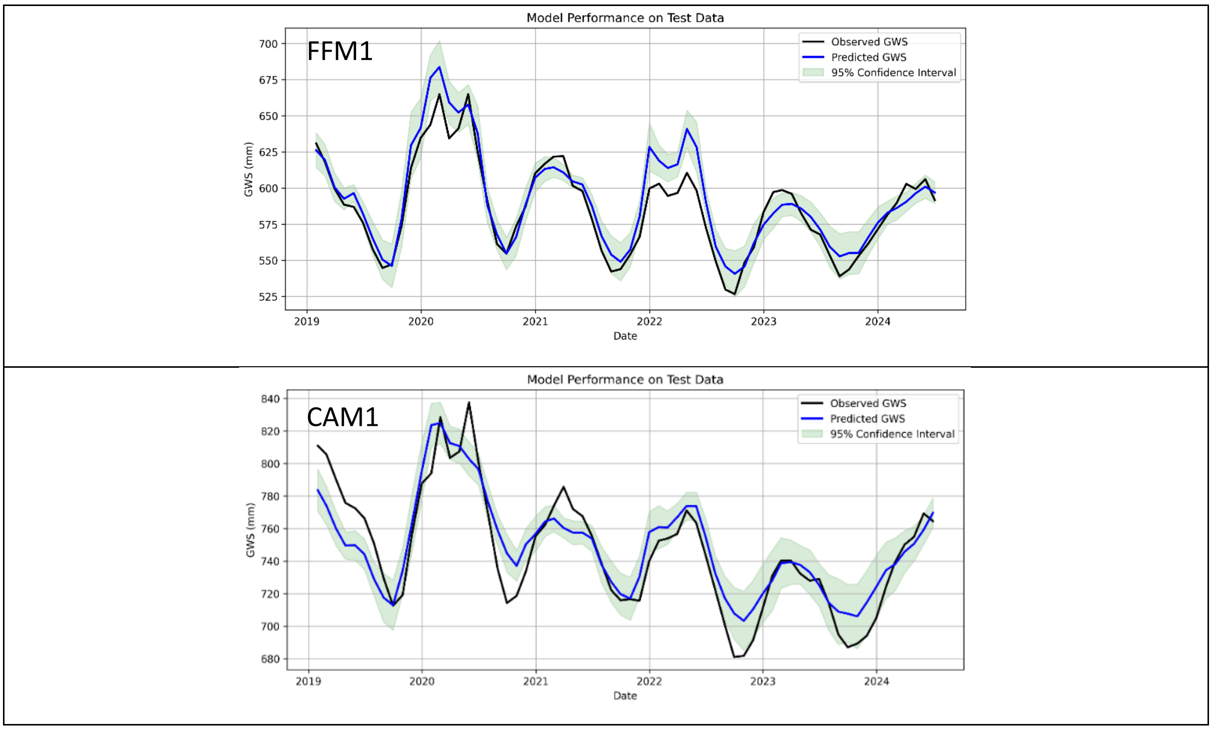

Figure 37 Model performance on test set

Table 15 Model Evaluation on test set (2019 -2024-06)

ID	Sequence length	Filters	Dense layer size	Batch size	LSTM Size	Learning rate	Dropout rate
FFM1	7	40	16	8	128	0.0055	0.2; 0.3
CAM1	7	221	64	8	128	0.0053	0.3; 0.4

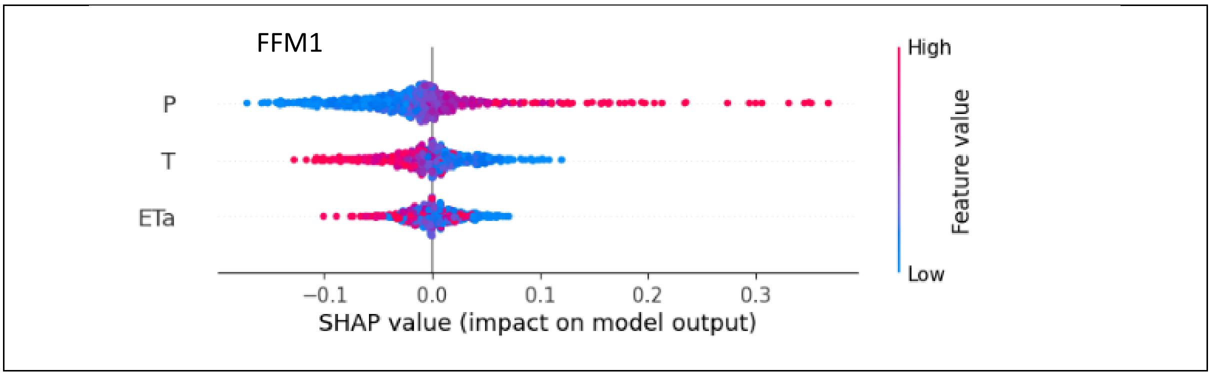

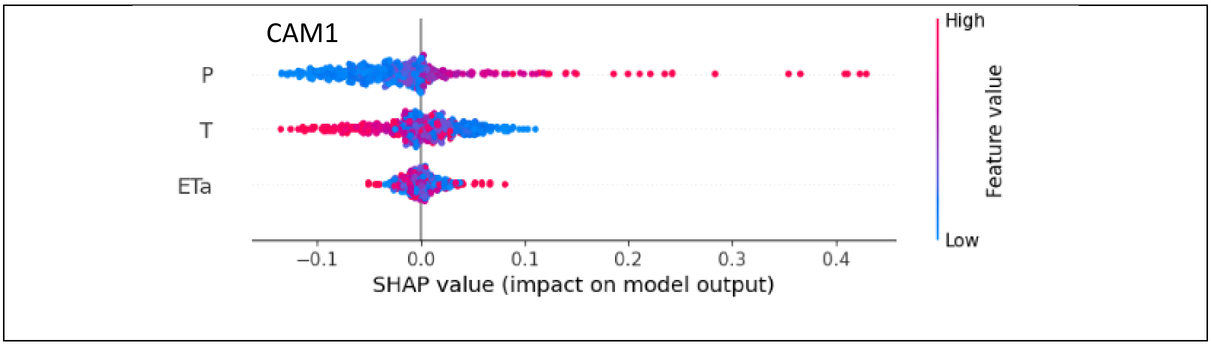

Figure 38 Beeswarm plot of SHAP analysis

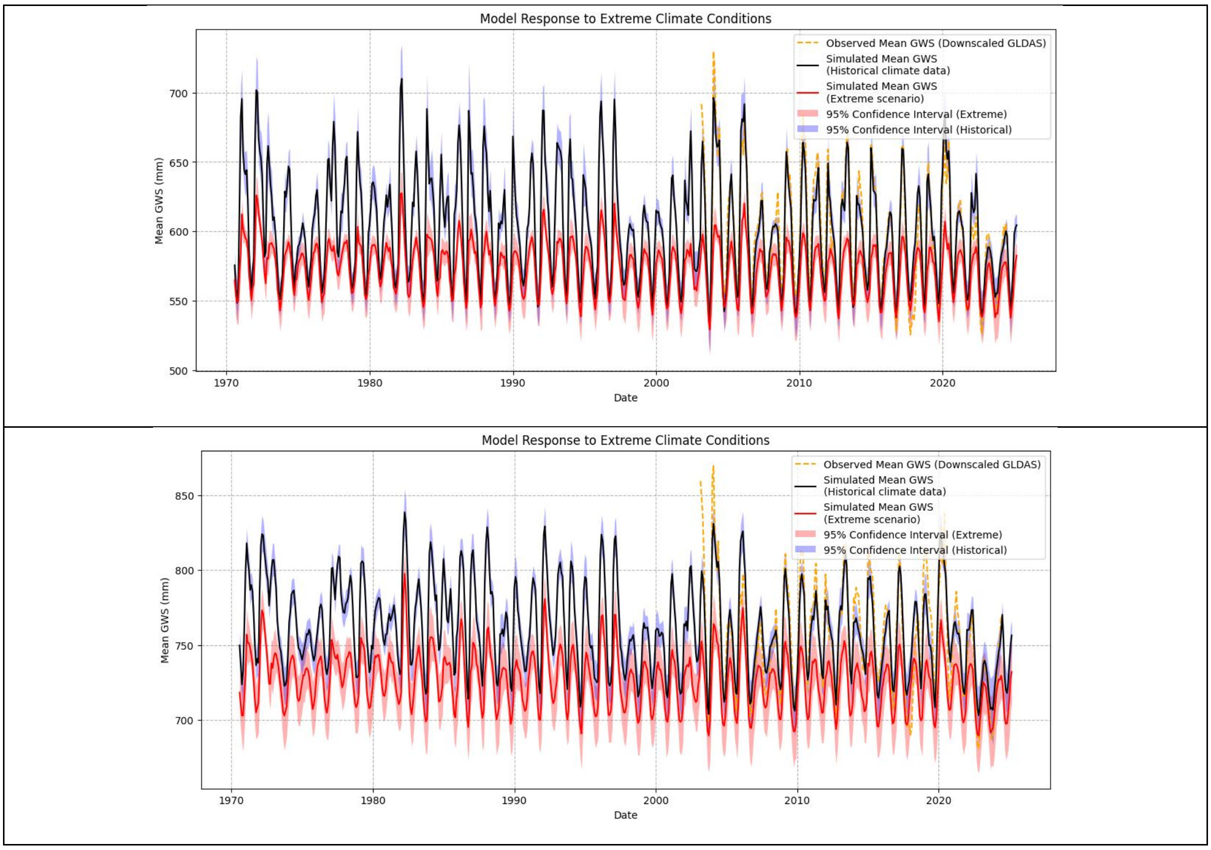

Figure 39 Model response under artificial extreme conditions in the past (modified ERAS)

- **Groundwater projections for Muga Coast**

The results show a continuous depletion in GWS in Costa Brava (Figure 40). Particularly, in the current to near future, all RCP scenarios present a negative trend, with a highly significant decrease of -0.392 mm/year expected under RCP4.5 (p-value < 0.01), and a significant decrease of -0.387 mm/year under RCP8.5 (p-value < 0.05). This negative trend is likely to persist through mid- and end-century projections.

Figure 41 illustrates a clear pattern of progressive groundwater depletion over time in comparison to ERA5 historical baseline (1970-2005). The most optimistic scenario, RCP2.6, shows only modest impacts, whereas RCP4.5 indicates moderate declines. Under the more severe RCP8.5 scenario, groundwater losses could reach up to 2% by the end of the century. Seasonal trends reveal that winter months consistently the most significant depletion across all scenarios and time periods, while summer tends to show positive changes. Despite the notable uncertainty, as depicted by the error bars, the persistence of negative trends across scenarios strongly suggests a sustained impact of climate change on groundwater resources in Muga aquifer.

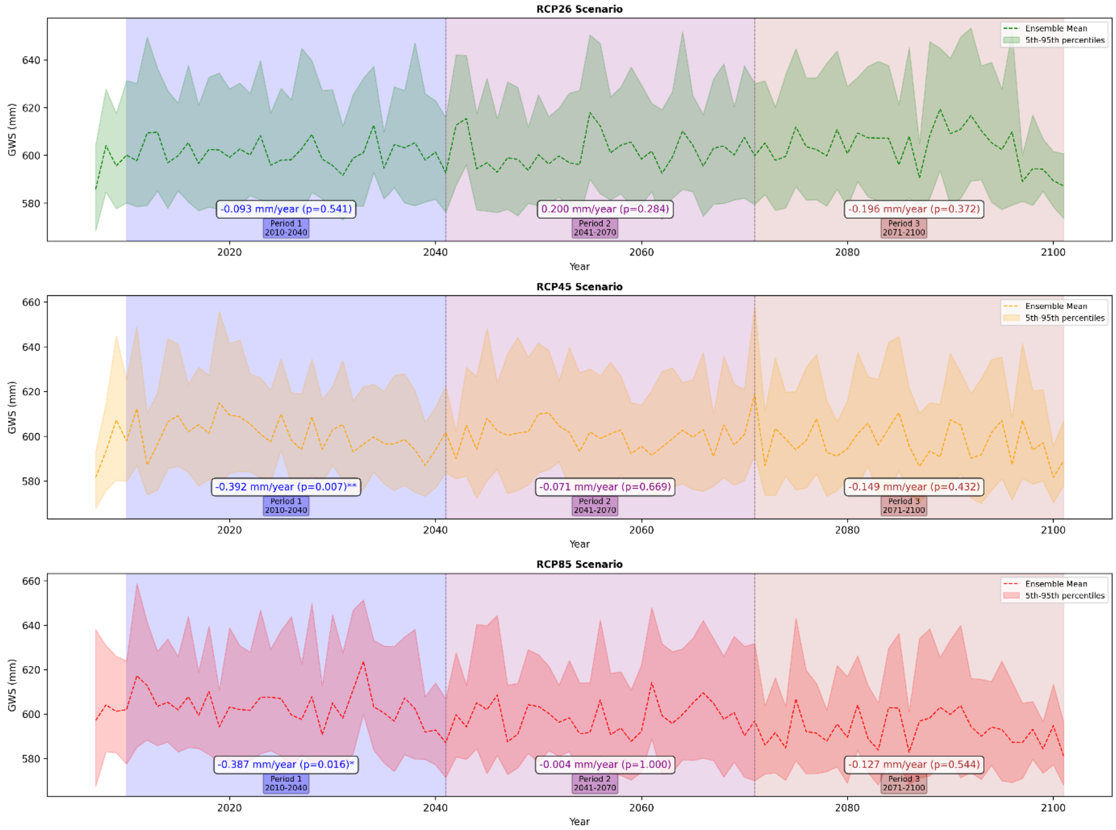

Figure 40 Projections of Ensemble Mean GWS Changes to 2100

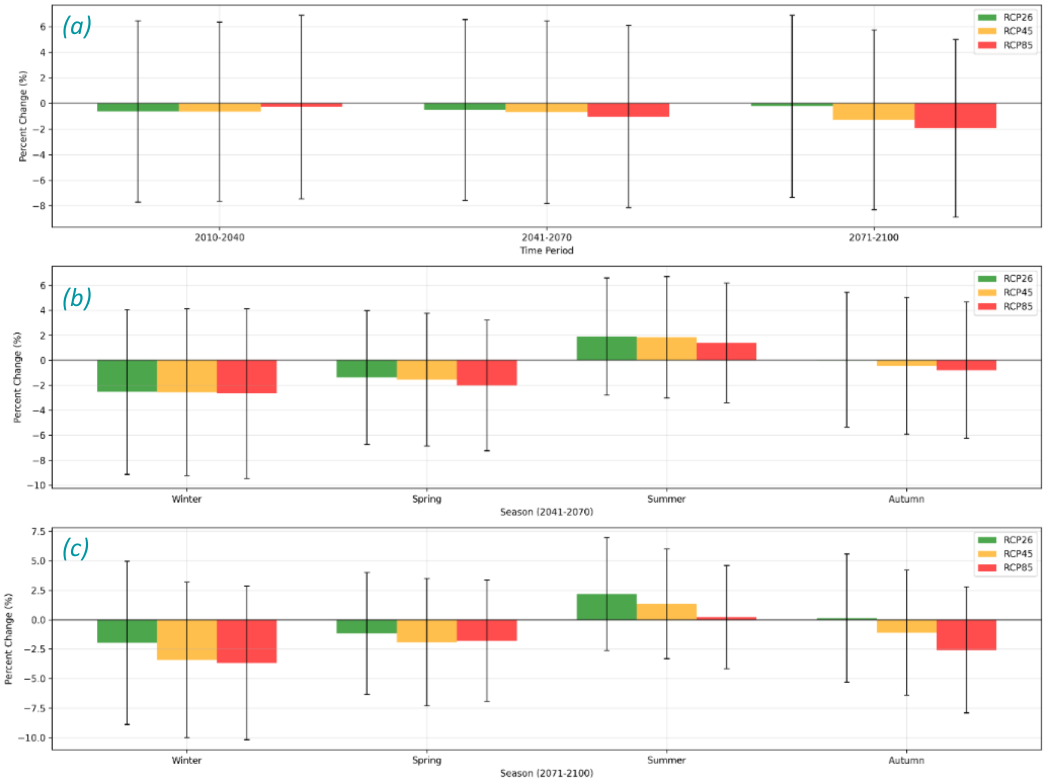

Figure 41 (a) GWL Change under RCP Scenarios by Period; (b-c) Seasonal GWL Percent Change.

- **Groundwater Projections Muga Inland**

Figure 42 presents the time series of ensemble means of GWS projections from the seven climate models for the Muga Alta aquifer. The results indicate a clear, significant negative trend in the current and near future (2010-2040), particularly under RCP4.5 (Mann-Kendall p-value < 0.01) and RCP8.5 (Mann-Kendall p-value < 0.05), with decreasing rates of -0.537 mm/year and -0.332 mm/year, respectively. It is also evident from the same figure that, by the end of the century, under all scenarios, the region is likely to experience a continued negative trend, with a pronounced rate of -0.278 mm/year under RCP8.5.

The histograms of percent changes by period and season are shown in Figure 43. The results demonstrate a clear decline in GWS, from -0.56% in the near future (2010-2040) to -2.36% by the end of the century (2041-2100) under RCP8.5. The percentage of change under RCP4.5 is smaller compared to RCP8.5, while RCP2.6 shows an inverse trend, with increasing values. Furthermore, a seasonal shift in percent change is observed. For both mid- and far-future periods, winter and autumn exhibit a decreasing trend, while summer shows an increase. A particularly pronounced decline is noted by the end of the century (2071-2100) under RCP4.5 (-3.72% in winter and -2.78% in autumn) and RCP8.5 (-4.24% in winter and -4.52% in autumn).

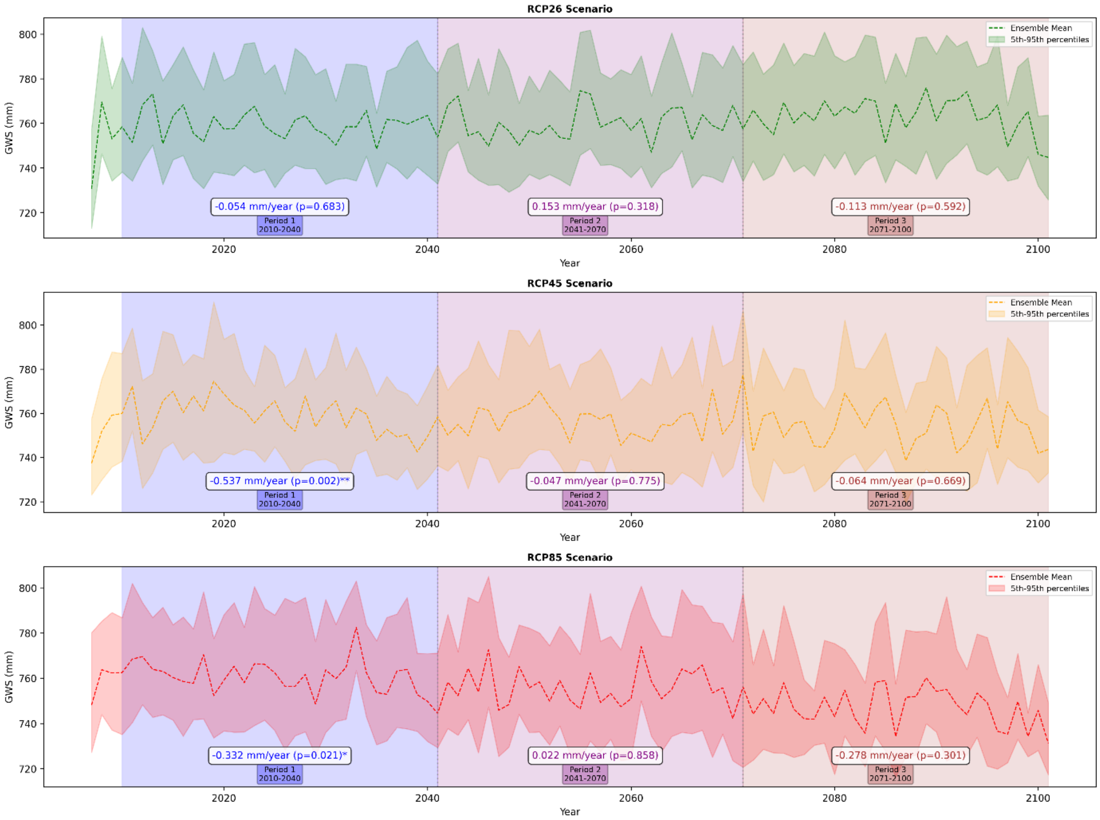

Figure 42 Projections of GWS changes to 2100 (Muga Alta)

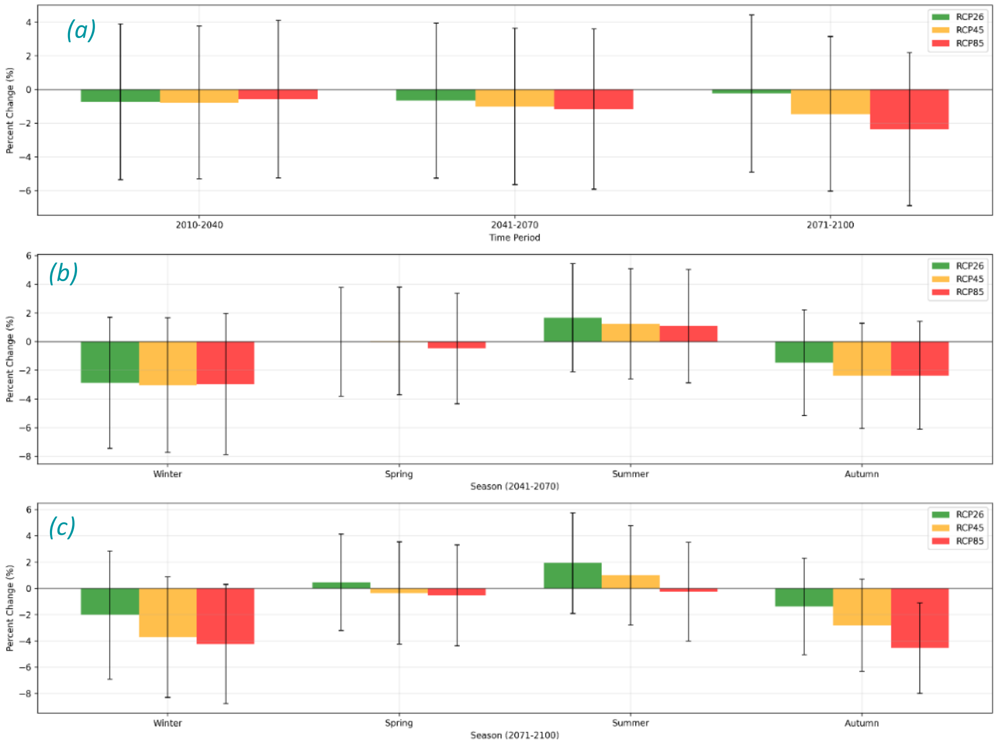

Figure 43 (a) GWS Change under RCP Scenarios by Period; (b-c) Seasonal GWS Percent Change

3.4 Demand Scenarios

3.4.1 CS1 North Holland

The drinking water demand in the Netherlands is expected to increase in the coming decades due to population growth, which is forecasted to reach around 20.6 million by 2070 (see Figure 44) (https://www.cbs.nl/en-gb/news/2023/50/forecast-nearly-18-million-inhabitants-19-million-projected-in-2037), along with increased economic activity. Simultaneously, climate change is exerting pressure on the freshwater supply, particularly during prolonged drought periods. The circular economy approach emphasizes the reuse and recycling of water, which can lead to a reduction in water consumption. By 2050, the Netherlands aims to achieve 100% circularity, which includes significant improvements in water management practices (United Nations Environment Programme, 2024). The Netherlands are currently aiming to reduce the per capita drinking water consumption to 100 L in 2035 from currently 125L and limiting low quality drinking water consumption. Additionally, large consumers of drinking water (mainly industries) are asked to reduce their drinking water consumption by 20%, thus limiting the effect on an increase in water demand in relation to the scarer water availability (Ministry of Infrastructure and Water, 2022). This demand reduction may come through greywater recycling and rainwater harvesting, and industrial circularity in manufacturing and construction. However, demand projections still come with high uncertainties; projections of total drinking water demand in the Netherlands in 2040 range from 1100 to over 1500 million m3/yr (current: around 1200 m3/yr) (Figure 45).

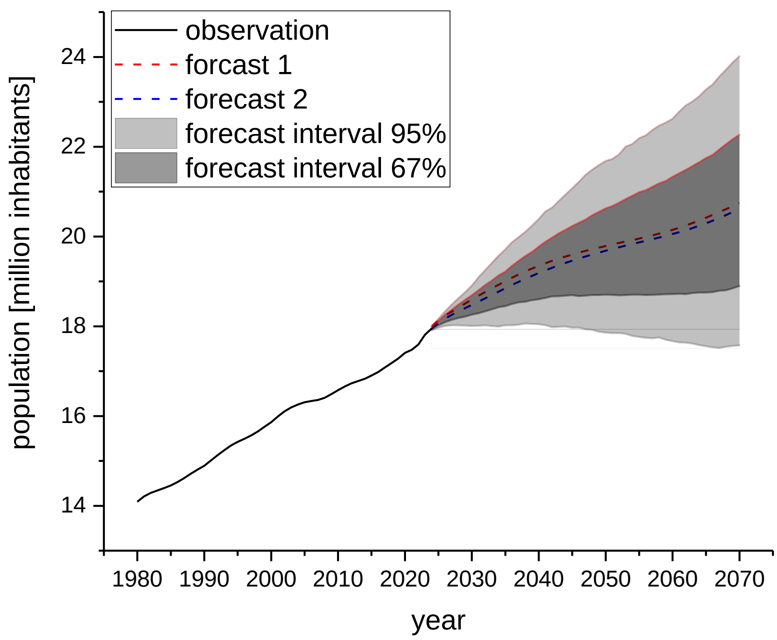

Figure 44 (a)Population forecast for Holland until the year 2070

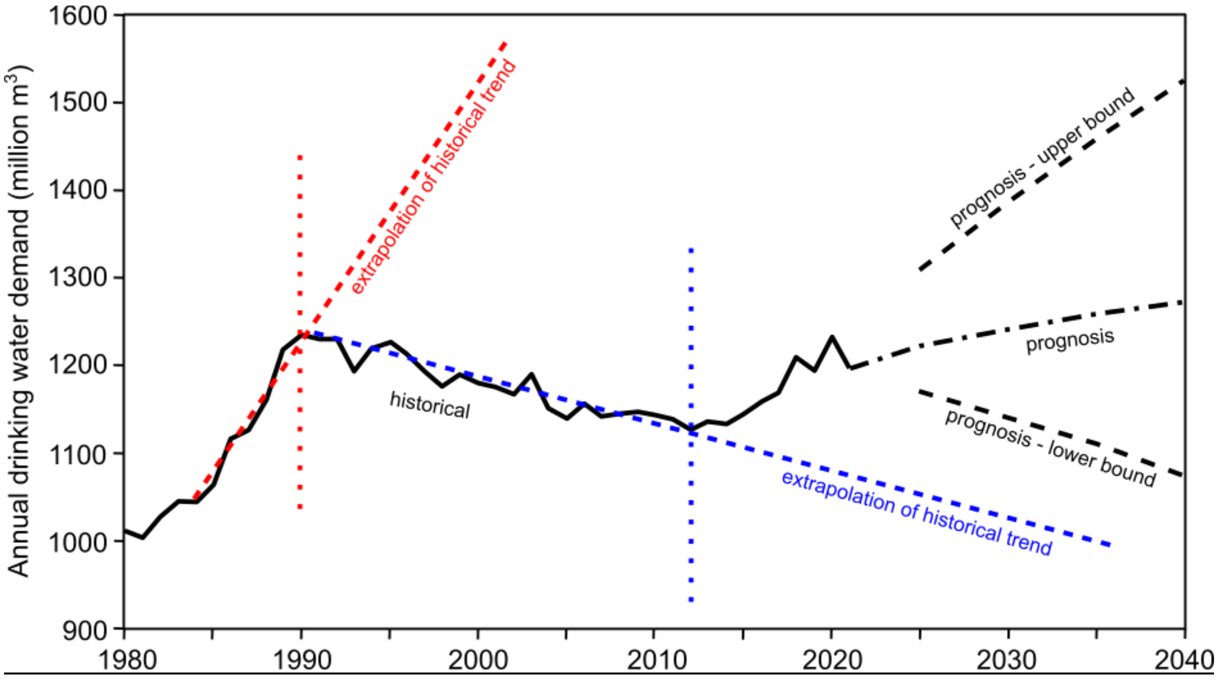

Figure 45 Past and projected drinking water consumption within the Dutch economy. Private households use over 70% of delivered tap water. (Baggelaar and Kuin, 2024).

Approximately 3 million people live and work in the province of Noord Holland, and drinking water is supplied by the utilities Waternet (Amsterdam) and PWN (province). PWN produces about 112 million m^3 of drinking water yearly, and utilises Lake Ijssel as its primary water resource. Given the general population forecast, the population of Noord Holland is expected to increase by approximately 300.000 people over the next 50 years. The main concern for Noord Holland, considering the transition to a circular economy and limited population growth, is not so much a direct increase in drinking water demand but rather a decline in water quality from the supply side. A significant concern is the salinisation of Lake IJssel. The surface water intake at Andijk / Lake IJssel is situated near the Afsluitdijk, the dam separating Lake IJssel (freshwater) from the Wadden Sea. During periods of low flow in the River Rhine, there is a risk of salinisation at the raw water intake due to seawater entering Lake IJssel via the locks that connect the lake with the sea. Other factors affecting the supply side include droughts and changing precipitation patterns, both of which have a direct impact on water supply and quality in Lake IJssel. Other water quality concerns may include pollution from possible incidents like illegal industrial wastewater discharge or shipwrecks near the water intake, PFAS contamination, and algae blooms during heatwaves.

The National Delta Scenarios (Van der Brugge, 2024) explore four different scenarios (Figure 46), which can be utilised to determine when and where alternative water resources will be required in the future. These scenarios are based on two significant impact factors that are both uncertain and beyond the direct control of water managers: climate change and socio-economic development. They provide both qualitative and quantitative information regarding climate, water systems, and water and land use. The qualitative information comprises storylines and maps that describe the backgrounds and identify connections among them. The quantitative information is presented as figures, covering time series for temperature, precipitation, river discharges, as well as geospatial land use databases, land subsidence, and salinisation in the Netherlands. The combination of the Delta Scenarios with climate change scenarios results in four combined demand scenarios (Busy, Steam, Warm, Rest). All are possible and must be considered. In each scenario, summers will become drier, and winters will become wetter due to climate change, leading to greater challenges. In Warm and Steam, the impact

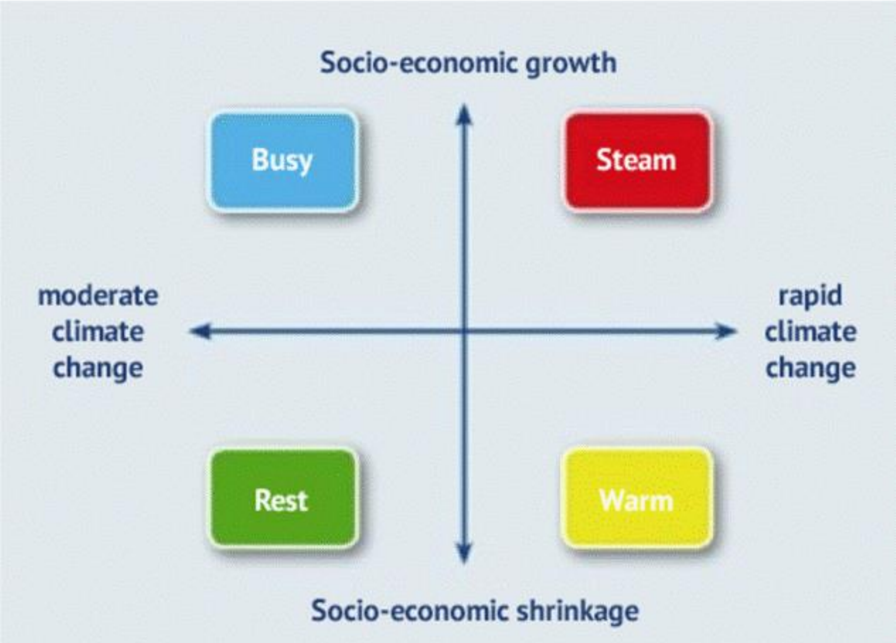

Figure 46 The four Delta scenarios combining climate change and Socio economic growth

of climate change is strongest, whereas in Busy and Rest, it is more modest. In Busy and Steam there is a socio-economic and population growth, while in Rest and Warm there is more space for nature and a lower socio-economic growth.

3.4.2 CS2 Kalundborg

Water demand in Kalundborg, a city known for its industrial symbiosis, is distributed across several key sectors: residential, public, commercial, industrial, and agricultural. The industrial sector is the primary user, accounting for approximately 70–75% of total water consumption. This includes 17 companies, including major users like Novo Nordisk, Novonesis, and a refinery. Surface water from Lake Tissø (4-5 million m^3 per year) is used for cooling, steam production and industrial water of potable water quality and thereby, it is often used for several purposes along a cascade of water supply. In total, industrial water consumption in Kalundborg is estimated to be around 8 million m^3 per year. The entire municipality of Kalundborg, which is home to approximately 48,000 residents (or 22,000 households), uses roughly 2.5 million m^3 per year for residential purposes and public services. Tourism contributes only minimally to overall water use. While agricultural water consumption is not precisely defined, it is estimated to be in the range of 4 to 5 million m^3 per year.

Over the next 50 years, water demand in Kalundborg will be shaped by key factors such as population growth, climate change, and advances in water management technologies. The most significant driver is expected to be industrial expansion, particularly from new biotech facilities and other sectors, including green hydrogen production. Depending on the socioeconomic development pathway, projections for 2070 show a wide range of possible outcomes (Figure 47, Figure 48):

- Under the SSP5 scenario (fragmented world with regional rivalry), total water demand could rise to 75 million m³ per year, with industry accounting for 84% of that demand.

- Under the SSP2 scenario (middle of the road), water demand is projected to reach 57 million m³ per year, with 84% allocated to industrial use.

- Under the more sustainable SSP1 scenario (focused on green growth and equality), water demand is projected to reach 40 million m³ per year, with industry still using 83% of total resources.

This is a substantial increase from current levels in 2024, where total water demand was approximately 15 million m³ per year, with 53% used by industry.

Population growth driven by industrial expansion is also expected to contribute significantly to increased water demand in Kalundborg. National projections estimate Denmark’s population will reach between 5.9 and 6.2 million by 2070. Internal migration—particularly the movement of workers to Kalundborg in response to industrial job opportunities—could substantially impact local water consumption. Under the SSP1 scenario, a 20–30% increase in Kalundborg’s population (equivalent to an additional 10,000–15,000 residents) would increase municipal water demand. However, the impact could be partially offset by the adoption of water-efficient appliances and greywater recycling systems, which offer a potential 15% reduction in household water use. In contrast, the SSP5 scenario anticipates a 100% population increase, which would place considerable strain on local water infrastructure and significantly elevate overall demand, especially when combined with industrial growth. Climate change is expected to significantly alter the regional water cycle in Kalundborg. Precipitation is projected to increase by 12–20%, with a notable rise in winter rainfall. Simultaneously, summer evapotranspiration is expected to grow by around 15%, potentially reducing water availability during warmer months. Additional hydrological impacts include increased winter discharge of 11-33%, an increase in drainflow of 16-32%, a rise in the mean groundwater levels by up to 18 cm and deep groundwater levels by up to 24 cm. These changes may help balance higher annual water demands driven by population growth, industrial expansion, and increased agricultural irrigation, partially offsetting some of the stress on local water resources.

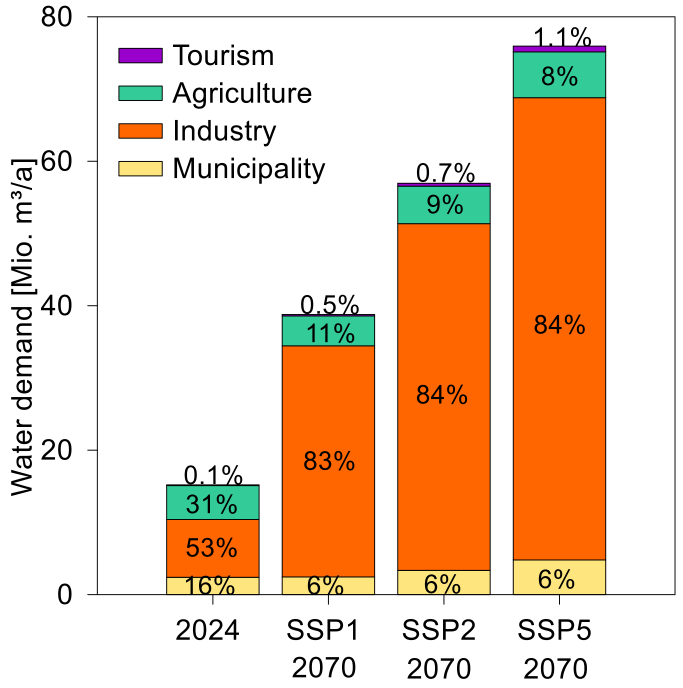

Figure 47 Water demand for different Scenarios and their percentage

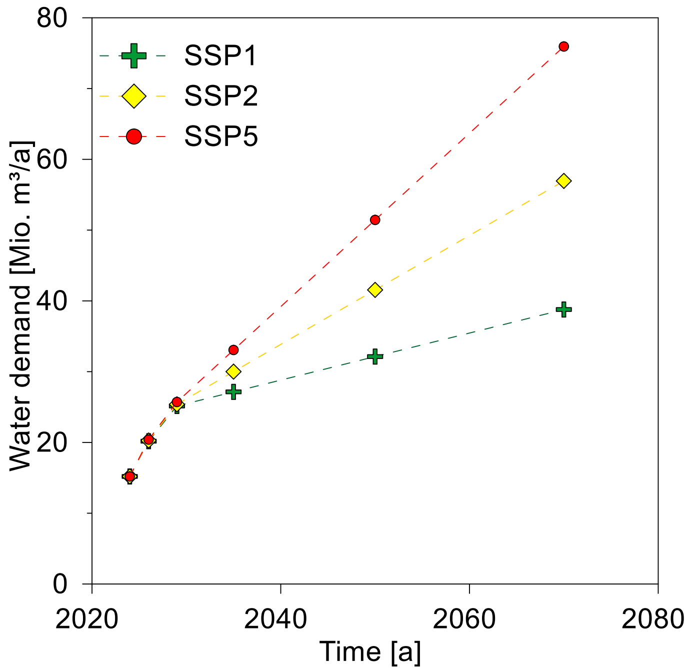

Figure 48 Water demand projections for different Socioeconoic pathways

3.4.3 CS3 Syros

The island of Syros, like many Greek islands, faces significant challenges in managing its water resources due to its unique geographical and climatic conditions, seasonal demand peaks, climate change and competing sectoral needs. The water demand on Syros is influenced by its inhabitants, agricultural activities, and tourism, all of which are expected to be further impacted by climate change.

The permanent population of Syros, projected to grow over the next 50 years, contributes to the island's baseline water demand, which includes drinking, sanitation, and other household needs. The approximately 22.000 inhabitants consume between 105 and 160 litres per person per day, which totals roughly 0.8 to 1.2 million m^3 annually, primarily supplied through desalination and groundwater abstraction. Legacy rainwater cisterns meet around 10% of household requirements, although modern construction often overlooks this practice. The island's water resources are already under pressure due to limited natural water availability and the necessity for sustainable management practices.

Agricultural activities on Syros, although not as extensive as in other regions, still require a reliable water supply. It relies heavily on irrigation, making it a significant water-consuming sector, accounting for approximately 1.6 million m^3 per annum.

Tourism on the island serves as a significant economic driver and has a notable impact on water demand, particularly during peak season. Tourists typically consume two to three times more water per capita than residents, estimated at around 240 litres per tourist per day, owing to frequent laundering, showering, recreational activities, and a lack of awareness regarding water restrictions.

Over the next 50 years, total water demand in Syros could rise by 1% to 14%, driven largely by population growth, an increase in water demand for agriculture, and a burgeoning tourism sector, depending on the Shared Socioeconomic Pathway (SSP) scenario. However, climate change is projected to reduce the availability of natural water resources and exacerbate water scarcity by altering precipitation patterns and raising average temperatures.

Based on downscaled projections from national demographic trends in Greece, SSP1 predicts a stable population, SSP2 a slight decline, and SSP5 an increase of up to 4,000 residents by 2070 (Figure 49).

In the agricultural sector, climate change is expected to gradually raise net irrigation requirements for major crops, resulting in an anticipated increase of at least 10% in irrigation demand. This may change due to change in irrigation type and efficiency as well as change in crops or use of highly efficient greenhouses, which use less water and reduce evapotranspiration.

Tourism is also expected to expand, with climate change likely to prolong the tourist season into spring and autumn. This could lead to a 15% rise in annual visitor numbers, placing additional pressure on water resources. Through the adaptation of water efficient appliances and encouragements to use less water, tourist driven water demand can be reduced (Figure 50).

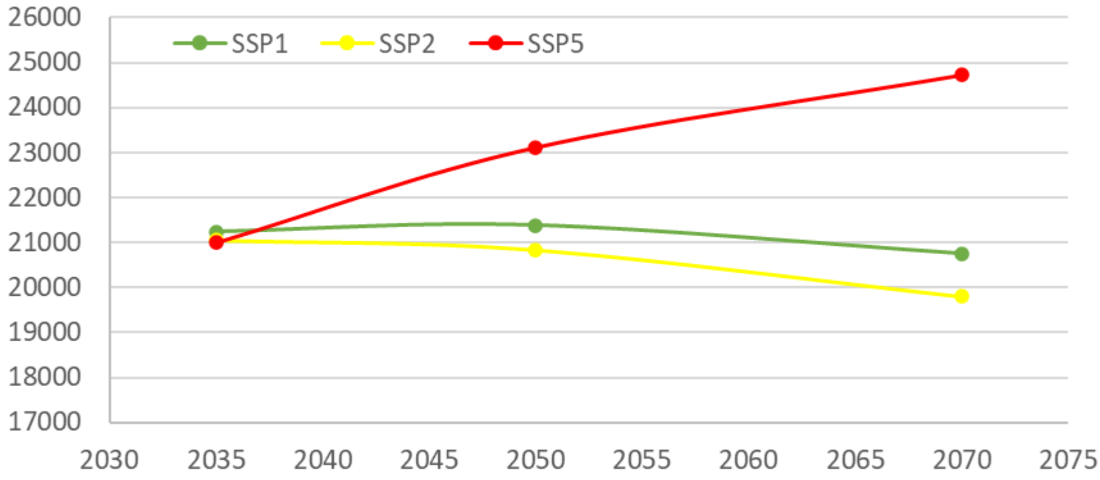

Figure 49 Population projection for Greece downscaled for Syros

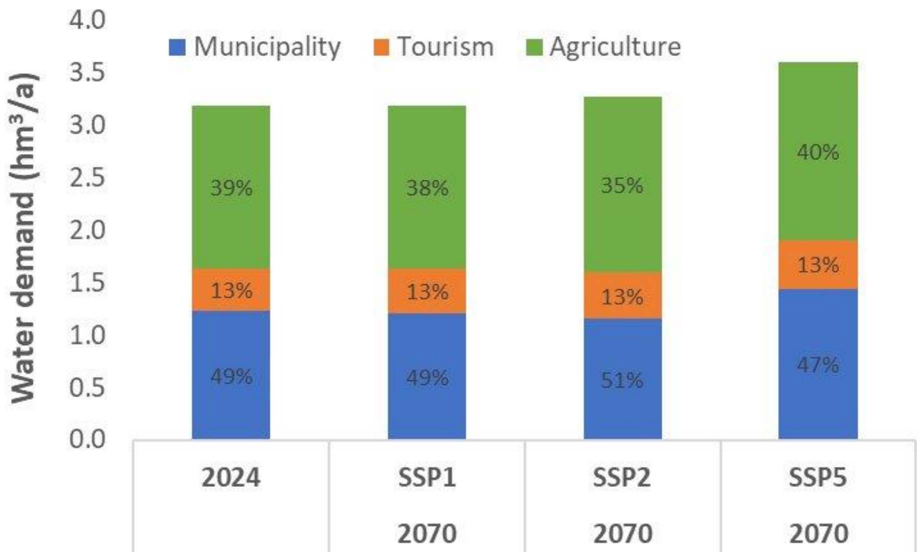

Figure 50 Water demand according to SSP scenarios

3.4.4 CS4 Costa Brava

The northern Costa Brava region, particularly the Alt Empordà comarca, like many Mediterranean areas, is experiencing increasing water demand driven by various sectors such as residents, agriculture, industry, and tourism. The region faces severe water stress due to seasonal demand spikes, prolonged droughts, salinisation of aquifers, and climate change. Current water demand is significantly influenced by population, tourism, and agriculture, while industry plays a minor role. The water demand for the 150.000 residents, approximately 12 million m^3/a, is met by the Fluvià-Muga aquifer and the Boadella Reservoir. During drought events, water restrictions of 200 litres per person per day were implemented to reduce consumption. The population in the region is projected to increase, particularly in urban centres, by approximately 50.000 people.

Agriculture in the Empordà region uses approximately 25 million m³ per annum and is highly sensitive to climatic changes. Additionally, the expansion of irrigated areas has significantly increased water demand, a trend that is expected to continue. Climate projections indicate a potential increase in net irrigation requirements by 60–100% by the 2070s under high-emission scenarios, due to rising temperatures and decreased precipitation. Under SSP1, sustainable practices (drought resistant crops) and technological advancements (deficit irrigation) could mitigate some of these demands by up to 40%. However, SSP5's emphasis on economic growth may exacerbate water stress and aquifer depletion by intensifying irrigation, which expands water demand by 50% for high-value crops.

The tourism sector, one of the primary economic drivers in the region, significantly contributes to water demand with 0.5 million m³/a, particularly during peak seasons when water resources are already under strain. Climate change may extend the tourist season into spring and autumn, potentially increasing annual visitor numbers by up to 15% and placing further pressure on water resources. Under SSP1, sustainable tourism practices (greywater recycling, vacuum sewerage) could reduce municipal usage by 25% and assist in managing this demand, whereas SSP5's emphasis on economic growth (unrestricted coastal development reliant on energy-intensive desalination) might result in increased water consumption without corresponding efficiency measures. Industrial activities with an consumption of approximately 5.2 million m3 annualy, while currently less dominant in the region, are expected to grow, particularly under SSP5. This growth could lead to increased water demand, especially in sectors like food processing and manufacturing. SSP1 envisions a shift towards water-efficient industrial processes, potentially offsetting some of the increased demand. Under SSP5, without significant efficiency measures, industrial water consumption could rise substantially.

Depending on the SSP scenario (Figure 51 and Figure 52), overall water demand will change significantly over the next 50 years. SSP1 will show a decline in water demand, from the current 42.7 million m³/a to 33 million m³/a, due to the implementation of reuse practices, infrastructure upgrades, and leak detection. SSP2 will experience an increase to 52 million m³/a, leading to aquifer salinisation, which will render 30% of groundwater unusable, thereby forcing reliance on desalination, which, in turn, will increase water prices due to a 20% rise in energy use. The fossil-fuelled development (SSP5) will result in a water demand of more than 71.5 million m³/a, causing total and irreversible aquifer depletion and salinisation, and tripling energy demand for desalination.

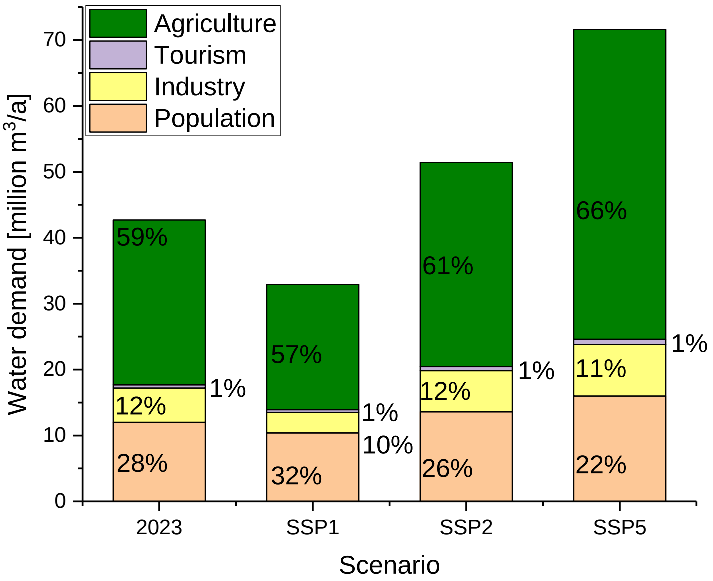

Figure 51 Respective water demand for Costa Brava by SSP scenario and section

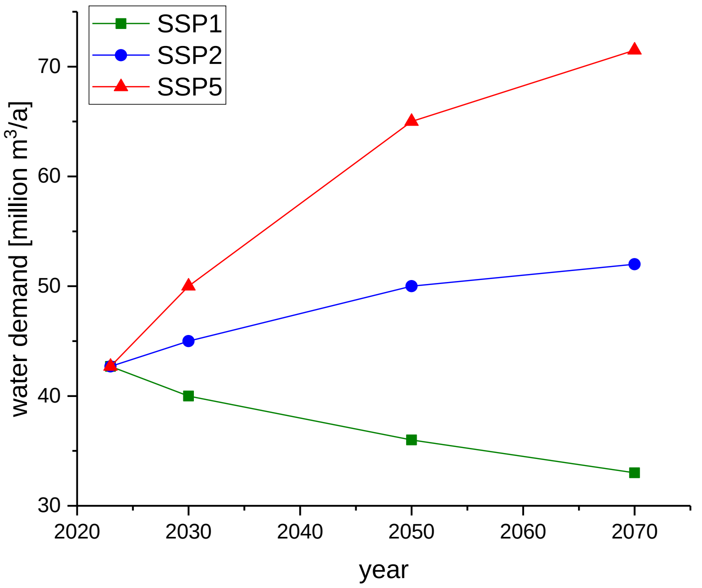

Figure 52 Overall water demand for the three selected SSP scenarios

4. Conclusion

4.1 General Observations on Structure and Data

The methodology employed in this report offers a consistent and comparative framework for assessing climate-related water supply vulnerability across four European case studies. Each case applies a four-tiered lens—climate predictions, surface water availability, groundwater availability, and water demand—utilising downscaled climate models and site-specific hydrological data. The strength of this structure lies in its ability to compare heterogeneous regions—industrial, urban, insular, and semi-arid—under a unified methodological umbrella. The use of ensemble model outputs smooths out uncertainties while allowing meaningful interpretation of relative changes and variability, which are increasingly more important than absolute values in climate impact studies.

One consistent finding across the dataset is that climate-induced hydrological changes are more clearly reflected in discharge than in precipitation. This is largely driven by enhanced evapotranspiration rates and altered soil moisture dynamics. In this sense, runoff projections serve as more informative indicators of water stress than rainfall alone. Furthermore, projected increases in interannual variability suggest that water systems must not only plan for average trends but also be designed to absorb extremes. Additionally, the report discusses aspects such as the frequency of heat spells, which are projected to increase, and this is relevant not only for ensuring sustainable water supplies but also for public health in general.

It should be noted that, while some of the observations may only become fully valid in the second half of the century and solely for the RCP8.5 scenario, our current trajectory is heading in this direction. Therefore, both climate change adaptation and climate change mitigation are becoming important strategies to pursue.

4.2 Case Study 1: North Holland, Netherlands

In North Holland, freshwater stress is driven not by absolute scarcity but by quality risks stemming from salinisation, particularly around Lake IJssel. The key climate vulnerability arises from the combination of sea level rise and reduced Rhine discharge during dry years, which weaken the hydraulic gradient that prevents seawater intrusion.

Although the region is unlikely to face net reductions in precipitation, the timing and variability of inflow into Lake IJssel are crucial. As dry summers align with peak irrigation, peak demands for water management of polder and nature areas, and domestic demand, there is a real risk of saltwater intrusion compromising freshwater abstraction points. Error bars in the projections for discharge also widen toward the end of the century, pointing to an increased frequency of extreme low-flow years.

Groundwater use is not a viable large-scale option due to salinity and subsidence risks. Therefore, reliance on Lake IJssel as a strategic freshwater reservoir must be carefully managed. Future scenarios may require either engineering interventions (e.g. strengthened sluice operations, upstream flow regulation) or a reconsideration of water allocation priorities between agricultural, water management and urban areas. As Lake IJssel is also fed by an international river catchment (the River Rhine), the political and international dimensions of river basin management must also be considered.

4.3 Case Study 2: Kalundborg, Denmark

Kalundborg demonstrates a mature model of integrated water reuse, supported by industrial symbiosis and circularity. The climate model results indicate slight increases in winter precipitation and stable runoff conditions, with minimal degradation projected for surface water availability. However, summer low-flow periods are likely to become more pronounced, jeopardising ecological flow requirements and seasonal water demands. Balancing industrial growth with Lake Tisso's capacity may necessitate stricter water abstraction quotas and enhanced cross-sector collaboration.

Groundwater resources are moderately resilient but remain under competing pressures, particularly from industry and agriculture, both sectors that may undergo changes in the future. Notably, Kalundborg benefits from existing infrastructure that supports reuse; however, less emphasis has been placed on natural seasonal buffering. There is a risk that the current balance-enabled by multiple reuse loops and shared industrial-municipal systems—could falter during heatwaves or prolonged dry spells if storage and alternative inflows are not scaled appropriately.

Water demand currently appears largely under control, thanks to long-standing efficiency strategies. However, any expansion in industrial activity or shifts in process water quality requirements may exert upward pressure on demand. These future quality demands can be addressed through infrastructure upgrades to ensure safe reuse. Kalundborg's system is highly adaptive, but further improvements may depend on upgrading seasonal storage and enhancing early warning for low-flow periods. Additionally, if changes in demand are disruptively high, rather than merely incremental, this necessitates adequate action to compensate.

4.4 Case Study 3: Syros, Greece

Although projected precipitation decreases are relatively small, the discharge declines are sharp-up to 30% in winter and spring due to increased evapotranspiration and soil dryness. This means that even normal-looking rainfall years may result in little effective surface runoff. Summer flows approach zero, threatening ecological stability and water availability during peak tourist season.

Groundwater is limited and has already been impacted by salinisation. Moreover, future projections indicate that recharge is expected to decline, signalling escalating water stress over time. Without careful extraction controls and artificial recharge, its role will diminish further. Meanwhile, water demand is projected to increase modestly, particularly from tourism. This could create flashpoint years where low inflow coincides with peak consumption.

Desalination will continue to be a cornerstone of resilience, yet it incurs high energy and operational costs. To ensure sustainability, Syros must invest in intelligent demand-side management, leakage control, and real-time monitoring, along with the potential expansion of seasonal water banking and dual-use systems.

4.5 Case Study 4: Costa Brava, Spain (Muga Catchment)

The Muga catchment's Darnius-Boadella Reservoir has already demonstrated its vulnerability to extended dry periods. From 2021 to early 2024, the reservoir dropped to as low as 11.5% capacity, only recovering after substantial autumn rainfall in late 2024.

Model projections show modest precipitation declines but more severe reductions in runoff (20–30%), especially in spring and summer. Discharge variability also increases markedly—error margins grow wider across all future time slices. This growing hydrological unpredictability places pressure on both supply planning and ecosystem services.

Groundwater availability is spatially heterogeneous, but a steady decline is observed under all climate scenarios. Additionally, seasonal analysis identifies winter as the most affected period, reinforcing long-term vulnerability to climate change. Consequently, while some agricultural zones may have access to aquifers, these are often shallow or vulnerable to quality degradation. With high agricultural and seasonal tourism demand, Costa Brava may face increased conflicts over water allocation and scheduling.

The relatively small storage volume of the Darnius-Boadella reservoir compared to regional demand underscores the urgency of investments in leak control, decentralized storage, reuse schemes, and efficient irrigation. Failure to act could result in escalating supply deficits, high dependency on desalination and growing socio-environmental tensions where rural communities face disparities in access to water during drought years as in fact had been observed also in recent history.

4.6 Commonalities and Differences Across Case Studies

Several core patterns emerge across the four case studies:

- Discharge, that is the run-off being generated from a surface or the discharge of a river, is a more climate-sensitive indicator than precipitation in all locations.
- Evapotranspiration and soil dryness significantly amplify the impact of warming, turning minor precipitation shifts into major runoff declines.
- Reservoir buffering capacity is a limiting factor: where storage is small (Syros, Boadella), resilience is weakest.
- GWS / recharge shows decreasing trends, with a clear seasonal shift characterized by increased recharge in summer and reduced recharge in winter.
- Seasonality and variability are increasing in all cases, raising the stakes for integrated, flexible water planning.
- Demand-side pressures are critical multipliers of vulnerability: industrial intensity (Kalundborg), population density (North Holland), tourism (Syros and Costa Brava) all amplify risk.

Yet key differences also shape adaptation pathways:

- North Holland faces systemic quality risks from salinization.
- Kalundborg’s strengths lie in circular water use and reuse.
- Syros must manage scarcity under isolation and cost constraints.
- Costa Brava’s challenge is coping with variability and limited capacity under high demand.

Together, these case studies show that context matters. Shared lessons that will be obtained within the RECREATE project around variability, storage, and demand-side governance will be highly transferable across Europe’s diverse water systems.

5. References

Akiba, T., Sano, S., Yanase, T., Ohta, T., & Koyama, M. (2019). Optuna: A Next-generation Hyperparameter Optimization Framework. *Proceedings of the ACM SIGKDD International Conference on Knowledge Discovery and Data Mining*, 2623–2631. https://doi.org/10.1145/3292500.3330701

Allen, R., Pereira, L., & Raes, D. (1998). FAO Irrigation and drainage paper No. 56. *Climasouth.Eu*. http://www.climasouth.eu/sites/default/files/FAO%2056.pdf

Arheimer, B., Dahné, J., & Donnelly, C. (2012). Climate change impact on riverine nutrient load and land-based remedial measures of the baltic sea action plan. *Ambio*, *41*(6). https://doi.org/10.1007/s13280-012-0323-0

Bonte, M., & Zwolsman, J. J. G. (2010). Climate change induced salinisation of artificial lakes in the Netherlands and consequences for drinking water production. *Water Research*, *44*(15). https://doi.org/10.1016/j.watres.2010.06.004

Copernicus Climate Change Service. (2022). *Copernicus Climate Change Service (C3S) (2022): ERA5-Land monthly averaged data from 1950 to present. Copernicus Climate Change Service (C3S) Climate Data Store (CDS)*.

D'Oria, M., Ferraresi, M., & Tanda, M. G. (2017). Historical trends and high-resolution future climate projections in northern Tuscany (Italy). *Journal of Hydrology*, *555*, 708–723. https://doi.org/10.1016/J.JHYDROL.2017.10.054

Gasparrini, A., Guo, Y., Hashizume, M., Lavigne, E., Zanobetti, A., Schwartz, J., Tobias, A., Tong, S., Rocklöv, J., Forsberg, B., Leone, M., De Sario, M., Bell, M. L., Guo, Y. L. L., Wu, C. F., Kan, H., Yi, S. M., De Sousa Zanotti Stagliorio Coelho, M., Saldiva, P. H. N., … Armstrong, B. (2015). Mortality risk attributable to high and low ambient temperature: A multicountry observational study. *The Lancet*, *386*(9991). https://doi.org/10.1016/S0140-6736(14)62114-0

Hamman, J. J., Nijssen, B., Bohn, T. J., Gergel, D. R., & Mao, Y. (2018). The variable infiltration capacity model version 5 (VIC-5): Infrastructure improvements for new applications and reproducibility. *Geoscientific Model Development*, *11*(8). https://doi.org/10.5194/gmd-11-3481-2018

Hengl, T., De Jesus, J. M., Heuvelink, G. B. M., Gonzalez, M. R., Kilibarda, M., Blagotić, A., Shangguan, W., Wright, M. N., Geng, X., Bauer-Marschallinger, B., Guevara, M. A., Vargas, R., MacMillan, R. A., Batjes, N. H., Leenaars, J. G. B., Ribeiro, E., Wheeler, I., Mantel, S., & Kempen, B. (2017). SoilGrids250m: Global gridded soil information based on machine learning. *Journals.Plos.OrgT Hengl, J Mendes de Jesus, GBM Heuvelink, M Ruiperez Gonzalez, M Kilibarda, A BlagotićPLoS One, 2017•journals.Plos.Org*, *12*(2). https://doi.org/10.1371/JOURNAL.PONE.0169748

Hengl, T., & MacMillan, R. (2018). *Predictive soil mapping with R*. https://books.google.com/books?hl=es&lr=&id=7M-JDwAAQBAJ&oi=fnd&pg=PA7&dq=Hengl,+T.,+MacMillan,+R.A.,+(2019).+Predictive+Soil+Mapping+with+R.+OpenGeoHub+foundation,+Wageningen,+the+Netherlands,+370+pages,+www.soilmapper.org,+ISBN:+978-0-359-30635-0.&ots=1X5nZ5MDzR&sig=mrKFdVVMoa1LS0lEeh7U99Sb-iA

Hersbach, H. , Bell, B. , Berrisford, P. , Biavati, G. , Horányi, A. , Muñoz Sabater, J. , Nicolas, J. , Peubey, C. , Radu, R. , Rozum, I. , Schepers, D. , Simmons, A. , Soci, C. , Dee, D. , &

Thépaut, J.-N. (2023). ERA5 hourly data on single levels from 1940 to present. Copernicus Climate Change Service (C3S) Climate Data Store (CDS), DOI: 10.24381/cds.adbb2d47 (Accessed on 06-Sep-2023). *Ecmwf*, *147*.

Hoyer, S., & Hamman, J. (2017). xarray: N-D labeled Arrays and Datasets in Python. *Journal of Open Research Software*, *5*(1). https://doi.org/10.5334/jors.148

IGRAC. (2025). *The Global Groundwater Monitoring Network (GGMN).* The Global Groundwater Monitoring Network (GGMN). https://ggmn.un-igrac.org

Jin, Z., Yezheng, W., & Gang, Y. (2005). General formula for estimation of monthly average daily global solar radiation in China. *Energy Conversion and Management*, *46*(2), 257–268. https://doi.org/10.1016/J.ENCONMAN.2004.02.020

Kling, H., Fuchs, M., & Paulin, M. (2012). Runoff conditions in the upper Danube basin under an ensemble of climate change scenarios. *Journal of Hydrology*, *424–425*, 264–277. https://doi.org/10.1016/J.JHYDROL.2012.01.011

Kotlarski, S., Keuler, K., Christensen, O. B., Colette, A., Déqué, M., Gobiet, A., Goergen, K., Jacob, D., Lüthi, D., Van Meijgaard, E., Nikulin, G., Schär, C., Teichmann, C., Vautard, R., Warrach-Sagi, K., & Wulfmeyer, V. (2014). Regional climate modeling on European scales: A joint standard evaluation of the EURO-CORDEX RCM ensemble. *Geoscientific Model Development*, *7*(4). https://doi.org/10.5194/gmd-7-1297-2014

Li, B., Rodell, M., Kumar, S., Beaudoing, H. K., Getirana, A., Zaitchik, B. F., de Goncalves, L. G., Cossetin, C., Bhanja, S., Mukherjee, A., Tian, S., Tangdamrongsub, N., Long, D., Nanteza, J., Lee, J., Policelli, F., Goni, I. B., Daira, D., Bila, M., … Bettadpur, S. (2019). Global GRACE Data Assimilation for Groundwater and Drought Monitoring: Advances and Challenges. *Water Resources Research*, *55*(9), 7564–7586. https://doi.org/10.1029/2018WR024618

Lundberg, S. M., Allen, P. G., & Lee, S.-I. (2017). A Unified Approach to Interpreting Model Predictions. *Advances in Neural Information Processing Systems*, *30*. https://github.com/slundberg/shap

Lundberg, S. M., Erion, G., Chen, H., DeGrave, A., Prutkin, J. M., Nair, B., Katz, R., Himmelfarb, J., Bansal, N., & Lee, S. I. (2020). From local explanations to global understanding with explainable AI for trees. *Nature Machine Intelligence*, *2*(1), 56–67. https://doi.org/10.1038/S42256-019-0138-9;SUBJMETA=117,308,639,692,705,794;KWRD=COMPUTER+SCIENCE,MEDICAL+RESEARCH,SOFTWARE

Ministry of Infrastructure and Water. (2022). *Water en bodem sturend, Policy note IENW/BSK-2022/283041*.

Muñoz Sabater, J. (2019). *ERA5-Land monthly averaged data from 1950 to present. Copernicus Climate Change Service (C3S) Climate Data Store (CDS)*.

O'Neill, B. C., Kriegler, E., Ebi, K. L., Kemp-Benedict, E., Riahi, K., Rothman, D. S., van Ruijven, B. J., van Vuuren, D. P., Birkmann, J., Kok, K., Levy, M., & Solecki, W. (2017). The roads ahead: Narratives for shared socioeconomic pathways describing world futures in the 21st century. *Global Environmental Change*, *42*. https://doi.org/10.1016/j.gloenvcha.2015.01.004

Save, H., Bettadpur, S., & Tapley, B. D. (2016). High-resolution CSR GRACE RL05 mascons. *Journal of Geophysical Research: Solid Earth*, *121*(10), 7547–7569. https://doi.org/10.1002/2016JB013007;WGROUP:STRING:PUBLICATION

Saxton, K. E., & Rawls, W. J. (2006). Soil Water Characteristic Estimates by Texture and Organic Matter for Hydrologic Solutions. *Soil Science Society of America Journal*, *70*(5), 1569–1578. https://doi.org/10.2136/SSSAJ2005.0117

Seidenfaden, I. K., Sonnenborg, T. O., Stisen, S., & Kidmose, J. (2022). Quantification of climate change sensitivity of shallow and deep groundwater in Denmark. *Journal of Hydrology: Regional Studies*, *41*, 101100. https://doi.org/10.1016/J.EJRH.2022.101100

Solomon, Susan. (2007). *Climate change 2007 : the physical science basis : Working Group I contribution to the fourth assessment report of the Intergovernmental Panel on Climate Change*. Cambridge University Press.

Spuler, F. R., Wessel, J. B., Comyn-Platt, E., Varndell, J., & Cagnazzo, C. (2024). ibicus: a new open-source Python package and comprehensive interface for statistical bias adjustment and evaluation in climate modelling (v1.0.1). *Geoscientific Model Development*, *17*(3), 1249–1269. https://doi.org/10.5194/GMD-17-1249-2024,

Steenhuis, T. S., & Van Der Molen, W. H. (1986). The Thornthwaite-Mather procedure as a simple engineering method to predict recharge. *Journal of Hydrology*, *84*(3–4), 221–229. https://doi.org/10.1016/0022-1694(86)90124-1

Taylor, K. E., Stouffer, R. J., & Meehl, G. A. (2012). An overview of CMIP5 and the experiment design. In *Bulletin of the American Meteorological Society* (Vol. 93, Issue 4). https://doi.org/10.1175/BAMS-D-11-00094.1

Team, R. C. (2023). R Core Team 2023 R: A language and environment for statistical computing. R foundation for statistical computing. https://www.R-project.org/. *R Foundation for Statistical Computing*.

Teutschbein, C., & Seibert, J. (2012). Bias correction of regional climate model simulations for hydrological climate-change impact studies: Review and evaluation of different methods. *Journal of Hydrology*, *456–457*, 12–29. https://doi.org/10.1016/J.JHYDROL.2012.05.052

Thornthwaite, C. W. (1948). An Approach toward a Rational Classification of Climate. *Geographical Review*, *38*(1), 55. https://doi.org/10.2307/210739

United Nations Environment Programme. (2024). Water as a Circular Economy Resource - Foresight Brief No. 033 February 2024. In *Water as a Circular Economy Resource - Foresight Brief No. 033 February 2024*. https://doi.org/10.59117/20.500.11822/44782

Van der Brugge, R. , R. C. de W. (2024). *Deltascenario's 2024 - Zicht op Water in Nederland.*

van Vuuren, D. P., Edmonds, J., Kainuma, M., Riahi, K., Thomson, A., Hibbard, K., Hurtt, G. C., Kram, T., Krey, V., Lamarque, J. F., Masui, T., Meinshausen, M., Nakicenovic, N., Smith, S. J., & Rose, S. K. (2011). The representative concentration pathways: An overview. *Climatic Change*, *109*(1). https://doi.org/10.1007/s10584-011-0148-z

Wunsch, A., Liesch, T., & Broda, S. (2022). Deep learning shows declining groundwater levels in Germany until 2100 due to climate change. *Nature Communications 2022 13:1*, *13*(1), 1–13. https://doi.org/10.1038/s41467-022-28770-2

Xue, D., Gui, D., Ci, M., Liu, Q., Wei, G., & Liu, Y. (2024). Spatial and temporal downscaling schemes to reconstruct high-resolution GRACE data: A case study in the Tarim River Basin, Northwest China. *Science of The Total Environment*, *907*, 167908. https://doi.org/10.1016/J.SCITOTENV.2023.167908

In case of any questions, please contact:

Wolfgang Gernjak

ICRA – Catalan Institute for Water Research

Contact: wgernjak@icra.cat

This project has received funding from the European Union's Horizon Europe research and innovation programme under grant agreement No. 101136598. This document reflects only the views of RECREATE consortium, neither the European Commission nor any associated parties are responsible for any use that may be made of the information it contains.